2011

Involvement of p53 in the S-phase Checkpoint during Nucleotide Deficiencies

Cortney Heyer
Virginia Commonwealth University

INVOLVEMENT OF P53 IN THE S-PHASE CHECKPOINT DURING NUCLEOTIDE DEFICIENCIES

A dissertation submitted in partial fulfillment of the requirements for the degree of Doctor of Philosophy at Virginia Commonwealth University.

by

CORTNEY L. HEYER

Bachelor of Science, St. Bonaventure University, 2005

RICHARD G. MORAN, PHD

PROFESSOR, DEPARTMENT OF PHARMACOLOGY AND TOXICOLOGY

Virginia Commonwealth University

Richmond, Virginia

April 26, 2011

Acknowledgements

I would like to recognize a number of individuals who have supported me and contributed to my graduate education. First, I would like to thank my mentor, Dr. Richard Moran, for his guidance, time and willingness to allow me to drive my own research. The education and experience obtained from his laboratory has provided me with a strong foundation for my scientific career which I am grateful for. I would also like to thank my committee members, Drs. Shirley Taylor, Jill Bettinger, Sumitra Deb and Larry Povirk for investing their time into my graduate education. I am thankful for insightful conversations with them and their questions, which ultimately gave me confidence in my own research. I would like to especially thank Dr. Shirley Taylor for sharing her expertise of cloning and cell culture with me and for her advice and guidance over the years.

Thank you to the members of the Moran and Taylor laboratory, both past and present, B. Ann Woodard, Lin Xie, Guoyan Gao, Amy Heineman, Dr. Shane Kasten, Dr. T. Britt Langston, Dr. Chen Wang, Dr. Alex Racanelli, Dr. Scott Lawrence, Dr. Scott Rothbart, Stuti Agarwal, Dr. Dolores Arjona, Erica Peterson, Lisa Shock, Prashant Thakkar. The conversation and time spent with all of you have made graduate school possible and enjoyable. I will be forever grateful for all of the conversations we have had troubleshooting experiments. I would like to especially thank Drs. Alex Racanelli and Scott Lawrence for your constant support, advice and encouragement, at both the personal and professional level, throughout my entire graduate education.

Thank you to all of my family and friends for giving me the extra push and believing in me when I did not believe in myself. I would like to thank my family: my parents, Wayne and Sharon Heyer, my sister and brother-in-law, Jennelle and Jon Malcos, and my brother, Brandon Heyer, for their endless love and support. Finally, I would like to thank my husband, Scott Lawrence, for being my biggest fan and for supporting and motivating me through difficult times.

Table of Contents

Page

List of Tables

Page

List of Figures

Page

Abbreviations

5-FU	**5-fluorouracil**
53BP1	**p53 binding protein 1**
9-1-1	**Rad9-Rad1-Hus1 complex**
AdR	**2-deoxyadenosine**
ADP	**adenosine-5′-diphosphate**
ATM	**ataxia telangiectasia mutated**
ATP	**adenosine-5′-triphosphate**
ATR	**ataxia telangiectasia mutated and rad3 Related**
Bax	**Bcl-2 associated X protein**
bp	**base pair**
BRCA2	**breast cancer susceptibility gene 2**
BSA	**bovine serum albumin**
ºC	**Celsius**
CBP	**CREB-binding protein**
CDP	**cytindine-5′-diphosphate**
ChIP	**chromatin immunoprecipitation**
cm	**centimeter**
CML	**chronic myelogenous leukemia**

CO-IP	**co-immunoprecipitation**
CTD	**C-terminal domain**
CTP	**cytidine-5′- triphosphate**
dATP	**deoxyadenosine triphosphate**
dTTP	**deoxythymidine triphosphate**
DDATHF	**5, 10-dideaza-5,6,7,8-tetrahydrofolic acid**
dFBS	**dialyzed fetal bovine serum**
dGTP	**deoxyguanosine triphosphate**
DNA	**deoxyribonucleic acid**
dNTP	**deoxyribonucleotide**
dTTP	**deoxythymidine triphosphate**
dUMP	**2′-deoxyuridine 5′-monophosphate**
GDP	**guanosine-5′-diphosphate**
GdR	**2′-deoxyguanosine**
γ-H2AX	**phosphorylated serine 139 on histone H2AX**
GTP	**guanosine-5′-triphosphate**
H3K4me3	**histone H3 trimethyl lysine 3**
HAT	**histone acetyltransferase**
HU	**hydroxyurea**
IP	**immunoprecipitation**
IR	**infrared radiation**

ITR	**inverted terminal repeats**
kb	**kilobase**
KDa	**kilodalton**
M	**molar**
MCM	**minichromosome maintenance**
MDM2	**murine double minute**
μg	**microgram**
μL	**microliter**
mL	**milliliter**
mRNA	**messenger ribonucleic acid**
μM	**micromolar**
mM	**millimolar**
ND	**no drug**
NES	**nuclear export signal**
nt	**nucleotide**
OA	**okadaic acid**
p53AIP1	**p53 regulated apoptosis inducing protein**
p53RE	**p53 response element**
PALA	***N*-(phosphonaceytl)-L-aspartate**
PARP	**poly (ADP-ribose) polymerase-1**
PCR	**polymerase chain reaction**

PIG3	**p53-inducible gene 3**
PTEN	**phosphatase and tensin homolog**
PTMS	**post-translational modifications**
PUMA	**p53 upregulates modulator of apoptosis**
Q-PCR	**quantitative PCR**
rAAV	**recombinant adeno-associated virus**
RNA	**ribonucleic acid**
RPA	**replication protein A**
RT-PCR	**reverse transcriptase PCR**
siRNA	**small interfering RNA**
ssDNA	**single-stranded DNA**
SDS-PAGE	**sodium dodecyl sulfate polyacrylamide gel electrophoresis**
TAF	**transcription TBP associated factor**
TAP	**tandem affinity purification**
TBP	**TATA-binding protein**
TEV	**tobacco etch virus**
TopBP1	**Topoisomerase II binding protein 1**
UV	**ultraviolet**
VP16	**etoposide**
Wip1	**wild-type p53-induced phosphatase**

Abstract

INVOLVEMENT OF P53 IN THE S-PHASE CHECKPOINT DURING NUCLEOTIDE DEFICIENCIES

By Cortney L. Heyer, B.S.

A dissertation submitted in partial fulfillment of the requirements for the degree of Doctor of Philosophy at Virginia Commonwealth University.

Virginia Commonwealth University, 2011

Advisor: Richard G. Moran, Ph.D.

Professor, Department of Pharmacology and Toxicology

Several classes of antimetabolites have been developed for the treatment of cancer, including numerous inhibitors of nucleotide biosynthesis. N-(phosphonacetyl)-L-aspartate (PALA) and hydroxyurea (HU) are two antimetabolites that inhibit nucleotide biosynthesis; PALA inhibits *de novo* pyrimidine synthesis and HU inhibits the conversion of ribonucleotide diphosphates to deoxyribonucleotide diphosphates. Due to the similar mechanisms, it was thought that cancer cells would respond similarly to HU and PALA treatment. However, studies in this dissertation revealed strikingly different responses to either HU or PALA treatment in HCT116 cells. A cytoprotective S-phase arrest was activated upon HU treatment while PALA treatment failed to activate the S-phase checkpoint,

resulting in p53-dependent apoptosis. The checkpoint effector kinase, Chk1, was not significantly phosphorylated during PALA treatment due to a failure to recruit ATR, the upstream kinase, to chromatin sites. The post-translational modifications of p53, phosphorylation of serines 46 and 392, suggested that PALA treatment promotes the accumulation of a transcriptionally active p53 while HU does not. ChIP analysis showed that p53 bound to pro-apoptotic promoters, therefore activating p53-dependent apoptosis during PALA treatment. To gain more insight into these differential cellular responses, we developed a tandem-affinity purification (TAP) tagged p53 cell line in which a TAP tag was inserted into the C-terminus of the endogenous p53 genetic locus through homologous recombination. This technology allows purification of p53 with its protein binding partners at endogenous expression levels. The tagged p53 accumulated and bound to promoters in response to DNA damage similar to the untagged p53, suggesting that the TAP tag did not interfere with the normal cellular functions of p53. Using mass spectrometry, we can identify the different p53 protein binding partners in response to PALA or HU treatment. We can also determine the variable pattern of post-translational modifications on different drug-stabilized p53 and determine which modifications are responsible for promoting apoptosis versus cytoprotective arrest. We can then exploit the identified proteins and post-translational modifications in the development of new chemotherapeutic agents.

Chapter 1: Overview and Introduction

Development of Cancer Chemotherapy

The origin of cancer chemotherapy dates back to World War I, when soldiers whom were exposed to mustard gases experienced dramatic symptoms, including significant bone marrow depression (Krumbhaar and Krumbhaar, 1919). Many years after this initial observation the biological action of mustard gases was investigated and it was found that proliferating cells are selectively vulnerable to mustard gases (Gilman and Philips, 1946). An initial clinical trial with a patient with non-Hodgkin lymphoma resulted in a dramatic anti-tumor effect with the use of mustard gas (Gilman, 1963). This experience with mustard gas was instrumental in the development of the concept that drugs could be administered systemically to induce tumor regression.

The next major advance in cancer chemotherapy was the development of antifolates. Syndey Farber made the discovery that administering folic acid to children with acute lymphoblastic leukemia (ALL) stimulated the proliferation of the cancer cells (Farber et al., 1947). This observation led to the development of aminopterin, a folic acid antagonist. Aminopterin induced remission in children suffering from ALL, the first time that induction of a temporary remission from cancer by drug was observed (Farber and Diamond, 1948). The concept of targeted therapeutics designed to inhibit cellular division led to the beginning of modern chemotherapy.

Antimetabolite development began to focus on DNA and RNA precursors in the early 1950's with the development of the purine analog 6-mercaptopurine (Hitchings and Elion, 1954), which was shown to have anti-cancer activity in mice with acute leukemia (Hitchings and Elion, 1954; Skipper et al., 1954). Pyrimidine analogs were also developed, the first being 5-fluorouracil, which was shown to inhibit the growth of transplanted tumors in mice (Heidelberger et al., 1957; Heidelberger et al., 1958). 5-FU is one of the oldest chemotherapeutic agents that is still in use for the treatment of several human cancers including colorectal, breast, stomach and pancreatic cancers, suggesting that this field of chemotherapy drugs is still very much alive.

A novel inhibitor of *de novo* pyrimidine synthesis

N-(phosphonaceytl)-L-aspartate (PALA) was synthesized in the search for specific inhibitors of nucleotide synthesis. Unlike 5-FU which requires cellular metabolism to convert it to its active form, 5-fluorodeoxyuridine monophosphate (FdUMP), which inhibits thymidylate synthase, PALA directly binds to and inhibits the second enzyme in *de novo* pyrimidine synthesis, aspartate transcarbamylase (Fig 1-1) (Collins and Stark, 1971). This enzyme consists of five subunits, two catalytic subunits and three regulatory subunits (Kantrowitz and Lipscomb, 1988). The end product of pyrimidine synthesis, cytidine triphosphate, interacts with the regulatory subunit decreasing the catalytic activity through negative feedback. Adenosine triphosphate also interacts with the regulatory subunit exerting the opposing effect, stimulating the catalytic activity of the enzyme (Gerhart and Pardee, 1962; Pardee and Yates, 1956). These feedback mechanisms maintain balanced levels of purines and pyrimidines in the cell for

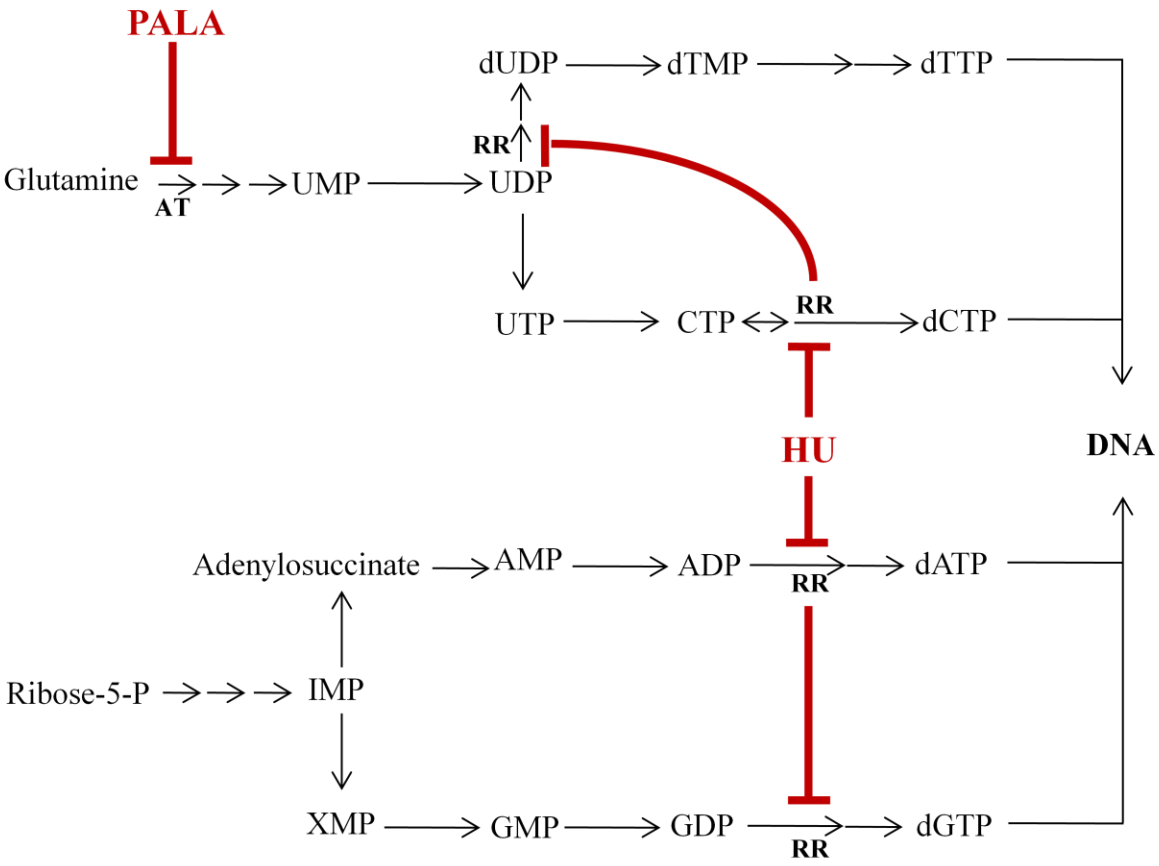

Figure 1-1. De novo pyrimidine and purine nucleotide synthesis pathway. Inhibition of the enzymes in this pathway by HU and PALA is indicated by red T-bars. AT, aspartate transcarbamylase and RR, ribonucleotide reductase.

nucleotide synthesis. The catalytic subunit binds L-aspartate and carbamyl-phosphate catalyzing the formation of carbamyl-L-aspartate, the first precursor committed exclusively to the biosynthesis of pyrimidines (Fig 1-2) (Reichard and Hanshoff, 1956).

Ultraviolet difference spectroscopy of the catalytic of subunit of *E. coli* aspartate transcarbamylase with various substrates demonstrated that the enzyme binds the transition state of the reaction more tightly than the substrates (Collins and Stark, 1969). The enzyme-carbamyl phosphate complex binds the inhibitor succinate more tightly than the natural substrate L-aspartate because it allows the conformational shift required for the reaction to occur without colliding with the carbamyl-phosphate. A model of the transition state of the aspartate transcarbamylase reaction was created on the basis of these observations in which the enzyme converts a portion of the electrostatic binding energy of L-aspartate into energy needed to force the two substrates together (Fig 1-2) (Collins and Stark, 1969). Using this model, PALA was synthesized as a transition state analog designed by combining structural features of the substrates (carbamyl phosphate and L-aspartate) and of the product (carbamyl-L-aspartate) of the aspartate transcarbamylase reaction (Fig 1-2) (Collins and Stark, 1971).

PALA simultaneously interacts with aspartate transcarbamylase at the binding sites for carbamyl-phosphate and L-aspartate with a Ki of 0.162 μM (Cohen and Schachman, 1986; Collins and Stark, 1971). It is a competitive inhibitor with carbamyl-phosphate at the catalytic subunit of the enzyme. Due to the ordered sequence of the reaction, carbamyl phosphate must first be bound to aspartate transcarbamylase in order for L-aspartate to bind; an excess of L-aspartate does not relieve PALA inhibition (Collins and Stark, 1971). Ultraviolet difference spectroscopy of PALA and aspartate transcarbamylase produced the same spectrum as was observed with carbamyl-phosphate and succinate, thus indicating that PALA inhibits the enzyme

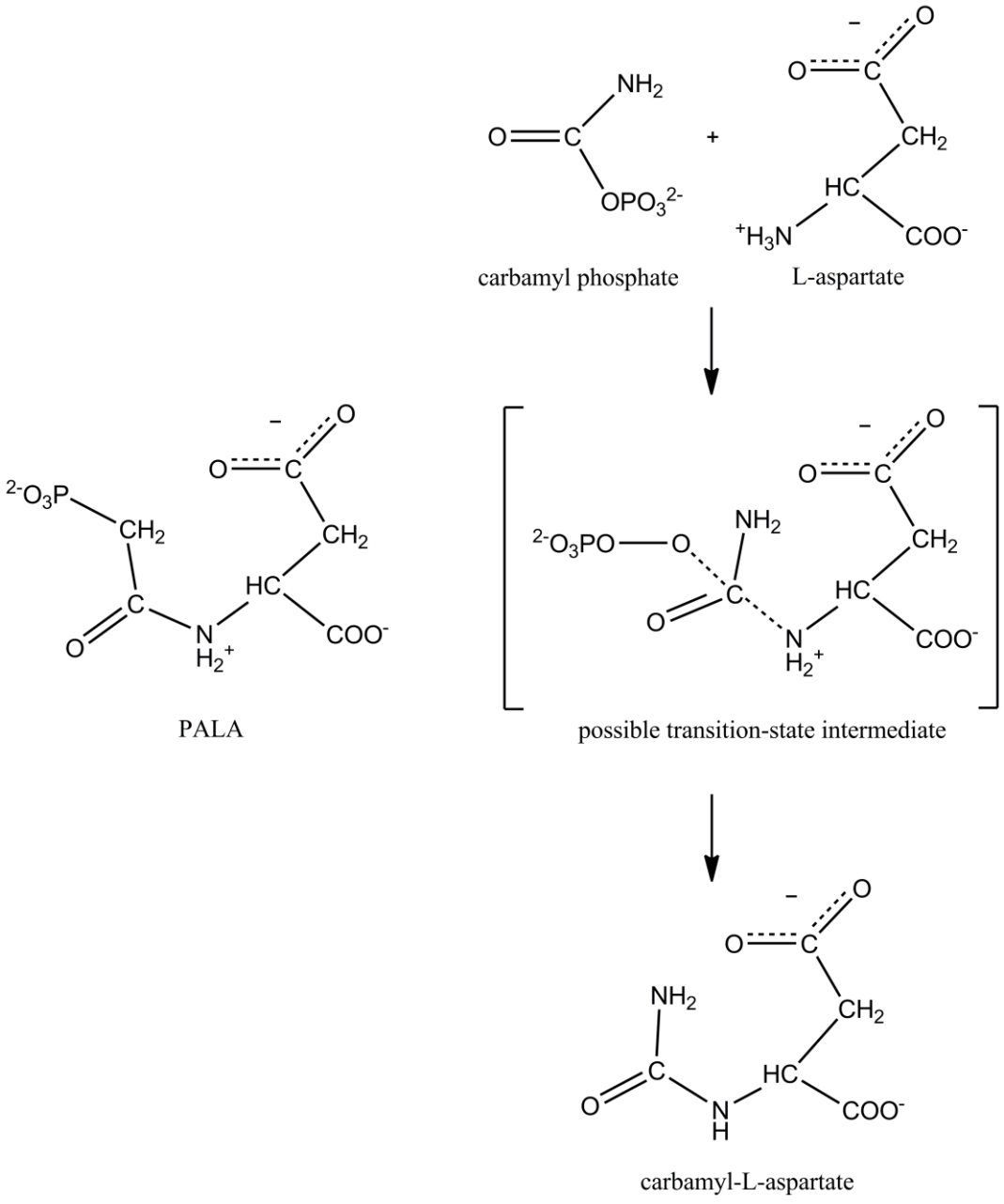

Figure 1-2. The chemical reaction catalyzed by aspartate transcarbamylase.

in a conformation closely resembling that associated with the transition state (Collins and Stark, 1971).

Initial studies with PALA in mammalian cells showed that PALA blocked proliferation and was cytotoxic. These effects were completely reversed with the addition of the nucleoside uridine indicating that PALA specially inhibits *de novo* pyrimidine synthesis (Swyryd et al., 1974). These initial studies suggested that PALA might have a clinical use in inhibiting cellular proliferation. In mice bearing transplanted tumors, PALA treatment delayed tumor growth and caused a partial regression. The most sensitive of these tumors was the Lewis lung carcinoma, a tumor that is refractory to most antiproliferative agents (Johnson et al., 1976). Doses of PALA which delayed the growth of Lewis lung carcinoma depleted the uracil and cytosine levels in the tumor without having an effect on the pyrimidine pools of liver, spleen or lung, indicating the specificity of PALA for rapidly proliferating cancer cells (Moyer and Handschumacher, 1979). This specificity was strictly found for solid tumors, including Lewis lung carcinoma, B16 melanoma and colon carcinoma 26, while L1210 and P388 leukemia are virtually insensitive to PALA (Johnson et al., 1976; Tsuboi et al., 1977). The spectrum of sensitivity of PALA to several experimental cancers inversely correlated with the cellular content of aspartate transcarbamylase. Interestingly, slow growing solid tumors in culture had lower levels of aspartate transcarbamylase than the fast growing leukemic cells (Johnson et al., 1978). This implies that PALA would potentially be an important drug for the slow growing, often drug refractory, solid human carcinomas.

The depletion of pyrimidine pools by PALA is considered to be essential for its antitumor activity. After 5 hours of PALA treatment in L1210 cells, UTP and CTP pools decreased to 10% of the control while ATP pools increased to 120% of control and GTP pools remain unchanged

(Moyer et al., 1982). Subsequently, DNA synthesis was 80% inhibited as measured by pulse labeling with ^{3}H-guanosine. Mice bearing transplanted tumors from L1210 cells were treated with PALA for 24 hours and showed similar trends and mirrored what was observed in Lewis lung carcinoma (described above); there were large decreases in CTP and GTP pools to 30-40% of the control, while ATP pools increased and GTP did not change (Moyer and Handschumacher, 1979; Moyer et al., 1982).

Clinical Evaluations of PALA

As a result of the promising preclinical antitumor effects of PALA, Phase I clinical trials were conducted in the late 1970's. In the first clinical trial, thirty-six patients were included, the majority of whom had either colon or lung cancer (Erlichman et al., 1979). All patients received a daily 15 minute intravenous infusion for a total of five consecutive days repeated every three weeks due to the rapid renal excretion of PALA with a plasma elimination $t_{1/2}$ of 4.6 hours. Dose limiting skin and gastrointestinal toxicities were observed at the highest doses. Only one patient with metastatic colon carcinoma showed signs of a clinical response to PALA after 8 months of treatment; in this patient, lung metastases decreased by more than 50% and several liver lesions also decreased in size (Erlichman et al., 1979). Phase II trials conducted in patients with colon, rectal or non-small cell lung cancer did not demonstrate significant antitumor activity, preventing further trials with PALA as a single agent (Carroll et al., 1980; Casper et al., 1980; Van Echo et al., 1980).

Experiments focusing on a possible combination therapy with PALA and other drugs began shortly after the completion of Phase II trials with PALA alone. When thymidylate synthetase is inhibited with 5-FU the conversion of dUMP to thymidylate is blocked causing an

accumulation of dUMP, which may interfere with FdUMP further binding and inhibiting thymidylate synthetase (Moran et al., 1979). If dUMP accumulation after 5-FU treatment could be prevented with the use of PALA, the inhibition of FdUMP on thymidylate synthetase might be enhanced. This hypothesis was tested; a 12-18 hour pretreatment with PALA followed by a two hour incubation with 5-FU increased FdUMP levels more than two fold and decreased dUMP levels three fold when compared to 5-FU alone in sarcoma cells (Liang et al., 1982). Encouraging experimental data led to a Phase I clinical trial consisting of 16 patients who received a 24-hour transfusion of PALA followed by an IV bolus of 5-FU daily for 5 days. This cycle was repeated every 28 days. Side effects included hair loss, diarrhea, skin rash, myelosuppression and dose-limiting gut toxicity (Meshad et al., 1981). One patient who was previously resistant to 5-FU responded to the combination treatment. A subsequent Phase II clinical trial with 57 patients treated with the same regimen concluded that 14% of the patients with the diseases responded to the drug combination. Of the responding patients, one with colon cancer and two with breast cancer had previously failed to respond to 5-FU alone. Although the outcome of the trials showed some promise, it was concluded that there was minimal advantage of PALA treatment in combination with 5-FU (Weiss et al., 1982).

Other drug combinations attempted to augment the incorporation of FUTP into RNA after administration of 5-FU, an alternative mechanism of the drug. When thymidine was administered before 5-FU in humans, it was shown to increase the half life of 5-FU by more than five-fold, an effect due to competition between 5-FU and thymidine at dihydropyrimidine dehydrogenase, the rate limiting process for 5-FU elimination (Woodcock et al., 1980). Subsequently, a Phase II clinical trial of the combination of FU, PALA, and thymidine was conducted in 37 patients with colorectal cancer. The dosing regimen consisted of an IV infusion

of PALA administered on day 1 followed by an IV infusion of thymidine 24 hours later on day 2 directly followed by an IV infusion of 5-FU. Treatment was repeated every four weeks (O'Connell et al., 1984). Although primary toxicities of leucopenia and ataxia were noted, there was a 27% response rate to this combination therapy over the historical response rate of 17% obtained after therapy with 5-FU alone. The dose-limiting leucopenia toxicity of the regimen prevented increasing the dosage of 5-FU.

Clinical trials using PALA in combination with other drugs, including methotrexate, ara-C and dipyridamole, continued until the mid 1990's but none resulted in any appreciable advantage in the treatment of cancer (Grem et al., 1988; Kemeny et al., 1989; Markman et al., 1987).

Hydroxyurea, a classic inhibitor of deoxynucleotide synthesis

Hydroxyurea, HU, was first synthesized in Germany by Dresler and Stein in 1869 (Fig 1-3) (Dresler and Stein, 1869). One hundred years after its original synthesis, it was discovered that HU inhibits ribonucleotide reductase, inhibiting the conversion of the four ribonucleotide diphosphates into deoxyribonucleotide diphosphates, the rate limiting step in the biosynthesis of DNA (Fig 1-1) (Krakoff et al., 1968). Mammalian and *Escherichia coli* ribonucleotide reductase consists of four subunits, two pairs of dimers, R1 and R2 (Reichard and Ehrenberg, 1983). Two active sites are formed at the interface between the R1 and R2 subunits. Each active site contains two sulfhydryl groups from the R1 subunit and a stable tyrosyl radical and two nonheme irons from the R2 subunit. Ribonucleotides bind to the R1 subunit and the sulfhydryl groups, tyrosyl radicals and nonheme irons participate in the reduction of the ribonucleotides (Atkin et al., 1973; Brown et al., 1969; Reichard, 1993). There are multiple levels of regulation of ribonucleotide

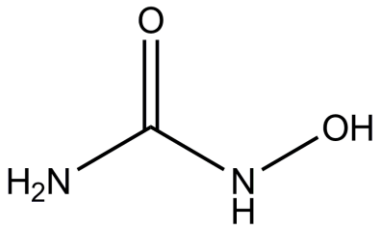

Figure 1-3. The chemical structure of hydroxyurea

reductase activity in place to obtain a balanced supply of dNTPS. Each R1 subunit contains two regulatory sites; one binds ATP activating the enzyme or dATP inactivating it, while the other binds effector molecules (ATP, dATP, dTTP or dGTP) altering the substrate specificity (Brown and Reichard, 1969; Reichard, 1987). HU scavenges the tyrosyl free radical, reducing it to a normal tyrosine residue, inhibiting the enzymatic activity of ribonucleotide reductase (Reichard and Ehrenberg, 1983). The –NH-OH segment of HU was shown to be essential for inhibition as detected in human recombinant holoenzyme-based *in vitro* assays (Shao et al., 2005). Using electron paramagnetic resonance, the inhibitory reaction between HU and purified R2 subunit of ribonucleotide reductase from mouse and *E. coli* was determined to be a one-electron transfer from HU to the tyrosyl radical (Lassmann et al., 1992). Studies with ribonucleotide reductase purified from Chinese hamster ovary cells demonstrated that HU noncompetitively inhibits the enzyme with a Ki of 0.08 mM for CDP reduction, 0.13 mM for ADP reduction and 0.07 mM for GDP reduction (Lewis and Wright, 1978). There are several other types of ribonucleotide reductase inhibitors (Reviewed in (Shao et al., 2006)). Other inhibitors that also scavenge the tyrosyl free radical include trimidox, nitric oxide and didox. Triapine chelates the iron groups in the R2 subunit inhibiting the enzyme. The R1 subunit is also a drug target. Caracemide and cisplatin inactivate the sulfhydryl groups and there are also several nucleoside analogs that bind to and inhibit the R1 subunit including, gemcitabine, tezacitabine and cytarabine.

The mechanism of action of HU was first linked to decreased nucleotide pools in *E. coli* (Neuhard, 1967). Further analysis in mouse embryonic fibroblast 3T6 cells showed that, after 10 minutes of HU treatment, dCTP, dGTP and dATP pools had decreased to 40% of the control while dTTP pools increased to 150% of the control (Bianchi et al., 1986). Thymidine incorporation into DNA was inhibited after 10 minutes of HU treatment indicating that the

decreases in nucleotide pools effectively inhibited DNA synthesis. When HU was given to animals, a marked leukopenia and anemia resulted, suggesting that HU might be active against leukemia (Rosenthal et al., 1928). Similar results were obtained when U251 human glioblastoma cells were treated with HU; after 2 hours dATP, dGTP and dCTP pools decreased while dTTP pools increased (Ostruszka and Shewach, 2003). Interestingly, after 24 hours of HU treatment, dATP pools remain decreased to 1% of the control while dGTP were 40% of control and both dCTP and dTTP pools increased to 175% of control. In 1963, HU was found to be active in L1210 mouse leukemia, doubling the life span of the treated mice (Stearns et al., 1963). This study resulted in clinical trials on patients with various types of cancer.

Clinical Evaluations of HU

Initial clinical trials of HU began in the 1960s in patients with a range of tumors. Patients with solid tumors experienced minimal improvement, while patients with chronic myelogenous leukemia, CML, experienced a decrease in leukocyte counts, a decrease in splenomegaly and an improvement in anemia (Fishbein et al., 1964; Thurman et al., 1963). A clinical trial focused on patients with CML administered a dose of 50 mg/kg/day of HU in two divided doses until the white blood cell count was 40% of the pretreated value, with the average length of treatment being ten days. The treatment of HU effectively controlled all nine patients with CML, but continuous therapy was required to maintain remission. Four of the nine patients were previously not responsive to busulfan, which led to the Federal Food and Drug Administration approving HU for the use in CML refractory to busulfan therapy (Kennedy and Yarbro, 1966). Subsequent trials proved that HU can be used as a primary therapy for CML and is currently

used in crises to rapidly reduce the number of white blood cells (Kennedy, 1972; von Bubnoff and Duyster, 2010).

When Chinese hamster ovary cells were treated with HU prior to or after IR treatment, the effects of radiation were more cytotoxic when compared to IR alone as measured by colony formation assays, implying HU is a radiosensitizing agent (Sinclair, 1968). Clinical trials began in 1969 for the combination treatment of head and neck carcinoma with IR and HU. Twenty patients received HU every third day with simultaneous treatment with IR over a period from three to ten weeks, while another 20 patients received IR with a placebo. Following the treatment with irradiation, patients continued receiving HU for six to eight weeks. Excluding the patients that underwent surgery, 6 out of the remaining 11 patients who received the combination therapy went into complete remission, while 2 out of the 11 patients who received placebo went into remission (Richards and Chambers, 1969). Several other clinical trials all demonstrated HU in combination with IR treatment is more beneficial than IR treatment alone in the treatment of head and neck carcinoma; HU and IR is clinically used to treat such cancers.

Other combination treatments with HU have been investigated but are currently not in clinical use. HU in combination with ara-C has been shown to enhance the cellular metabolism to the active metabolite ara-CTP (Robichaud and Fram, 1987). A phase II clinical trial in which 21 patients with non-Hodgkin's lymphoma treated with HU for six days followed by a three day infusion of ara-C resulted in 43% treated patients going into partial or complete remission (Schilsky et al., 1987). In combination with 5-FU, HU improved the survival of mice with L1210 mouse leukemia compared with treatment of either alone, although a clinical trial on patients with colon cancer showed only modest improvement (Lokich et al., 1975; Moran et al., 1982).

Currently, HU is also approved for the treatment of melanoma and inoperable, metastatic or recurrent ovarian cancer. Interestingly, HU is also used to treat the painful crises of sickle cell anemia, decreasing the need for blood transfusions (Platt et al., 1984). HU has been shown to increase fetal hemoglobin in patients with sickle cell anemia. The increased level of fetal hemoglobin limits sickle-cell hemoglobin polymerization, which is responsible for the painful episodes (Rodgers, 1992).

Cellular events induced by nucleotide synthesis inhibitors

Although PALA is not clinically used due to limiting efficacy at maximal tolerated doses, HU and PALA were shown to efficiently reduce tumor growth and in some cases even induce remission. The cellular and molecular mechanisms responsible for growth arrest and kill by nucleotide synthesis inhibitors have been investigated. This section will summarize what is presently known and how this dissertation research adds to the current understanding of the cytotoxicity induced by this class of antimetabolites.

Previous studies demonstrated that when fibroblasts with a functional p53 are treated with PALA, a G_1 arrest results whereas cells lacking p53 were able to progress into S-phase after treatment, therefore indicating that p53 contributes to the G_1 checkpoint (Yin et al., 1992). In contrast to the p53-dependence of the PALA-induced cell cycle arrest, HU caused arrest in early S-phase regardless of the p53 status, suggesting that fibroblasts respond differently to various types of nucleotide synthesis inhibitors (Linke et al., 1996). This concept raised a question which was central to this dissertation, namely, how do cancer cells molecularly respond to treatment with different nucleotide synthesis inhibitors? The data suggesting p53 is not required for the apparent S-phase checkpoint activated by inhibitors of dNTP synthesis also raises the

question of whether p53 is involved in the cellular response to HU. The molecular events of the G_1 arrest induced by PALA treatment were shown to include p53 accumulation, p21 activation and hypophosphorylation of Rb (Linke et al., 2003). Analysis of metaphase chromosomes demonstrated that PALA treatment did not cause chromosomal aberrations and did not cause DNA damage, yet p53 still accumulated. This led to the idea that p53 could detect levels of nucleotide pools, activating the G_1 checkpoint when pools become unbalanced (Linke et al., 2003). If this is true, how does this explain the observation that regardless of p53 status, HU treated cells arrest in early S-phase? Can p53 only detect nucleotide pools imbalances when pyrimidine or purine synthesis is inhibited and not when all dNTP synthesis is inhibited? The observed arrest induced by PALA treatment was not universal across all cell lines; out of five fibroblast cell lines studied that had wild-type p53, two arrested in S-phase while the other three underwent a functional G_1 arrest (Agarwal et al., 1998). Those cells that arrested in S-phase exhibited reduced BrdU staining and a three-fold decrease in thymidine incorporation, both suggesting that the arrested cells are not efficiently synthesizing DNA. This was not observed in fibroblasts lacking a functional p53; these cells continued synthesizing DNA and entered mitosis, suggesting p53 is inhibiting DNA synthesis during an arrested S-phase (Taylor et al., 1999). Synthesizing DNA in the presence of limited pyrimidine pools resulted in apoptosis as observed from positive staining in the TUNEL assay, DNA laddering, cytochrome c release, and cleavage of caspases 3 and 9 (Agarwal et al., 2006). Cells containing a wild-type p53 that arrested in S-phase appeared to be protected from cellular death by MIC-1 (macrophage inhibitory cytokine 1), a member of the TGF-β superfamily. A follow-up study addressed how p53 is stabilized during PALA treatment and suggested that when normal actively dividing fibroblasts are treated with PALA, reversible DNA damage occurs activating ATR and subsequent phosphorylation of

Chk1 and p53, leading to p53 accumulation, MIC-1 induction and S-phase arrest (Hastak et al., 2008). There appear to be contradictions on what checkpoint, if any, is activated in p53 competent cells treated with PALA. Some studies indicate p53 activates the G_1 checkpoint (Linke et al., 1996) while others suggest p53 activates the S-phase checkpoint (Agarwal et al., 1998). The reason for this discrepancy is not clear. This dissertation work is aimed at clarifying this field and understanding the molecular activities of p53 during PALA and HU treatment.

HU was identified to be an S-phase specific drug when Chinese hamster ovary cells traversing through S-phase were killed during HU treatment while the non-S-phase cells accumulate at the G_1-S boundary of the cell cycle and survived (Sinclair, 1965). Flow cytometry analysis of G_1 synchronized Chinese hamster ovary cells released into HU for 10 hours demonstrated that cells accumulated at the G_1/S border, with approximately 10% cells entering S-phase as compared to the control (Tobey and Crissman, 1972). After HU was removed, the cells entered S-phase synchronously and divided 6 hours later. These experiments led to the use of HU as a synchronization agent that has been a very valuable approach for generating an S-phase enriched cell population. In the early characterization of cell-cycle checkpoints, HU was often used for this reason, as well as to understand how incomplete DNA replication is detected by cellular mechanisms. A screen for *Schizosaccharomyces pombe* mutants that failed to arrest in the cell-cycle, and therefore initiated mitosis when DNA replication was blocked by HU, identified five genes named hus (hydroxyurea sensitive) 1-5, (Enoch et al., 1992). The analyses of these mutants in yeast have led to the discovery of what is now known as the S-phase checkpoint. It is now understood that HU activates the protective S-phase checkpoint and this compound is commonly used as a tool to study this cell cycle checkpoint, raising the question of whether other drugs that inhibit the synthesis of nucleotides will also activate this checkpoint,

which has been almost exclusively characterized with the use of HU. The S-phase checkpoint is described in detail in the introduction of the next chapter.

Focus of this Dissertation

Through the course of this dissertation, we investigated the cellular responses resulting from treatment with nucleotide synthesis inhibitors. The precedent literature suggested that PALA and HU treatment would activate the same molecular event within the cell, the protective ATR activated S-phase arrest. As described in Chapter 2, we determined that when human colon carcinoma HCT116 cells are treated with PALA or HU, both of which inhibited enzymes within the nucleotide synthesis pathways and thus, slowing the progress of the replication fork, the cancer cells respond differently at the molecular level. PALA is cytotoxic to the tumor cells, while HU is cytoprotective, preventing further tumor cell growth with little immediate cytotoxicity. The cellular signaling resulting from drug treatment is strikingly different, although both drugs cause a slowed S-phase and robust accumulation of p53. The differences in the molecular response of HCT116 cells to HU and PALA will be described. During these studies, we have developed a HCT116 cell line in which one allele of the p53 gene has been endogenously modified with a tandem affinity purification (TAP) tag. This cell line will be very useful in investigating the role of p53 in the cellular events leading to the cytotoxic versus cytoprotective response after treatment with these nucleotide synthesis inhibitors. The development and functional characterization of this cell line is detailed in Chapter 3. The implications of the results presented here will be discussed in Chapter 4.

Chapter 2: Differential Cellular Responses to Nucleotide Synthesis Inhibitors

Introduction

This Chapter will investigate the cellular and molecular responses of human colon cancer cells to different inhibitors of nucleotide synthesis. The role of p53 in the signaling pathways activated by the drugs as well as the possible mechanisms causing the observed responses will also be addressed. The following introduces the tumor suppressor p53, its cellular functions and the molecular events involved in the S-phase checkpoint.

The Tumor Suppressor p53

Structure of p53

p53 was discovered in 1979 as a phosphoprotein that co-immunoprecipitated with the simian virus large T antigen after SV40 infection and traveled at 53,000 Daltons on sodium dodecyl sulfate polyacrylamide gel electrophoresis (SDS-PAGE) (Lane and Crawford, 1979). p53 was originally hypothesized to have oncogenic properties after a temperature sensitive mutant of the SV40 large T-antigen gene was found to cause p53 accumulation after a temperature shift suggesting that p53 was involved in SV40-mediated transformation (Linzer et al., 1979). It is now know that the accumulation of p53 under these conditions reflects inactivation of p53 function by binding to the large T-antigen. p53 was later identified as a tumor suppressor after the loss of p53 was found to promote cancer. This was first reported in 1984 when p53 was inactivated by a retroviral insertion into a leukemia virus-transformed mouse

cell line (Wolf and Rotter, 1984). p53 was cloned shortly afterwards, allowing experimental manipulation of the gene and investigation of the consequences of such manipulations (Oren and Levine, 1983).

The p53 gene is located on the short arm of human chromosome 17 (17p13) and consists of 11 exons spanning approximately 20 kb of DNA (Benchimol et al., 1985; Lamb and Crawford, 1986). The p53 protein consists of 393 amino acids organized into four functional domains (Fig 2-1). The amino terminus of p53 contains two acidic transactivation domains, amino acids 1-42 and 43-60 (Fields and Jang, 1990). Activation of gene transcription by p53 is facilitated through the binding of several transcription factors at the amino terminus of p53 including the TATA binding protein (TBP) and TBP associated factors (TAFs) (Seto et al., 1992; Thut et al., 1995). One nuclear export sequence is located within the transactivation domain at amino acids 12-27 containing two serine residues (serine 15 and serine 20), which are known to be phosphorylated after DNA damage, resulting in nuclear retention of p53 (Zhang and Xiong, 2001). Downstream from the transactivation domain there is a proline rich domain (amino acids 64-92), which contains five repeats of the src homology 3 (SH3) binding motif PXXP where P represents proline and X any other amino acid (Walker and Levine, 1996). This region has been linked to p53-mediated apoptosis and appears to be dispensable for transactivation and cell growth arrest (Sakamuro et al., 1997). Amino acids 102-292 constitute the DNA binding domain that enables p53 to bind to specific DNA sequences (Kern et al., 1991). This domain of p53 specifically binds to the consensus binding sequence (p53 response element, p53RE) within gene promoters that contains two copies of the 10 bp motif 5′-PuPuPuC(A/T)(T/A)GPyPyPy-3′ separated by 10-13 bps where Pu is a purine base and Py is a pyrimidine base (el-Deiry et al., 1992). There are four conserved regions within the DNA binding domain responsible for

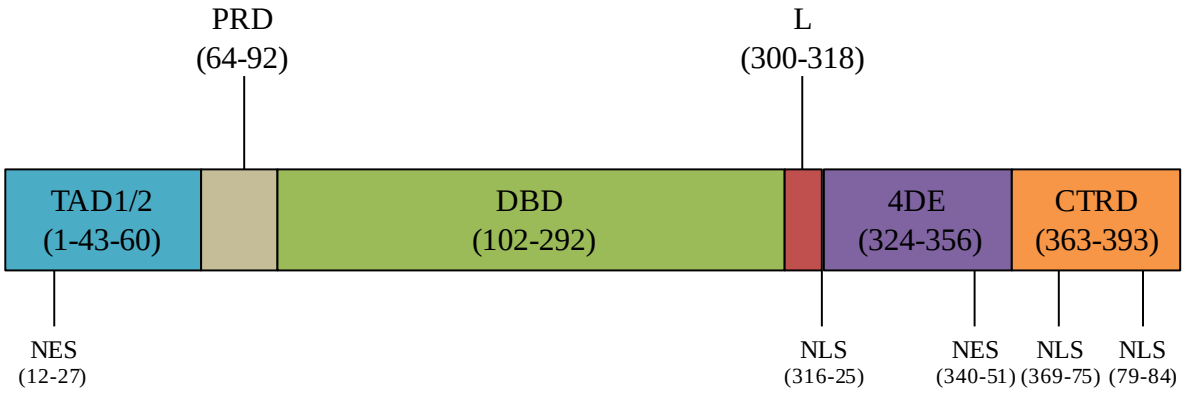

Figure 2-1. Structure of the p53 protein. Map of the functional domains of the p53 protein, the amino-acid residues spanning each domain are indicated below the domain name. p53 consists of two amino terminal acidic transactivation domains (TAD), a proline rich (PRD), a central DNA binding domain (DBD), a flexible linker (L), a tetramerization domain (4DE) followed by the C-terminal regulatory domain (CTRD). The nuclear export sequence (NES) and nuclear localization signals (NLS) are also noted.

contacting the minor and major grooves of the DNA within the p53-binding site. The DNA binding domain contains the majority of mutation hotspots in human cancer; the most frequently occurring mutations are in the peptides that make the closest contacts with DNA, explaining why many p53 mutants are unable to bind DNA (Cho et al., 1994).

The C-terminal region of p53 contains a flexible linker connecting the central core domain to the oligomerization domain, a 32 amino acid peptide required for the formation of tetramers, which are the form of p53 that bind to DNA (Fig 2-1) (Kraiss et al., 1988). Each monomer contains a turn, a β-strand, a second turn and an α-helix. Two monomers form a dimer in which the α-helix is anti-parallel to the β-strand in the corresponding monomer. Tetramers are formed by two dimers interacting through their α-helices and therefore the p53 tetramer is known as a dimer of dimers (Jeffrey et al., 1995). This tetramerization is required for efficient p53 transactivation *in vivo* and subsequent growth suppression (Pietenpol et al., 1994). A nuclear export sequence (NES) is located at amino acids 340-351 within the oligomerization domain and tetramerization masks the NES resulting in nuclear retention of p53 (Stommel et al., 1999). The extreme C-terminal basic domain, amino acids 363-393, was initially thought to be a negative regulator of sequence specific binding (Hupp and Lane, 1995). It was shown that DNA binding increased when the C-terminus of p53 was blocked with an antibody. This view has recently changed with the discovery that p53 binds nonspecifically to DNA via the C-terminal domain (CTD) and then slides along the DNA searching for p53 consensus sequences and therefore the CTD promotes DNA binding (McKinney et al., 2004). There are three known nuclear localization signals within p53, one located in the flexible linker sequence and the other two within the CTD (Addison et al., 1990; Shaulsky et al., 1990).

Accumulation and Stabilization of p53 by Post Translational Modifications

p53 is rapidly turned over in unstressed cells through its interaction with MDM2, a RING family type E3 ligase, which promotes poly-ubiquitination and proteasomal degradation (Honda et al., 1997). After the genotoxic stress of IR-induced DNA damage, p53 protein levels increased, apparently due to a post-translational mechanism. (Kastan et al., 1991). Post-translational modifications (PTMs) of p53 play a role in p53 accumulation by uncoupling the interaction between MDM2 and p53 thereby inhibiting its degradation (Shieh et al., 1997). PTMs of p53 have been extensively investigated; modifications can include phosphorylation, acetylation, methylation, ubiquitination, neddylation and/or sumoylation (Reviewed in (Toledo and Wahl, 2006)). After different cellular stresses, PTMs are thought to act as a barcode dictating the multiple cellular functions of p53. This section will address the phosphorylation sites which were investigated in this dissertation work. Figure 2.2 summarizes the known PTMs of p53.

Serine 15

The role of serine 15 phosphorylation in p53 biology appears to be complex. Phosphorylation of serine 15 is not required for p53 accumulation or transcriptional activation but enhances subsequent phosphorylations on neighboring residues (Fuchs et al., 1995). Nonetheless, MDM2 interacts with amino acids 18-23 of p53, therefore phosphorylation at serine 15 undoubtedly promotes p53 accumulation by alleviating this inhibitory interaction (Shieh et al., 1997). This residue lies within a nuclear export signal and when phosphorylated, results in nuclear retention of p53 (Zhang and Xiong, 2001). After IR, phosphorylation of serine 15 increases the ability of p53 to recruit and associate with the transcriptional coactivator proteins

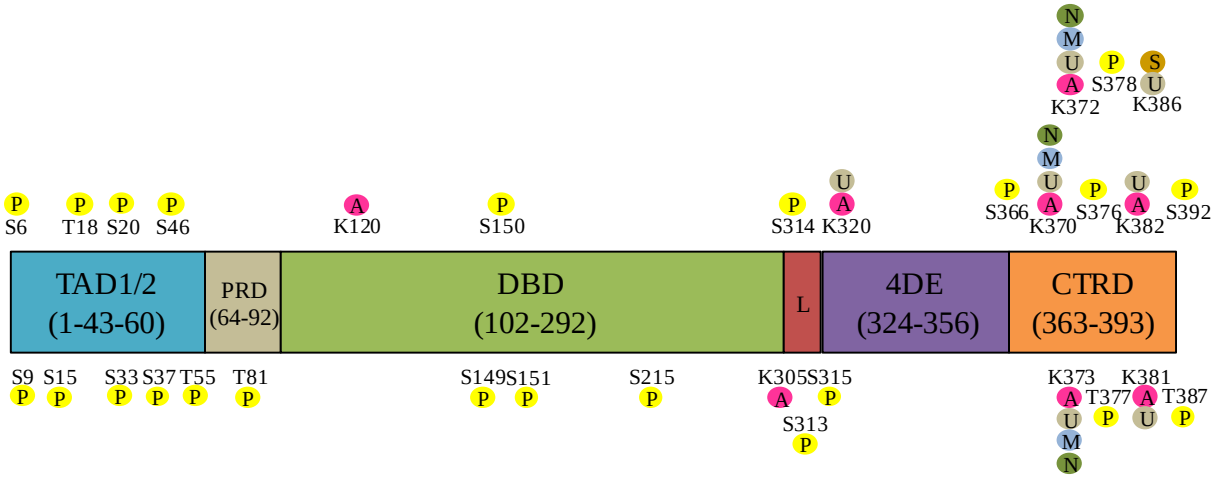

Figure 2-2. Post-translational modifications of p53. A map of the post translational modifications of p53 where each residue known to be modified is shown. Phosphorylation (P) sites are indicated in yellow, acetylations (A) in pink, ubiquitination (U) in grey, methylation (M) in as blue and neddylation (N) in green.

CBP and p300 (Lambert et al., 1998). The acetyltransferase activity of p300 recognizes the C-terminal domain of p53 as a substrate and acetylates it at lysines 373 and 382 enhancing the sequence-specificity of p53 binding to DNA (Gu and Roeder, 1997). Several kinases have been linked to phosphorylation of serine 15, including ATM, ATR, AMPK, DNA-PK, ERK, p38 and CDK9 (Reviewed in (Toledo and Wahl, 2006)). In this dissertation we are most interested in the activity of ATR, which is known to phosphorylate serine 15 after IR and UV treatment and is involved in the S-phase checkpoint (see below) (Tibbetts et al., 1999).

Serine 20

Phosphorylation of serine 20 also aids in p53 accumulation and nuclear retention in a similar fashion as was described for serine 15 phosphorylation. It is also not required for p53 stabilization and activation (Chehab et al., 1999). Chk1, among several other kinases, have been identified to be capable of phosphorylating serine 20 and, rather surprisingly, other than facilitating p53 stabilization, no further functions of this modification have been elucidated (Shieh et al., 2000).

Serine 37

Phosphorylation at serine 37 after UV and IR treatment appears to be important in p53-dependent transcription. Mutating this serine residue to an alanine significantly impairs the transactivating ability of p53 in a MDM2-luciferase reporter assay (Dohoney et al., 2004). Sequence-specific DNA binding of p53 is also enhanced when serine 37 is phosphorylated. The phosphorylation of serine 37 was shown to stimulate the interaction between p53 and the transcriptional coactivators p300 and PCAF which acetylate p53 at lysine 382 and lysine 320, respectively, activating the sequence-specific DNA-binding of p53 (Sakaguchi et al., 1998).

Serine 46

Phosphorylation of serine 46 has been implicated in p53 dependent apoptosis. When this residue is mutated to an alanine, cells have a reduced ability to induce apoptosis after UV treatment when compared to cells containing wild-type p53. Phosphorylation of p53 at serine 46 by the kinase HIPK2 induces the p53 dependent transcription of p53AIP1, a protein known to induce apoptosis by disrupting the mitochondrial membrane potential (D'Orazi et al., 2002; Oda et al., 2000). One study demonstrated that the phosphorylation status of serine 46 dictates the promoter selection of p53 (Mayo et al., 2005). Thus, during mild VP16-induced DNA damage, serine 46 is not phosphorylated and p53 thereby activates the transcription of MDM2 inducing the autoregulatory feedback loop. After extensive VP16-induced DNA damage, serine 46 is phosphorylated and the transcriptional activation by p53 becomes more extensive, for instance, PTEN transcription is activated favoring apoptosis (Mayo et al., 2005).

Serine 392

Thermodynamic studies demonstrated that phosphorylation of serine 392 significantly enhanced tetramer stability, possibly through hydrogen bonds between the phosphorylated residue and the N-terminal region of p53 (Sakaguchi et al., 1997). DNA binding and transcription activation of p53 is also enhanced after phosphorylation of serine 392 during UV treatment (Hupp et al., 1992; Keller et al., 2001). All of these effects of phosphorylation of serine 392 appear to be important for the anti-proliferative activity of p53. When SV3T3 mouse cells were transfected with p53 containing an alanine at this residue, this mutant p53 was unable to suppress colony formation as compared to cells transfected with wild-type p53 (Milne et al., 1992).

Transcriptional Regulation by p53

As described in the previous section, p53 contains a DNA binding domain which specifically binds the p53 response element (p53RE) within promoter regions of various genes, and a C-terminal domain, which has been shown to non-specifically bind DNA and then coordinate the linear search of DNA for p53REs (el-Deiry et al., 1992; McKinney et al., 2004). This section will further explain how p53 regulates gene transcription from binding to the p53RE to transcriptional elongation.

p53 Response Element

The p53RE contains two copies of the 10 bp motif 5′-PuPuPuC(A/T)(T/A)GPyPyPy-3′ separated by 10-13 bps where Pu is a purine base and Py is a pyrimidine base (el-Deiry et al., 1992). However, p53 is somewhat promiscuous when binding to promoters. It has been shown that tetrameric p53 is able to recognize, bind and transactivate genes from noncanonical consensus sequences containing only half of the consensus sequence (Jordan et al., 2008). Overall, the literature suggests that different p53RE have different binding affinities for p53. A study using a red-white p53 reporter system in *Saccharomyces cerevisiae* measured the ability of p53 to transactivate the reporter gene from various p53REs. It was shown that there is as much as a 1000-fold difference between the transactivation from weaker p53RE to stronger p53RE. The upstream p21 p53RE had the highest affinity, while the p53RE within the BAX promoter had the weakest affinity (Inga et al., 2002). *In vitro* thermodynamic studies using fluorescence anisotropy to measure the ability of purified p53 to bind to fluorescein labeled p53RE oligonucleotides agreed with the yeast model, demonstrating that the upstream p21 p53RE has greatest affinity and the promoters of other p53-regulated cell cycle genes, cyclin G, 14-3-3σ and

GADD45 also have higher binding affinity than the proapoptotic genes PUMA, BAX and p53AIP (Weinberg et al., 2005). Post translational modifications of p53 and p53 binding partners also contribute to the diversity of the transcriptional response. For instance, the phosphorylation of serine 46 discussed above has been shown to selectively induce p53 to transactivate the pro-apoptotic gene *p53AIP* (Oda et al., 2000). The ASPP family of proteins bind to p53 and promote transactivation of the pro-apoptotic gene *bax*; this is not observed with the cell cycle regulator p21 (Samuels-Lev et al., 2001). The control of genes transactivated by p53 is an enormously complex process for which multiple p53 post translational modifications and protein interactions with binding partners effect promoter selectivity.

Transcriptional Initiation

Prior to transcriptional initiation the chromatin around a promoter must be modified to open the chromatin structure allowing the general transcriptional initiation machinery to bind to the DNA. The role of p53 in this process is intricate. After p53 has bound to the p53RE, histone acetyltransferases (HATs) are recruited to acetylate the histones surrounding p53 (Lill et al., 1997). One such HAT that is recruited to promoters is p300/CBP following the interaction of CBP with the transactivation domain of p53. Not only does p300/CBP acetylate the histones bound to DNA in the vicinity of p53, it also acetylates the CTD of p53 increasing the activation of gene transcription (Gu and Roeder, 1997). After the opening of chromatin, the general transcription machinery can be recruited to form the preinitiation complex (PIC). p53 is known to act with several components of the PIC to initiate transcription. The assembly of complexes containing p53, TBP, the TBP associating factors (TAF), $TAF_{II}60$, $TAF_{II}40$ and $TAF_{II}250$ can activate transcription. When leucine 22 and tryptophan 23 residues of p53 that have been shown

to interact with the transcriptional machinery, were mutated to alanine, the transcriptional activity of the complex decreased (Thut et al., 1995).

The composition of the PIC required for transcriptional activation differs between gene loci as well as the stress stimuli. Two examples of this are the p21 and FAS promoters. Prior to any cellular stress, p53 is poised at the p21 promoter along with components of the PIC, TBP and paused RNA polymerase (Espinosa et al., 2003). After UV stress, increased levels of p53 leads to completion of the transactivation process by p53-dependent recruitment of $TAF_{II}250$ and stimulating the phosphorylation of serine 2 in the C terminal domain (CTD) of the paused RNA polymerase, converting it to the elongation form. In contrast, the FAS promoter does not contain a TATA box. Prior to any stress, p53 is also poised but the levels of paused RNA polymerase are significantly lower than found at the p21 promoter (Espinosa et al., 2003). After UV treatment, p53 levels increase recruiting HATs and $TAF_{II}250$ to the promoter. There is no net loss of paused RNA polymerase at the promoter after the appearance of the elongation form, suggesting that the initiation and elongation rates were similar. The difference between these two promoters demonstrate that cell cycle genes, such as p21, are poised for rapid transcriptional activation after cellular stress while the transcriptional activation of the proapoptotic gene *Fas* is slower due to the lower levels of RNA polymerase poised at the promoter. Once RNA polymerase is loaded onto the promoter and transcription is initiated, transcription of FAS remained constant because there is no net loss of paused RNA polymerase while p21 transcription fluctuates due to varying levels of loaded RNA polymerase (Espinosa et al., 2003).

Transcriptional Elongation

After RNA polymerase is cleared from the promoter, its processivity is facilitated by several elongation factors, some of which interact with p53. The phosphorylation of serine 392 of p53 is often implicated in complexes with elongation factors and, as described above, this phosphorylation promotes oligomerization of p53 and subsequent DNA binding (Hupp et al., 1992; Sakaguchi et al., 1997). During the discovery that casein kinase 2 (CK2) is able to phosphorylate serine 392 of p53 after UV treatment, p53 was found to be in a complex with subunits from the FACT (facilitated chromatin transcription) complex, a known elongation factor (Keller et al., 2001). The human p-TEF (positive transcription elongation factor) is responsible for converting the paused RNA polymerase to elongating polymerase through phosphorylation at serine 2 in the carboxy terminal domain (Marshall et al., 1996). The Cdk9 kinase is the component of p-TEF responsible for phosphorylating serine 5 of the CTD of RNA polymerase (Ramanathan et al., 2001; Zhu et al., 1997). Cdk9 is known to interact with p53 and phosphorylate it at serine 392; the stabilized p53 then promotes transcription of Cdk9, thereby promoting transcriptional elongation in a feed-forward system (Claudio et al., 2006).

Transcriptional Repression

A less studied role of p53 is transcriptional repression. After binding to certain promoters, p53 interacts with mSin3a recruiting HDAC1 (histone deactetylase), which removes the acetyl moieties from the chromatin causing the chromatin to close around the promoter, repressing transcription (Murphy et al., 1999). The physical binding of p53 to promoters may occlude the binding of other transcription factors required for transcriptional activation. This is observed during hypoxic stress: under these conditions p53 binds to the alpha-fetoprotein promoter, inhibiting the binding of the transcriptional activator HNF3 and, hence, repressing

transcription (Lee et al., 1999). Although the mechanism of transcriptional repression is not understood yet, p53 binds to the Rad51 promoter repressing transcription of this protein critical to homologous recombination during DNA damage (Arias-Lopez et al., 2006). As will be discussed below, this repression is of interest for this dissertation.

p53 Dependent Apoptosis

It was first shown that p53 was involved in the apoptosis pathway when tumor cells null for p53 underwent spontaneous cell death after the introduction of a wild-type p53 by transfection (Yonish-Rouach et al., 1991). Bax was found to be a direct transcriptional target of p53 and the first example of a proapoptotic gene directly regulated by p53 (Miyashita and Reed, 1995). The restoration of p53 in murine leukemia cells caused an increase of Bax mRNA and protein levels (Selvakumaran et al., 1994). Since then several other pro-apoptotic genes have been identified that are regulated by p53, including p53AIP1, APAF1, Caspases 1, 6 and 10, FAS, PUMA, DR4 and DR5. Upon binding to the promoters of these genes, p53 activates transcription, thereby promoting the downstream components of the apoptosis cascade (Reviewed in (Riley et al., 2008)).

Evidence for a role of p53 in the regulation of apoptosis that was independent of transcription was first hypothesized after transcriptionally inactive mutants of p53 were found to induce cell death (Haupt et al., 1995). After DNA damage, p53 translocates to the surface of mitochondria prior to the release of cytochrome c from the mitochondrial intramembrane space and caspase 3 cleavage in the cytosol, suggesting that p53 has a direct role in the intrinsic pathway of apoptotic signaling (Marchenko et al., 2000). Once at mitochondria, p53 specifically binds to the Bcl-2 family proteins. The interaction between p53 and Bak releases the anti-

apoptotic inhibitory protein Mcl-1 from complexes with Bak, allowing oligomerization of Bak and subsequent cytochrome c release from the mitochondria (Leu et al., 2004). Similarly, p53 also interacts with Bax releasing the anti-apoptotic protein Bcl-xl from Bax-Bcl-xl complexes and promoting Bax oligomerization and cytochrome c release (Chipuk et al., 2004). The anti-apoptotic proteins Bcl-xl and Bcl-2 are also modulated by p53 within mitochondria. The DNA binding domain of p53 binds to Bcl-xl and Bcl-2 inhibiting their anti-apoptotic activity, again facilitating the release of the central mediator of the intrinsic pathway, causing cytochrome c release (Mihara et al., 2003; Tomita et al., 2006).

p53 senses cellular stresses induced by chemotherapeutic agents

Due to the several roles of p53 in response to chemotherapeutic agents, the question arose as to what cellular changes p53 could detect after such treatments. Most cellular responses have been studied in response to IR or UV; much less is known about the p53 response to nucleotide pool deprivations. Ionizing radiation, camptothecin and bleomycin directly and rapidly induce DNA strand breaks, promoting the accumulation of significant levels of p53 within one hour of treatment. Cells electroporated with DNaseI or the restriction enzyme *Alu*I also accumulated p53, leading to the conclusion that DNA strand breaks initiate p53-dependent signaling pathways (Nelson and Kastan, 1994). Further analyses showed that only one single DNA strand break per cell was sufficient to induce a p53 dependent growth arrest (Huang et al., 1996).

The concept that p53 could sense nucleotide levels and then would become stabilized was first proposed by Linke *et al.* (Linke et al., 1996). In their experiment, treating WS1 embryonic skin cells containing a wild-type p53 with antimetabolites inhibiting different parts of *de novo* pyrimidine and purine synthesis resulted in a G_1 cell cycle arrest. In cells null for p53 the effect

did not occur and cells slipped into early S-phase and then arrested. Interestingly, dNTP biosynthesis inhibitors caused arrest in early S-phase regardless of p53 status. This dissertation addresses the question of what role, if any, does p53 have in the S-phase checkpoint. In the studies of Linke and colleagues, the G_1 arrest was reversed upon the addition of the limiting nucleotides and no apparent DNA damage was detected by metaphase chromosome analysis, therefore, the p53 dependent arrest was not caused by DNA damage. This was a central paper to this dissertation in that it demonstrated the accumulation of p53 in response to deoxynucleotide deficiencies promoted cell cycle arrest. This unique p53 dependent cell cycle arrest caused by nucleotide depletion is of substantial importance because if cells are allowed to divide in the presence of limiting nucleotides, chromosome breakages could arise due to incomplete DNA replication, putting the genome at risk of becoming highly unstable and tumorigenic (Linke et al., 1996).

p53 mutations and cancer

In approximately 50% of human cancers p53 is mutated, making it the most commonly mutated gene in human malignancies (Vogelstein, 1990). As described above, p53 is capable of triggering apoptosis or growth arrest, both of which aid in maintaining genome stability. Due to the involvement of p53 in these pathways protecting the cell from tumorigenesis, extensive research has been done to further understand mutant p53 and its cellular effects. The majority of p53 mutations in human cancers disrupt the ability of p53 to bind to DNA (Kato et al., 2003). In a study including 280 tumors containing p53 with somatic base substitution mutations, 98% of the mutations fell within a 600 base pair region of p53 encompassing exons 5 through 8 (amino acids 110-307). Out of the 280 analyzed, 227 were from solid tumors. Colon, esophagus, breast

and non-small cell lung cancer containing the most mutations (Hollstein et al., 1991). In heterozygous cells, a mutant p53 allele can alter the function of the wild-type p53 allele, have a dominant negative effect on wild-type p53, or results in gaining new oncogenic properties independent of the wild-type p53 (Baker et al., 1989). Analysis of tumors containing allelic deletions in the short arm of chromosome 17, specifically the region encoding p53, showed that the remaining allele contained point mutations indicative of loss of heterozygosity (Baker et al., 1989). Upon co-translation of mutant p53 and wild-type p53, mutant p53 was found to oligomerize with wild-type p53, driving it to a mutant phenotype characteristic of a dominant negative effect (Milner and Medcalf, 1991). Transfection of mutant p53 into p53 null tumors resulted in lethal tumors, demonstrating that mutant p53 may gain oncogenic properties (Wolf et al., 1984).

DNA Replication

DNA replication in eukaryotic cells is an intricate process; this section will serve as a brief overview of the main proteins that are present at replication forks during an unperturbed S-phase (See Figure 2-3). Replication is initiated at multiple origins along the DNA in mammalian cells as was shown by audioradiography of chromosomal DNA fibers isolated from Chinese hamster fibroblasts (Huberman and Riggs, 1966). The origins are marked by the formation of pre-replicative complexes (preRC) in G_1. The origin recognition complex (ORC) binds to the preRC as well as the additional replication factors, including Cdc6, Cdt1 and minichromosome maintenance helicase complex (MCM2-7) (Bell and Stillman, 1992). Initiation of DNA synthesis is regulated by two protein kinases: S-phase specific cyclin-dependent kinase (S-CDK) and Cdc7-Dbf4 (DDK). The exact mechanisms of how these kinases enhance the initiation of

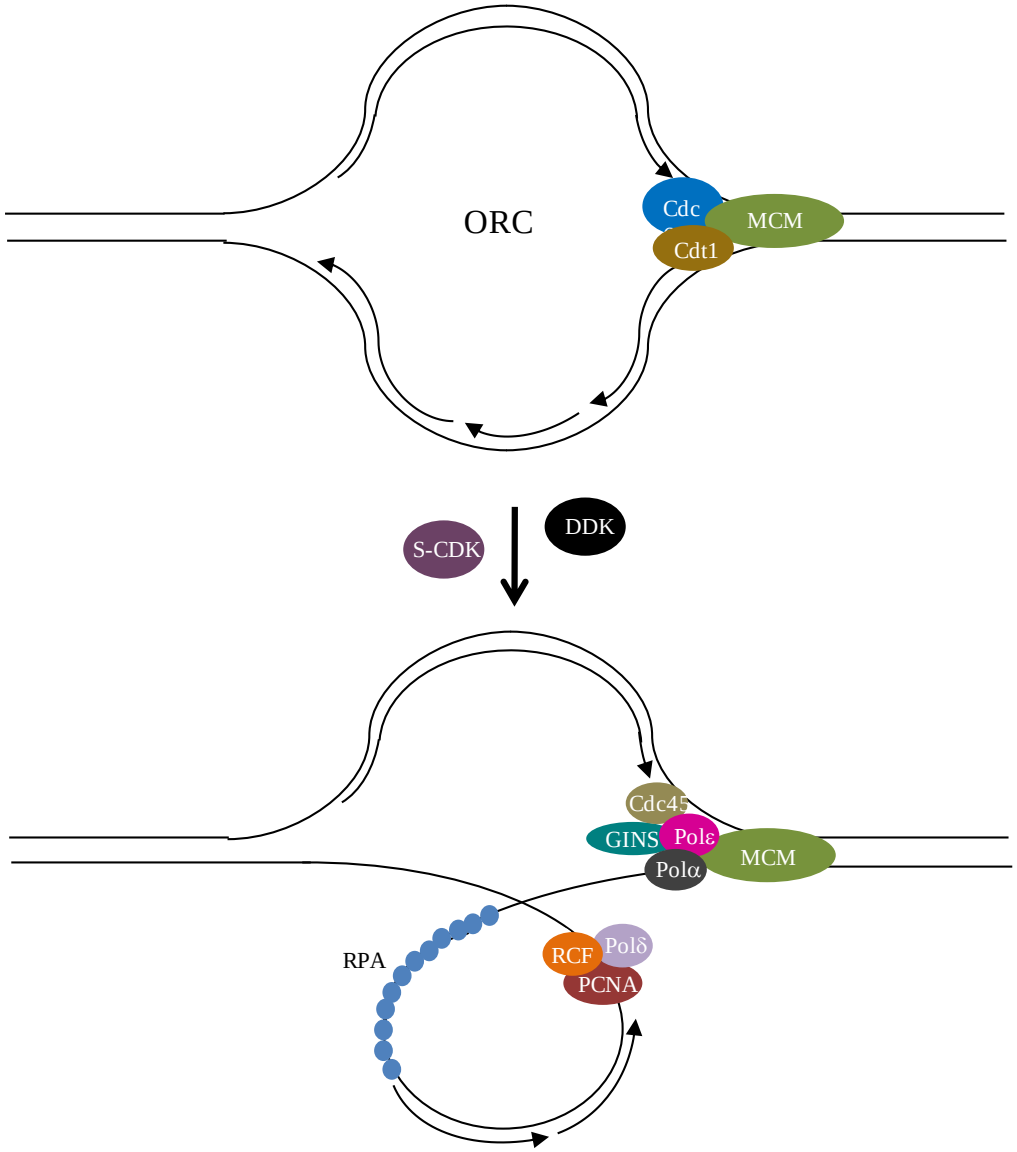

Figure 2-3. Model of eukaryotic DNA synthesis. Modifications of the origin of replication complex (ORC) by S-CDK and DDK initiates DNA replication. MCM helicase unwinds the DNA allowing access to replisome proteins. Replication protein A (RPA) binds to and stabilizes the ssDNA during DNA synthesis. The replication clamp PCNA is loaded onto the complex by RCF forming a complex with polδ. The leading strand is indicated by the continuous arrow while the lagging strand is indicated by the discontinuous arrows.

replication in eukaryotes remain to be elucidated but it is thought that they are involved in promoting the assembly of the active helicase CMG complex, consisting of Cdc45, MCM and GINS (Moyer et al., 2006). DDK was shown to phosphorylate the N-terminus of MCM4 in *Saccharomyces cerevisiae* (Sheu and Stillman, 2006). A mutant of MCM4 with the N-terminus removed was able to progress through S-phase in the absence of DDK indicating that the phosphorylation of MCM4 by DDK relieves an inhibitory activity (Sheu and Stillman, 2010). During S-phase, fired origins consist of two replication forks moving away from the origin in opposing directions as the DNA is unwound by the MCM helicase allowing access to replisome proteins including DNA polymerase-α primase, replicative DNA polymerase-δ and polymerase-ε, which elongate the primers, and Cdc45 (Aparicio et al., 1997; Aparicio et al., 1999). As the DNA is unwound by MCM2-7 helicase and DNA is replicated by the components of the replisome, the replication protein A (RPA) binds and stabilizes the ssDNA as was observed by colocalization of the RPA subunits with newly synthesized DNA (Dimitrova and Gilbert, 2000).

The S-phase Checkpoint

The accurate completion of DNA replication is of utmost importance for maintaining genomic stability and preventing carcinogenesis. Although DNA damage can occur throughout all phases of the cell cycle, cells are most susceptible to genotoxic stress during S-phase and M-phase. The S-phase checkpoint is in place to inhibit progress through S-phase and the subsequent mitosis when the conditions for accurate DNA replication have not been met. This checkpoint would then allow time for DNA repair, recombination or apoptosis (Kastan and Bartek, 2004; Zhou and Bartek, 2004).

Function of the S-phase Checkpoint

The function of the S-phase checkpoint is to maintain functional replication forks in times of replication perturbations, to ensure successful chromosome replication. This was shown in yeast when kinase dead mutants of the yeast homolog to mammalian ATR (Ataxia telangiectasia mutated and Rad3 Related), mec1, had a significant increase in the rate of replication fork breakdown during HU treatment which led to replication fork collapse and generation of lethal double strand breaks. When the yeast effector kinase homologous to human checkpoint effector kinase, Chk1, was put under the control of a Gal promoter allowing induction by galactose, non-induced cells were unable to recover from HU treatment, resulting in a decrease in viability. This suggests that DNA damage is caused by stalled replication forks which are not stabilized through Chk1 signaling and this is catastrophic for the cell (Tercero et al., 2003). The RecQ helicase BLM and the homologous recombination protein Rad51 are proteins within the ATR-Chk1 signaling cascade that have both been implicated in the restart of stalled replication forks after the removal of HU (Davies et al., 2007; Petermann et al., 2010). The S-phase checkpoint regulates BLM and Rad51 so that stalled replication forks are not restarted in the presence of replicative stress, which could possibly lead to replication fork collapse (see below) and subsequent catastrophic DNA damage.

In order to explain the mechanisms in which the S-phase checkpoint stabilizes stalled replication forks, it is necessary to discuss the remodeling of the stalled replication fork structures prior to the restart of S-phase events, which remain largely speculative (summarized in Fig 2-4). One central model is that when a replication fork encounters a lesion in the template DNA, the leading and lagging strand unwind and pair with the newly replicated sister strand,

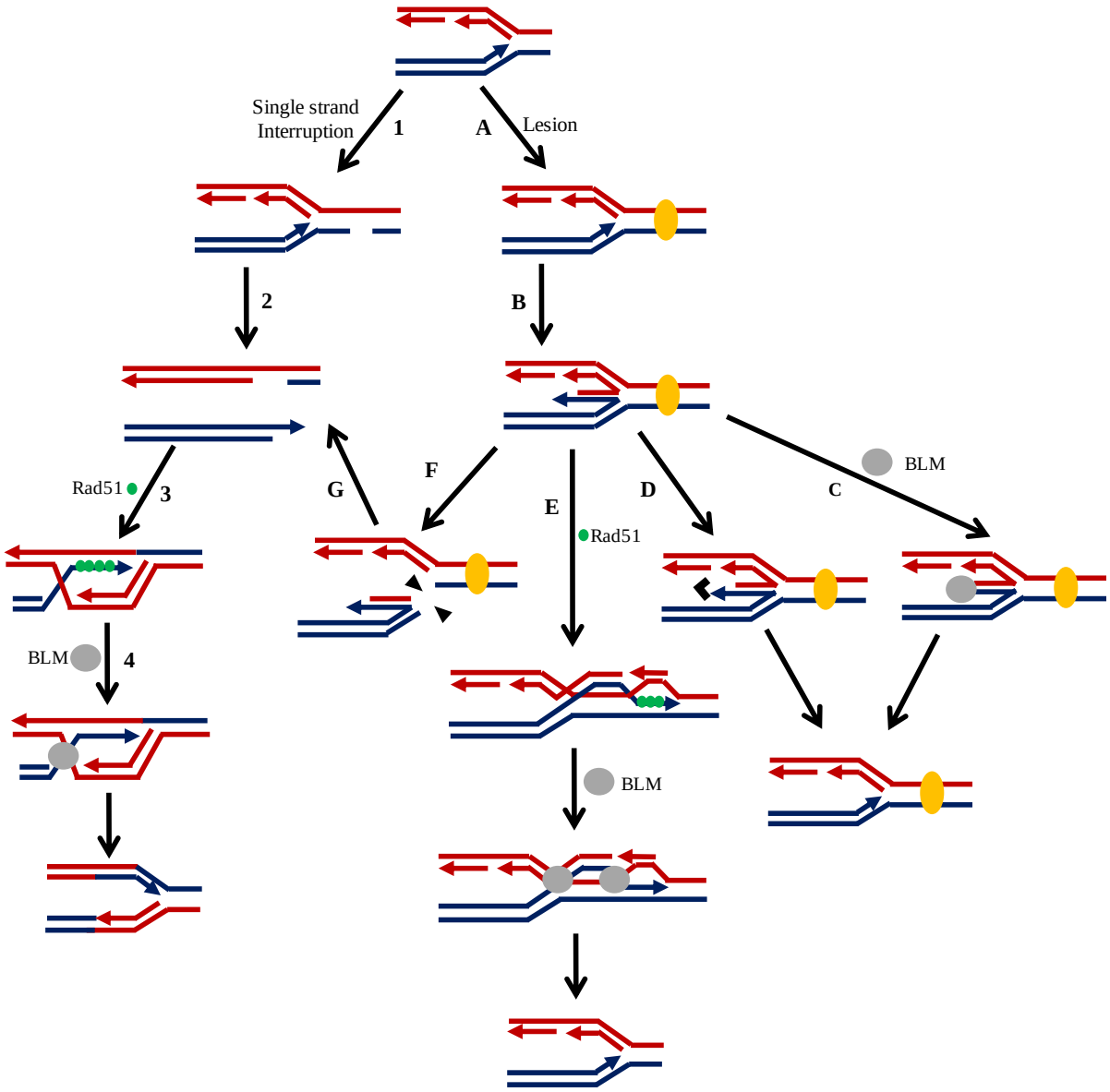

Figure 2-4. Pathways for restart of stalled replication forks. Consequences of a collision of a replication fork with a single strand interruption (1) or a lesion (A) are shown. After collision with a lesion, the stalled replication fork can become stabilized by pairing with the newly synthesized strand forming a Holliday Junction (A→B) Pathway F, E, D and C all show possible outcomes of the Holliday junction. Pathway E resolves the lesion through Rad51-mediated homologous recombination and BLM-mediated resolution of double Holliday junctions. The other pathways stabilize the stalled replication without repair of the lesion and F results in a double strand break due to collapse of the replication fork by DNA junction-processing enzymes (G). Collision with a single strand interruption also results in double strand break due to replication fork collapse. Rad51-mediated homologous recombination and resolution of the Holliday junction by BLM repairs the damage allowing replication restart. Leading strand is represented in blue and lagging strand is represented in red. DNA junction-processing enzymes are represented by black triangles and exonucleases are represented as a ◀.

creating a four-stranded DNA structure, termed fork regression. This resembles a Holliday junction commonly found during recombination (A→B). The fork regression can be reversed by branch migration (A→B→C), or can undergo exonuclease degradation (A→B→D) and the replication fork will be restored to its original conformation. The newly paired sister strand can also be used as a substrate for homologous recombination to repair the lesion (A→B→E). If a replication fork encounters a single strand interruption in the template DNA, the fork collapses, generating a double strand break (1→2). A similar structure results if the regressed fork is resolved by DNA junction-processing enzymes which ultimately breaks the fork into a double strand break ((A→B→F→G)). These structures can be repaired by strand invasion of the double-strand end into the corresponding sister chromatid followed by homologous recombination (2→3→4). (Reviewed in (Atkinson and McGlynn, 2009; Budzowska and Kanaar, 2009; Petermann and Helleday, 2010; Weinert et al., 2009)). The proteins involved in the current model of replication fork recovery are part of the S-phase checkpoint and will be discussed in detail below. The phosphorylation and recruitment of the majority of the proteins during the S-phase checkpoint efficiently recruit and modulate the functions of BLM and Rad51 at the stalled replication fork.

Activation of the S-phase Checkpoint

The initial groundbreaking research that defined the S-phase checkpoint was done in the yeast *Saccharomyces cerevisiae* in the presence of hydroxyurea (HU). Human homologs of the checkpoint proteins discovered in yeast have since been identified and the area of research has expanded into mammalian cells. HU is an important tool in studying the S-phase checkpoint in both mammalian and yeast systems. ATM (Ataxia telangiectasia mutated) and ATR are

members of the phosphatidylinositol kinase-related protein family and are essential for cell cycle checkpoint signaling in the presence of DNA damage or of stalled replication forks (Reviewed in Durocher and Jackson, 2001; Shiloh, 2001). The overexpression of kinase-inactive ATR in fibroblasts from Ataxia Telangiectasia (AT) patients sensitizes cells to UV, IR and HU treatment and abolishes the activation of the checkpoint, thus implicating ATR in the S-phase checkpoint (Cliby et al., 1998; Wright et al., 1998). ATR exists in a complex with ATR-interacting protein (ATRIP) and colocalizes to nuclei after UV and HU treatment. ATRIP and ATR are mutually dependent on each other in human cells, that is, if one is deleted or knocked-down, expression of the other diminishes and cell cycle checkpoint control is lost (Cortez et al., 2001).

Electron microscopy analyses of the DNA structures accumulating during HU treatment in *S. cerevisiae* demonstrated that cells exhibit normal replication forks when treated with HU but sustain very slow DNA synthesis at a rate of 50 base pairs per a minute. Interestingly, there is an increase of about 100 nucleotides of single stranded DNA (ssDNA) present at replication forks during HU, a substantially larger ssDNA fragment when compared to those in untreated cells, a fact that has led to the suggestion that the increase of ssDNA may activate the S-phase checkpoint (Sogo et al., 2002). Replication protein A (RPA) has been known to coat ssDNA within mammalian and yeast cells; when RPA was mutated in *S. cerevisiae,* the S-phase cell cycle checkpoint was defective allowing progression through S-phase into G_2 after UV treatment (Longhese et al., 1996; Wold, 1997). Recruitment of ATR and ATRIP to nuclear foci depends on the presence of RPA which stimulates ATRIP binding to ssDNA (Zou and Elledge, 2003). A substrate of ATR is Chk1, which is phosphorylated in response to UV and HU treatment (Liu et al., 2000). Interestingly, this phosphorylation was shown to be dependent on the presence of

RPA lending evidence to the concept that RPA-coated ssDNA is the molecular trigger initiating the S-phase checkpoint (Zou and Elledge, 2003).

S-phase Checkpoint Signaling

After nuclear localization of ATR and ATRIP and binding of this complex to RPA-coated ssDNA, ATR phosphorylates a series of proteins and recruits them to the stalled replication fork in mammalian cells (Fig 2-5). Activation of the checkpoint is thought to require the recruitment of the Rad9-Rad1-Hus1 (9-1-1) complex and the Rad17-replication factor C complex (RCF)-dependent loading of Rad9 onto the chromatin (Weiss et al., 2003; Zou et al., 2002). The 9-1-1 complex is a PCNA-related complex that is thought to sense DNA damage and the recruitment of the 9-1-1 complex to sites of DNA damage is independent of ATR, suggesting that it may enable ATR to recognize the damaged DNA (Volkmer and Karnitz, 1999; Zou et al., 2002). TopBP1 (Topoisomerase II beta binding protein 1) is recruited to stalled replication forks by Rad9 (Greer et al., 2003). ATR kinase activity is activated through the interaction of TopBP1 and ATRIP and the direct contact between TopBP1 and the PRD (PIKK phosphoinositide 3-kinase related kinase Regulatory Domain) of ATR (Mordes et al., 2008). ATRIP further stimulates the kinase activity of ATR resulting in autophosphorylation of ATR, phosphorylation of ATRIP and the RPA32 subunit (Cortez et al., 2001; Unsal-Kacmaz and Sancar, 2004). Rad9 and Rad17 are also phosphorylated by ATR (Furuya et al., 2004; Zou et al., 2002). The above-mentioned series of localization and phosphorylation events are the current standing model of ATR activation.

Like ATR, the main S-phase checkpoint effector kinase Chk1 is an essential gene and deletion of either results in an embryonic lethal phenotype in mice, indicating an irreplaceable

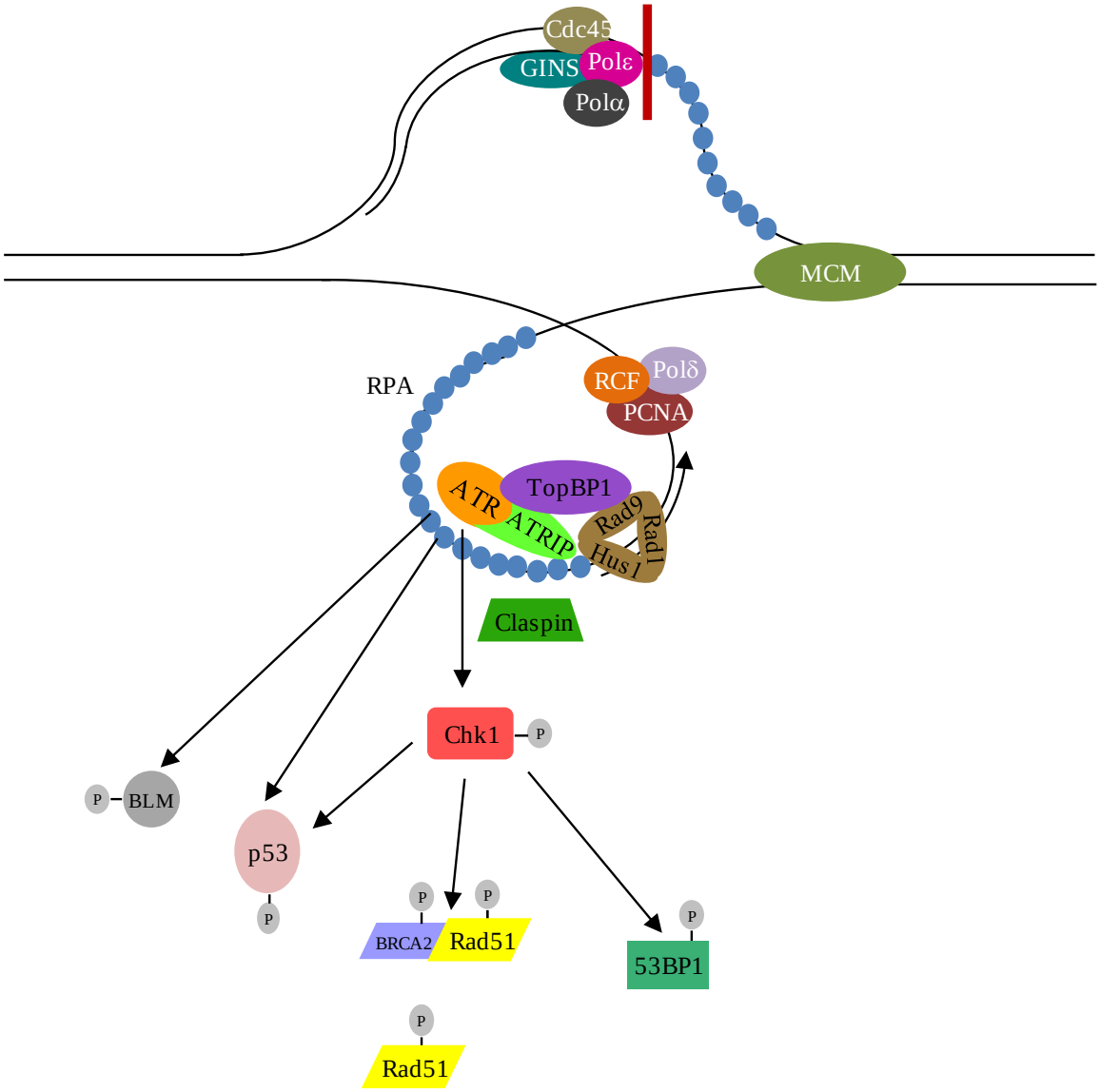

Figure 2-5. The signaling involved in the S-phase checkpoint. Long lengths of RPA-coated single-stranded DNA activates the checkpoint signaling. RPA-dependent binding of ATRIP to DNA and interaction with TopBP1 activates ATR kinase activity. ATR phosphorylates several key checkpoint proteins, including Chk1 which is dependent on the presence of Claspin. Phosphorylated and activated Chk1 is the central kinase in the S-phase checkpoint. Phosphorylation of signaling proteins by Chk1 leads to recruitment of these proteins to the stalled replication fork and subsequent replication fork stabilization.

role for both kinases in development (Brown and Baltimore, 2000; Takai et al., 2000). Activated ATR phosphorylates Chk1 at serines 317 and 345 in response to HU and subsequently activates Chk1 as detected by the phosphorylation of the known Chk1 substrate Cdc25C (Zhao and Piwnica-Worms, 2001). Phosphorylation of serine 345 is required for Chk1 activation and is dependent on phosphorylation of serine 317 (Lopez-Girona et al., 2001; Walker et al., 2009). Phosphorylation of Chk1 also requires other nuclear proteins, for instance through the interaction of Tipin and RPA, Timeless binds to Tipin recruiting the adaptor molecule Claspin which then facilitates the phosphorylation of Chk1 by ATR (Kemp et al., 2010). Claspin is required for ATR-dependent Chk1 phosphorylation (Chini and Chen, 2003; Kumagai and Dunphy, 2000). Activated Chk1 phosphorylates downstream proteins including p53 at serine 20, BRCA2, Rad51, Cdc25C, 53BP1 and FANCE (Bahassi et al., 2008; Sanchez et al., 1997; Shieh et al., 2000; Sorensen et al., 2005; Tripathi et al., 2008; Wang et al., 2007). The implications of these phosphorylations will be discussed in the next section.

Chk1 is not the only substrate of ATR in the S-phase checkpoint. ATR phosphorylates BLM at threonines 99 and 122 during HU-induced stalled replication forks (Davies et al., 2004). Mutant forms of BLM transfected into BLM -/- cells in which these residues have been changed to alanine fail to recover from the replication blockade following HU and arrest in G_2/M, demonstrating that the phosphorylation of BLM by ATR is required for proper recovery from S-phase arrest. BRCA1 is phosphorylated by ATR during HU or UV treatment and this phosphorylation is independent of ATM (Chen, 2000; Gatei et al., 2001). Serine 15 of p53 is phosphorylated by ATR after IR, UV or HU treatment. Kinase inactive mutants of ATR interfere with phosphorylation of p53 in late S-phase during IR treatment and completely suppress p53 phosphorylation after UV treatment, supporting the obligatory role of ATR in the

S-phase checkpoint (Tibbetts et al., 1999). During replication-mediated double strand DNA breaks induced by camptothecin, ATR phosphorylates H2AX (γH2AX) an event required to recruit DNA repair proteins Mre11, Rad50 and NSB1 (MRN) (Furuta et al., 2003). It is now known that although ATM and ATR have overlapping targets, ATM is the kinase involved in the G_1/S and G_2/M checkpoint signaling after IR treatment while ATR is activated after UV treatment and is involved in the S-phase checkpoint (Reviewed in (Cimprich and Cortez, 2008; Kastan and Bartek, 2004)).

BLM and p53

Plasmid based assays in *E. coli* show that when a replication fork encounters a lesion and stalls, the leading and lagging strand of DNA replication uncouple and DNA synthesis continues on the lagging strand, generating ssDNA gaps which may activate homologous recombination (Pages and Fuchs, 2003). In 1990, prior to the identification of BLM in mammalian cells, RecQ was characterized as a 3′ to 5′ DNA helicase in *E. coli*. It was shown to initiate homologous recombination and unwind a broad range of DNA substrates representative of structures generated during recombination or replication including 3′ and 5′ ssDNA overhangs, 4-way junctions and 3-way junctions, thus implicating RecQ in repair of stalled replication forks (Harmon and Kowalczykowski, 1998; Umezu et al., 1990). The mammalian homolog of RecQ is BLM, which is the gene product mutated in and causative of Bloom's syndrome. Cells from Bloom Syndrome patients exhibit chromosomal instability due to an elevated rate of sister-chromatid exchange suggesting that a protein involved in recombination is mutated in these cells (Chaganti et al., 1974). BLM selectively recognizes Holliday junctions, a four-way DNA junction, and promotes the branch migration of these junctions, thereby preventing homologous

recombination of the regressed fork from occurring (Karow et al., 2000). It has been hypothesized that, when replication forks stall, Holliday junctions may arise and resolution of these structures would result in a double-strand DNA break that is repaired by homologous recombination returning the replication fork to its original structure (Sharples et al., 1999). p53 has been shown to bind to BLM modulating the associated helicase activity (Yang et al., 2002). By inhibiting the resolution of the Holliday junctions at stalled replication forks, modulation of BLM by p53 prevents the collapse of the replication fork, further DNA damage, and the threat of tumorigenesis. Interestingly, BLM is required for efficient localization of p53 to stalled replication forks during HU (Sengupta et al., 2003). Once recruited, p53 is found to bind to and inhibit the pro-recombinogenic protein Rad51 as well as inhibiting BLM helicase activity. This inhibition is thought to stabilize stalled replication forks by inhibiting unnecessary recombination. It is also thought that the presence of p53 recruits other proteins to the stalled replication fork, so that the necessary homologous recombination can occur after the replication stress has been resolved to reinitiate the replication fork, allowing for an accurate S-phase to continue (Sengupta et al., 2003).

Rad51

The double strand breaks resulting from replication fork collapse and resolution of the fork regression are a lethal form of DNA damage that can be repaired error-free by homologous recombination using the undamaged sister chromatid as a template (Johnson and Jasin, 2000; van Gent et al., 2001). Homologous recombination is tightly regulated in the S-phase checkpoint to prevent further DNA damage during replicative stress. Expression of Rad51 is induced in late S-phase and G_2 and binds to single stranded DNA during the initial steps of homologous

recombination (Benson et al., 1994; Flygare et al., 1996). Rad51 possesses DNA-dependent ATPase activity which catalyzes the homologous pairing and strand exchange of the sister chromatid during homologous recombination leading to the formation of a Holliday junction as a DNA intermediate (Baumann et al., 1996). When Chk1 was inhibited with either UCN-01 or caffeine during HU treatment, an increase in double strand breaks and Rad51 nuclear DNA foci formation resulted, suggesting that Chk1 modulates Rad51 function (Sorensen et al., 2005). Chk1 phosphorylates Rad51 at threonine 309 during HU treatment. When this residue is mutated to alanine, cells are more sensitive to HU treatment, indicating that phosphorylation of Rad51 by Chk1 is required for survival after replication stress. Importantly, less than 1% of Chk1 was found to immunoprecipitate with Rad51 during HU treatment in cells containing a Chk1 mutant where serines 317 and 345 are mutated, preventing ATR phosphorylation and activation of Chk1. That is, if Chk1 phosphorylation is blocked it cannot form a complex with Rad51. Therefore the ATR dependent activation of Chk1 and subsequent nuclear localization and phosphorylation of Rad51 is important for survival after replication–stress induced DNA damage (Sorensen et al., 2005).

When p53 was transfected into normal human fibroblast cells along with wild-type Rad51, the homologous recombination frequency decreased compared to cells containing only Rad51, suggesting that the direct binding of p53 to Rad51 inhibits the homologous recombination activity of Rad51 (Linke et al., 2003; Sturzbecher et al., 1996). Rad51 and p53 both co-localize to stalled replication forks induced by HU and their interaction inhibits the Rad51-driven homologous recombination at the stalled replication fork, maintaining genome integrity by stabilizing the stalled replication fork (Sengupta et al., 2003; Yoon et al., 2004). During VP16-induced DNA damage, p53 binds to the Rad51 promoter, repressing transcription

of Rad51, indicating that p53 controls homologous recombination when the genome integrity is compromised at two levels; through protein-protein interactions and through transcriptional repression (Arias-Lopez et al., 2006).

BRCA2

In vitro kinase assays demonstrated that Chk1 phosphorylates BRCA2 at threonine 3387 (Bahassi et al., 2008). This phosphorylation was found to be required for the nuclear localization of Rad51 after DNA damage. Interestingly, when the Chk1 phosphorylation site of BRCA2 is mutated, there is a significant increase in Rad51 binding to BRCA2 after IR treatment comparable to the levels observed in untreated cells with wild-type BRCA2. After cells were cotransfected with BRCA2 and either a wild-type Rad51 or mutated Rad51 at the residue phosphorylated by Chk1, the mutant form associated with BRCA2 after UV treatment while the wild-type form did not. Together these studies suggest a model of Rad51 control by Chk1 where BRCA2 binds Rad51 under normal cellular conditions and upon the generation of DNA damage, Chk1 phosphorylates BRCA2 and Rad51 releasing Rad51 allowing for Rad51 to localize to sites of DNA damage within the nucleus (Bahassi et al., 2008).

53BP1

53BP1 was identified as a p53 binding partner in a two-hybrid yeast screen and was later found to rapidly localize to the nucleus after exposure to DNA DSB-inducing agents, implicating 53BP1 in the cellular response to DSBs (Iwabuchi et al., 1994; Schultz et al., 2000). Initially, 53BP1 was found to be required for the nuclear localization of BLM and p53 during HU treatment in an ATR-Chk1 dependent fashion (Sengupta et al., 2004). Co-immunoprecipitation

studies demonstrated that, during HU treatment, 53BP1 forms a complex with Rad51 and BLM (Tripathi et al., 2008). Phosphorylation of 53BP1 by Chk1 enhanced the interaction between 53BP1 and Rad51. In a study on defects in cells lacking BLM, it was shown that BLM enhances the localization and interaction of 53BP1 and Rad51 during HU-induced replication stress. The heterotrimeric complex ultimately inhibits Rad51 as was shown by a decrease in homologous recombination as measured by fluorimetric assay where a homologous recombination substrate is transfected and homologous recombination results in an emission of green fluorescence. This assay also included a mutated BLM where the residue that ATR phosphorylates is mutated to an alanine and the homologous recombination frequency increases, indicating that this phosphorylation is required for the anti-recombinogenic activity of BLM (Tripathi et al., 2008).

Reversal of the S-phase Checkpoint

After DNA damage has been repaired or the replication stressor is resolved, the S-phase checkpoint must be turned off to allow cells to continue replication for an accurate completion of S-phase. The serine/threonine phosphatase Wip1, also called PPM1D, is the protein responsible for dephosphorylating Chk1, attenuating the S-phase checkpoint (Lu et al., 2005). Wip1 was first identified in a screen for genes induced by IR treatment in WBM Burkitt lymphoma cells. While comparing mRNA Wip1 transcript levels between the WBM cells containing a wild-type p53 to several cell lines with varying p53 status from null to mutated, a clear correlation was observed between p53 status and induction of Wip1 mRNA. Thus, the newly discovered gene was name Wip1, wild-type p53-induced phosphatase (Fiscella et al., 1997). More than ten years later p53 was found to bind to the Wip1 promoter, transactivating the transcription of Wip1 after UV

IR treatment. Transcription of Wip1 is p53 dependent; in cells without p53 there are very low levels of Wip1 mRNA (Rossi et al., 2008).

Wip1 is a member of the PP2C phosphatase family. The Wip1 sequence shows region-specific homology at the three conserved regions among the PP2C family of phosphatase and is dependent on Mg^{2+} and insensitive to the inhibitor okadaic acid, all characteristics of the PP2C family (Fiscella et al., 1997). Phosphatase assays demonstrated that Wip1 dephosphorylates Chk1 at serine 345 but not at serine 317 and that this dephosphorylation decreases Chk1 kinase activity by more than two fold (Lu et al., 2005). Similarly, Wip1 was found to dephosphorylate p53 at serine 15. Wip1 was knocked down with siRNA in U2OS cells: Wip1-tet on cells, or overexpressed following tetracycline induction and then treated with UV and the percentage of ^{3}H-thymidine incorporated in DNA was measured. In the absence of Wip1 there was 70% reduction of incorporation, while cells overexpressing Wip1 incorporated more ^{3}H-thymidine than the control cells, indicating Wip1 attenuates the S-phase checkpoint as observed by an increase in DNA synthesis in the presence of Wip1 (Lu et al., 2005).

Focus of this Chapter

The experiments presented in this chapter address the molecular and cellular response of human colon cancer HCT116 cells to nucleotide pool deficiencies induced by nucleotide synthesis inhibitors. Treatment with PALA and HU resulted in slowed S-phase progression and p53 accumulation, yet the cellular consequences of pyrimidine deficiencies versus dNTP deficiencies were very different. For example, ATR was not recruited to the chromatin during PALA treatment, resulting in a deficient S-phase checkpoint, and cells subsequently underwent p53-dependent apoptosis. During HU treatment the S-phase checkpoint was found to be intact

and as a result, cells were protected from the nucleotide deficiencies. The observations that the PTMs of p53 were asymmetrically opposed during the two treatments and that p53 was bound to pro-apoptotic promoters during PALA treatment, led us to hypothesize that p53 has a central role in determining the cytotoxic versus cytoprotective response to nucleotide pool deficiencies.

Materials & Methods

Drug Solutions

Solutions of HU (Sigma) and PALA (National Cancer Institute) were made by dissolving the drug in phosphate-buffered saline (PBS) containing 1.06 mM KH_2PO_4, 155.17 mM NaCl, 2.97 mM Na_2HPO_4-$7H_2O$, pH 7.4. VP16 (Sigma) was dissolved in DMSO then diluted in PBS prior to use. DDATHF (Eli Lilly) was dissolved in 0.2 M Tris-Cl, pH 8.9. HU was made fresh prior to every use and PALA and DDATHF stocks were made and stored at -80ºC until use.

Cell Culture

Human colon carcinoma HCT116 p53 +/+ and p53 -/- cells were generously provided by Dr. Bert Vogelstein (John Hopkins University). They were grown in RPMI 1640 (Invitrogen/Life Technologies) supplemented with 10% dialyzed fetal bovine serum (dFBS) in a humidified atmosphere of 5% CO_2 at 37ºC. G_o/G_1 synchrony was achieved by plating cells at a high density of 2.5×10^6 cells/T-25 flask, allowing them to reach confluency (approximately 72 hours) feeding once after 48 hours, and holding them at confluence for an additional 48 hours. Cells were released from postconfluent synchrony by replating at low density of 2×10^6 cells/10 cm dish.

Western Blotting

Cellular Lysate preparation

HCT116 cells were plated at 8 x 10^5 cells/10 cm dishes and allowed to adhere for 24 hours prior to drug treatment. Stock solutions of drug were made as previously described, filter sterilized through a 0.22 μM syringe filter, and added to the appropriate volume of RPMI 1640 containing 10% dFBS to achieve the working drug concentrations. After the time point was reached, cells were washed with cold PBS once and scraped into PBS containing 1x protease inhibitor complete mixture (Roche). Cells were pelleted by centrifugation at 4,000 x g for 5 minutes at 4ºC and lysed in 10x volumes of lysis buffer containing 62.5 mM Tris, pH 6.8, 5% glycerol, 2% SDS, 5% 2-mercaptoethanol, 0.2 mM Na_3VO_4, 10 mM NaF, and 1x protease inhibitor complete mixture (Roche Applied Science). The samples were passed through a 22 gauge needle ten times and debris was pelleted by centrifugation at 10,000 x g for 10 minutes at 4ºC. Protein concentrations were determined using the Bradford assay against a standard of bovine serum albumin (BSA) according to manufacturer's (Bio-Rad) instructions. Lysates were aliquoted and stored at -80ºC.

SDS PAGE and Immunoblotting

Laemmli sample buffer (Bio-rad) was added to 25 μg of total cellular protein and the solution was boiled for 5 minutes. Proteins were resolved by electrophoresis on 5%, 7.5%, 10% or 15% SDS-polyacrylamide gels, at 150 V in running buffer containing 25 mM Tris base, 250 mM glycine and 0.1% SDS. Immobilon-P polyvinylidene fluoride membrane (PVDF) was activated in 100% methanol for 2 minutes prior to use. The gel and PVDF membrane were equilibrated in cold transfer buffer containing 25 mM Tris base and 192 mM glycine for 15 minutes. Proteins were transferred to the PVDF membrane for one hour at 100 V using a wet

transfer. Following transfer the membrane was immersed into 100% ethanol for 15 seconds and dried for 15 minutes. Non-specific protein binding was blocked in either Starting Block Buffer (Pierce) or a Blotto solution containing 5% milk, 0.1% Tween 20, 0.01 M Tris, pH 7.4, 0.15 M NaCl for 1 hour at 25ºC with gentle rocking. Blots were washed three times for five minutes each with TBS-T containing 0.5 M Tris pH 7.5, 0.14 M NaCl, 2.7 mM KCl, 0.05% Tween 20 at 25ºC with vigorous rocking then incubated with primary antibody diluted in Starting Block Buffer or 5% milk and TBS-T for 16 hours at 4ºC with gentle rocking. Primary antibodies were polyclonal phospho-Chk1 (S317, S345) both at 1:1000 (Cell Signaling Technology, #2344, #2341), polyclonal Chk1 at 1:1000 (Cell Signaling, #2345), monoclonal p21 at 1:100 (Calbiochem Ab-1, OP64) monoclonal beta Actin at 1:5000 (Abcam, #8226), monoclonal p53 at 1:100 (Calbiochem Ab-6, OP43), polyclonal Wip1 at 1:1000 (Santa Cruz H-300, sc-20712), polyclonal BLM at 1:500 (Santa Cruz C-18, sc-7790), polyclonal ATR at 1:1000 (Santa Cruz H-300, sc-28901), polyclonal trimethyl-Histone H3 (Lys4) at 1:1000 (Upstate, 07-473), polyclonal phospho p53 (S15, S20, S37, S46, S392) all at 1:1000 (Cell Signaling, #9284, #9287, #9289, #2521, #9281) and polyclonal PARP (Cell Signaling, #9542), cleaved PARP (Asp214) (Cell Signaling, #9541), cleaved Caspase-9 (Asp330) (Cell Signaling, #9501), cleaved Caspase-7 (Asp198) (Cell Signaling, #9491) all at 1:1000, monoclonal phospho-H2AX (S139) at 1:1000 (Millipore JBW301, #16-193). Following three TBS-T washes as described above, the membranes were incubated for 1 hour at 25ºC with secondary antibodies conjugated to horseradish peroxidase (Pierce) diluted in Starting Block Buffer or 5% milk and TBS-T and complexes were detected by enhanced chemiluminescence using the Supersignal West Pico Chemiluminescent Substrate Kit or SuperSignal West Dura Extended Duration Substrate Kit (Pierce). For the p53 post-translational modification blot, 25 μg of cell lysates were probed for

p53 and the densities of the corresponding p53 signals were measured with a FluorChem SP Imager (Alpha Innotech). The amount of protein required to be loaded for each treatment lane was calculated from the obtained densities and a second gel was set up so that equal amounts of p53 were present in every lane by loading different volumes of the different samples.

Chromatin Immunoprecipitation (ChIP)

Formaldehyde cross-linking and chromatin shearing

The ChIP assay was adapted from Bronder *et al* (Bronder and Moran, 2003). Approximately 1 x 10^7 cells per condition were crosslinked at room temperature with 1% formaldehyde for 10 minutes, the reaction was then quenched for 5 minutes by the addition of 0.125 mM glycine. Cells were washed twice with PBS, scraped, washed in buffer I containing 10 mM HEPES pH 7.5, 0.5 mM EGTA pH 7.5, 10 mM EDTA pH 8.0, 0.25% Triton X-100, then in buffer II containing 10 mM HEPES pH 7.5, 0.5 mM EGTA pH 7.5, 1 mM EDTA pH 8.0, 200 mM NaCl. All ChIP buffers contained 1 μg/mL aprotinin, 1 μg/mL leupeptin, 1 μg/mL pepstatin, 1 mM PMSF, 0.2 mM Na_3VO_4 and 10 mM NaF. Cells were lysed in lysis buffer containing 25 mM Tris pH 7.5, 5 mM EDTA pH 8.0, 150 mM NaCl, 1% Triton X-100, 0.1% SDS, 0.5% Na Deoxycholate. Aliquots of 2 x 10^6 cells in 600 μL lysis buffer were sonicated with a Diagenode bath bioruptor for a total of 20 minutes with consecutive duty cycles of 30 seconds on, 30 seconds off at 4ºC (5 minute cycles repeated a total of 4 times). These conditions were found to yield DNA fragments less than 1000 bp in size.

Immunoprecipitation

Lysates corresponding to 2 x 10^6 cells were precleared for 1 hour at 4ºC with a 50% slurry of protein G-Sepharose (Amersham Biosciences) beads previously blocked with 8 μg of BSA and either 5 μg of sonicated lambda DNA or 6 μg of sonicated salmon sperm DNA, then incubated with 2 μg p53 Ab-6 (Calbiochem) antibody or 2 μg IgG (Millipore) antibody overnight. Antibody-protein-DNA complexes were captured by the addition of 30 μL of 50% blocked protein G-Sepharose bead slurry for 1 hour at 4ºC. Beads were pelleted at 4,500 x g for 5 minutes at 4ºC and the supernatant from the IgG immunoprecipitation was saved and the DNA contained within was referred to as input DNA. Beads were washed extensively twice with RIPA buffer (150 mM NaCl, 50 mM Tris pH 8.0, 0.1% SDS, 0.5% Na Deoxycholate, 1% NP-40), once with High Salt Buffer (500 mM NaCl, 50 mM Tris pH 8.0, 0.1% SDS, 1% Na Deoxycholate), once with LiCl Buffer (250 mM LiCl, 50 mM Tris pH 8.0, 0.5% Na Deoxycholate, 1% NP-40), and twice with TE (10 mM Tris pH 8.0, 1 mM EDTA pH 8.0) for 10 minutes each at 4ºC rotating end-over-end. Protein-DNA complexes were eluted with elution buffer (2% SDS, 10 mM DTT, 0.1 M $NaHCO_3$) while rotating end over end at 25ºC for 15 minutes and the cross-links were reversed by the addition of 0.2 M NaCl and incubation at 65ºC overnight. DNA was treated with 10 μg of RNase for 30 minutes at 37ºC and with 20 μg Proteinase K in 10 mM Tris pH 7.5, 5 mM EDTA pH 8.0, 0.25% SDS for 1 hour at 42ºC, phenol-chloroform extracted, ethanol-precipitated and dissolved in 100 μL TE.

Quantitative PCR (Q-PCR)

Quantitative PCR was performed with 1 μL of input DNA or ChIP DNA for each 25 μL reaction containing 12.5 μL Quantitect SYBR Green PCR Master Mix (Qiagen) and 0.3 μM of each primer. The sequences of the primers flanking the p53 binding sites of the analyzed

promoters can be found in Table 2-1. The amplification conditions were 95ºC for 15 minutes, 40 cycles of 95ºC for 45 seconds, for the noted Tm of each primer set in Table 2.1 for 45 seconds, 72ºC for 45 seconds with a plate read, and concluding with a 5 minute extension at 72ºC and a melting curve from 45ºC to 100ºC. Absolute quantities were calculated using a standard curve ranging from 100 ng to 0.8 ng of input DNA.

One Parameter Flow Cytometry

Cells were synchronized as previously described. At indicated times cells were collected by trypsinization, centrifuged at 300 x g and washed twice in PBS. Cells were resuspended in propidium iodide fluorochrome stain containing 50 μg/mL propidium iodine, 0.1% Triton X-100, 7 K-units/mL ribonuclease B in 3.2 mM sodium citrate buffer at a density of 1 x 10^6 cells/mL. Cell solutions were wrapped in foil and stored at 4ºC in the dark until analysis, up to 48 hours. Prior to analysis, cells were filtered through a 35 μm nylon mesh to obtain a single cell suspension. Flow cytometry was performed on a Beckman Coulter Elite XL-MCL single-laser flow cytometer**.**

Growth Rescue with deoxyribonucleotides

Inosine and deoxyadenosine (AdR) (Sigma) were dissolved in PBS. Deoxyguanosine (GdR) (Sigma) was dissolved in PBS and 10% the total volume of 1N NaOH was added to aid in solubilization. HCT116 cells were plated in 12-well plates at 2.4 x 10^4 cells/well and allowed to adhere overnight. Triplicates were plated for every drug treatment. Filter-sterilized drugs were added to RPMI 1640 supplemented with 10% dFBS and HEPES/MOPS buffer containing 20 mM HEPES, 10 mM MOPS, pH 7.4 to obtain the working concentration and added to the plated cells for 72 hours. Cells were fed after 48 hours with fresh drug-containing medium. Cells were

Promoter	Sense Primer	Antisense Primer	Tm
p21 5′ RE	5′-CTTTCCACCTTTCACCATTCC-3′	5′-AAGGACAAAATAGCCACCAGC-3′	53ºC
Rad51	5′-CCTCGAACTCCTAGGCTCAGA-3′	5′-CCGCGTCGACGTAACGTAT-3′	54ºC
WIP1	5′-ACGCCTGATTTGTGTGGTGG-3′	5′-ACGCAGCCCGCCGAATCCG-3′	55ºC
PUMA	5′-TGGGGGTGTGGATCTGTG-3′	5′-AAGTCAGGACTTGCAGGCG-3′	55ºC
FAS	5′-GCGGACAGGAATTGAAGCGGAAG-3′	5′-GGACCTTTGGCTTGGCTTGTCA-3′	58ºC
PIG3	5′-CCTTTCTCTTCTCTTAGCAGCACC-3′	5′-GTGCGATTCTAGCTCTCACTTCAAGG-3′	55ºC
BAX	5′-GCTCATGCCTGTAATCCCAGCG-3′	5′-ACCTGGATCTAGCAATATAGCCCACG-3′	58ºC
AIP1	5′-ATCTCTGGATGGGTAGGAGG-3′	5′-GTTCATGTCAGGGAGGTGC-3′	53ºC

Table 2-1. Sequence of primers used in ChIP assays to quantitate the levels of p53 residence at various promoters. The sense and antisense primers are denoted next to the specific promoter. The melting temperature (Tm) of each primer set follows the primers.

trypsinized and counted with the Beckman Coulter Z1 Coulter Particle Counter. For the purine nucleotide rescue of HU treatment, the above solutions were used scaled up to 10 cm plates for lysate preparation.

Co-immunoprecipitation

HCT116 cells were grown in RPMI 1640 supplemented with 10% dFBS. Cells were plated at 3 x 10 cells/15 cm dish and allowed to adhere overnight. Twenty-four hours after drug treatment plates were washed once with PBS and then scraped in 2 mL modified RIPA buffer containing 50 mM Tris-HCl pH 7.4, 1% NP40, 0.25% Na deoxycholate, 1 mM EDTA pH 8.0. All buffers contained 1 μg/mL aprotinin, 1 μg/mL leupeptin, 1 μg/mL pepstatin, 1 mM PMSF, 0.2 mM Na_3VO_4 and 10 mM NaF. Cells were lysed through gentle rocking for 15 minutes at 4ºC. Cell debris was pelleted at 14,000 x g for 15 minutes at 4ºC. Protein concentration of the supernatant was determined with the Bradford assay as previously described. BLM was immunoprecipitated from 0.75 mg of total protein with 1 μg polyclonal BLM antibody (Santa Cruz C-18, sc-7790) adding 4 M NaCl to obtain a final concentration of 100 mM NaCl. The volume of the above solution was raised to 750 μL with CO-IP buffer containing 50 mM Tris-HCl pH 7.5, 15 mM EGTA pH 7.5, 100 mM NaCl, 0.1% Triton X-100 and was incubated on ice for 90 minutes with occasional inverting. Nonspecific aggregates were pelleted by centrifugation at 14,000 x g for 10 minutes at 4ºC. The supernatant was incubated for 60 minutes while rotating end over end with 50 μL 50% protein G bead slurry that was previously washed three times with Co-IP buffer. Beads were pelleted by centrifugation at 4,500 x g at 4ºC for 1 minute and washed three times with 500 μL CO-IP buffer, with three tube inversions between washes. The beads were resuspended in 25 μL sample buffer containing 62.5 mM Tris-

Cl pH 6.8, 5% glycerol, 2% SDS, 5% 2-mercaptoethanol and boiled for 5 minutes. Beads were pelleted by centrifugation at 4,500 x g at 4ºC for 1 minute and the supernatant was stored at -20ºC until further analysis by western blot, as described above. Prior to loading on to a polyacrylamide gel, samples were boiled for 5 minutes and 1 μL 0.4% bromophenol blue was added to each sample.

Reverse Transcriptase Quantitative PCR

Total RNA was isolated using the TRIzol reagent according to manufactures instructions (Invitrogen). RNA (1 μg) was treated with 10 units of DNase I (Invitrogen) for 15 minutes at 25ºC in a 100 μL volume reaction containing 10 mM Tris HCl (pH 8.4), 2 mM $MgCl_2$ and 5 mM KCl. DNase I was inactivated for 10 minutes at 65ºC with 2.5 mM EDTA (pH 8). RNA was precipitated with the addition of $1/10^{th}$ the total volume of 3 M NaOAc and 2.5 times the total volume of 100% ethanol overnight at -80ºC. The integrity of the RNA was verified on a 1% agarose gel containing ethidium bromide. cDNA was synthesized from 2 μg RNA using random hexamers in the Superscript III First-Strand Synthesis System according to the manufacturer's instructions (Invitrogen). Quantitative PCR was performed with 1 μL cDNA in a 25 μL reaction containing 12.5 μL Quantitect SYBR Green PCR Master Mix (Qiagen), 0.3 μM of each primer in a three-step amplification plus melt-curve as described previously. Primers to measure the Wip1 transcript were 5′-TGCCGCCGCCGTTCCTCCGTG-3′ (sense) and 5′-GCCCCGAATGATGACCACACT-3′ (antisense); primers to measure β-actin as the normalizing control were 5′-CACGAAACTACCTTCAACTCC-3′ (sense) and 5′-TCATACTCCTGCTTGCTGATCC -3′ (antisense).

RNA Interference

HCT116 cells were plated at 1.5 x 10^5 cells/well in a 6-well plate, in 2 mL of RMPI 1640 with 10% dFBS and 1% pen/strep, and were allowed to adhere overnight. siRNA (Wip1 siGENOME SMARTpools or non-targeting siRNA pool #1, Dharmacon) was resuspended to a concentration of 20 μM in 1x siRNA buffer containing 60 mM KCl, 0.2 mM $MgCl_2$ and 6 mM HEPES pH 7.5. siRNA was diluted to 2 μM in the above mentioned 1x siRNA buffer and an equal volume of serum free RPMI 1640 was added. Dharmafect reagent #2 was diluted down to 0.2% in serum-free RPMI 1640. Both sets of solutions were incubated at 25ºC for 5 minutes and then mixed together and incubated for another 20 minutes at 25ºC. RPMI 1640 with 10% dFBS was added to the transfection solutions to a final siRNA concentration of 100 nM. Each well received 2 mL of the transfection-medium and after 24 hours the transfection medium was removed and replaced with RPMI 1640 containing 10% dFBS and 100 U/mL of penicillin and 100 mg/mL of streptomycin replaced the transfection medium. The 24 hour drug treatment began 48 hours after transfection.

Chromatin Fractionation

Cells were synchronized at G_o/G_1 as previously described and chromatin fractionation was performed as previously described (Mendez and Stillman, 2000). Synchronized HCT116 cells were released at 2 x 10^6 cells/10 cm dish containing 10 mL. 24 hours after drug treatment, cells were washed with PBS once and scraped into PBS containing 1x complete protease inhibitor mixture (Roche). Cells were pelleted at 1000 x g for 5 minutes at 4ºC. The pellet was resuspended in Buffer A containing 10 mM HEPES pH 7.9, 10 mM KCl, 1.5 mM $MgCl_2$, 0.34 M Sucrose, 10% glycerol, 1 mM DTT, and Triton X-100 was added to obtain a final

concentration of 0.1%. All buffers contained 0.5 μg/mL aprotinin, 0.5 μg/mL leupeptin, 0.5 μg/mL pepstatin, 0.1 mM PMSF, 2 mM Na_3VO_4 and 10 mM NaF. Cells were incubated on ice for 8 minutes and nuclei were pelleted by low speed centrifugation at 1300 x g for 5 minutes at 4ºC. The supernatant was saved as the cytosolic fraction. The nuclei were washed twice with Buffer A and lysed with 50 μL for ND treatment, 40 μL for HU and 30 μL for PALA (volumes which were previously determined to yield equal nuclear fractions from control and drug treated cells) of buffer B containing 3 mM EDTA pH 8.0, 0.2 mM EGTA pH 7.5, 1 mM DTT and incubated on ice for 30 minutes. The chromatin was pelleted at 1700 x g for 5 minutes at 4ºC and the insoluble nuclear fraction supernatant was saved. The pellet was washed twice with buffer B and resuspended in 40 μL for ND and 25 μL for HU and PALA samples of 1x sample buffer containing 62.5 mM 1 M Tris pH 6.8, 10% glycerol, 2% SDS and 10% 2-mercaptoethanol and sonicated at 4ºC with the Diagenode bioruptor for a total of 15 minutes with consecutive duty cycles of 30 seconds on, 30 seconds off (5 minute cycles repeated a total of 3 times). All fractions were aliquoted and stored at -80ºC.

Clonogenic Survival

For colony formation assays, HCT116 p53 +/+ and HCT116 p53 -/- cells were plated at 150 cells/10 cm dish and allowed to adhere for 5 hours. Cells were then incubated with RPMI medium containing 10% dFBS and a range of HU or PALA concentrations for 24 hour. Plates were replenished with fresh RPMI with 10% dFBS medium the following day and every 2-3 days for a total of 8 days. For the adapted version of the colony formation assay, HCT116 cells were synchronized as previously described and released into drug for 24 or 48 hours. Adherent and floating cells were collected and plated at 100 cells/60-mm^2 dish and allowed to attach

overnight. Plates were replenished with fresh RPMI with 10% dFBS medium the following day and every 2-3 days. After 8 days in both assays, colonies were fixed with methanol, stained with 5% Wright-Giemsa reagent and all visible colonies were counted manually.

Results

The experiments presented in Chapter 2 address the question of whether treatment of HCT116 cells with different nucleotide synthesis inhibitors result in similar cellular responses. Besides p53 stabilization and slowed S-phase progression, the cellular responses to HU and PALA treatment are strikingly different. The results presented herein suggest that PALA treatment fails to recruit ATR to the chromatin resulting in a p53-dependent apoptosis while HU-treatment activates a S-phase checkpoint that is cytoprotective.

Cell Cycle Effects of Nucleotide Synthesis Inhibitors

Both HU and PALA stabilize p53 and minimally activate p21 transcription

Given the significant role p53 plays in a multitude of cellular responses within the cell, the ability of nucleotide-deprived cells to promote the accumulation of p53 was investigated. HCT116 cells were treated with HU, PALA or the positive control DNA damaging agent VP16 for 24 hours and lysates were then western blotted to determine the effect on p53 accumulation. All three drug treatments led to the accumulation of p53. VP16 and PALA treatment resulted in the highest accumulation of p53, but p53 levels after HU were also quite high (Fig 2-6). The activation of p21 was investigated by immunoblotting to determine if the accumulated p53 was promoting transcription of this critical cell cycle inhibitor. As expected VP16 caused significant p21 activation; p21 activation by PALA treatment was very low but still clearly detectable, while

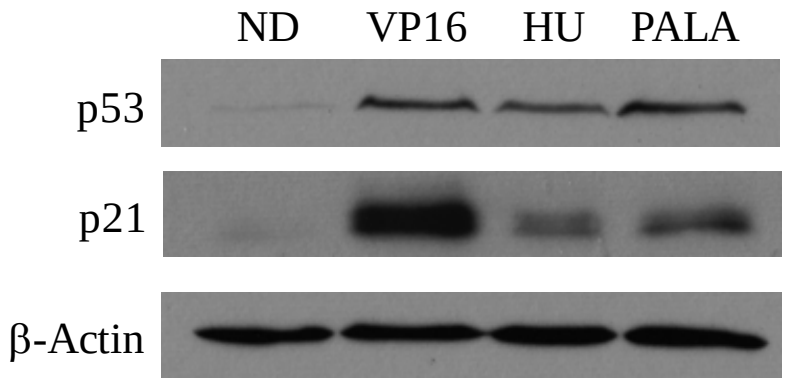

Figure 2-6. Nucleotide deficiencies promote p53 accumulation with minimal p21 activation. This figure shows a western blot analysis of p53 and p21 levels in asynchronous HCT116 cells exposed to 10 μM VP16, 1.5 mM HU or 100 μM PALA for 24 hours. Total cell lysate protein (25 μg) was subjected to SDS-PAGE and immunoblotted with antibodies against p53, p21 or β-Actin. VP16 was used as the positive control for p53 accumulation and p21 activation. Protein loading was assessed with β-Actin.

HU treatment resulted in minimal p21 activation, even though a significant amount of p53 stabilization was seen in all three drug treatments (Fig 2.6). The poor transcriptional activation of p21 after HU was expected from previous work in Prives' laboratory, but that observed after PALA treatment was surprising but reproducible. Previously in our lab, Julie Bronder observed a similar defect in p21 transcription during treatment of HCT116 cells with DDATHF, an antifolate *de novo* purine synthesis inhibitor. In her studies, p53 was bound to p53RE sites at the p21 promoter but, due to the lack of PTMs on p53 and the closed chromatin structure of the promoter, transcription was not activated (Bronder and Moran, 2003). To determine if the minimal activation of p21 transcription during HU treatment was due to failure of p53 to bind to the p21 promoter or events downstream of binding to the p53REs in the p21 promoter, a ChIP experiment was performed, with DDATHF included as a control for a nucleotide synthesis inhibitor exhibiting a similar p21 defect as HU. After DDATHF and HU treatment, approximately threefold more p53 was detected at the upstream p53RE of the p21 promoter than was seen in the no drug control. There was over a five-fold enrichment of p53 at the p21 promoter during PALA treatment and VP16 resulted in a four-fold enrichment of p53 bound at this promoter (Fig 2-7). The inability of the p53 that accumulated in HU-treated cells to transactivate p21 in spite of binding at the p21 (Mattia et al., 2007) promoter had previously been observed in Carol Prives' laboratory (Gottifredi et al., 2001), but the mechanism for this effect is still not clear.

The post translational modifications of stabilized p53 after nucleotide synthesis inhibition

The PTMs of the p53 that accumulated in HCT116 cells during the treatments with HU,

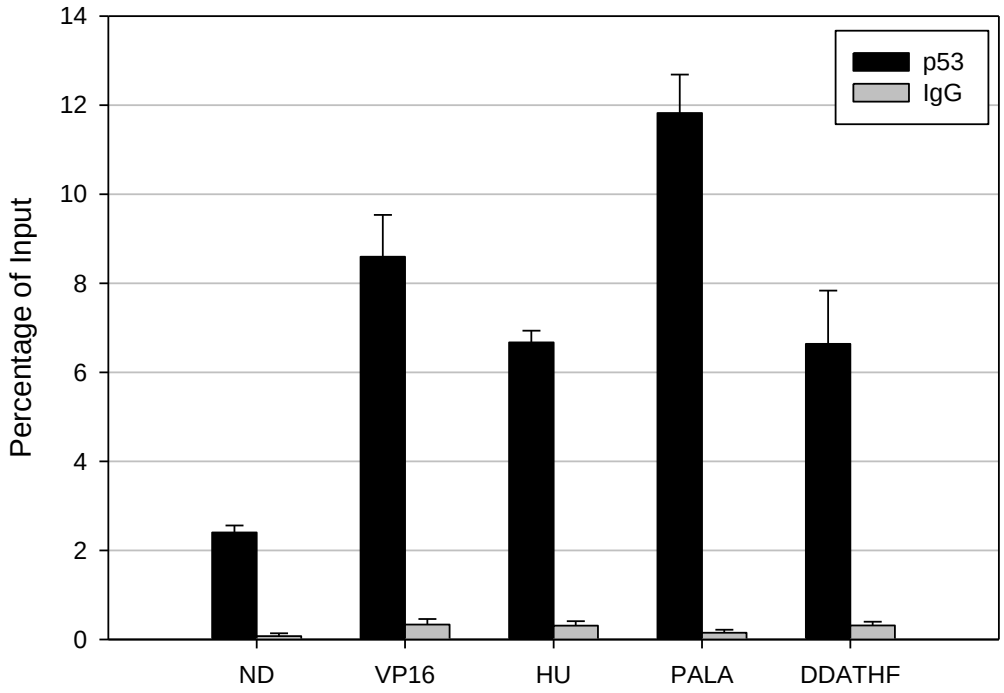

Figure 2-7. Nucleotide deficiencies induce p53 binding at the p21 promoter. ChIP analysis of p53 enrichment at the p21 promoter in asynchronous HCT116 cells after 24 hours of drug treatment. p53-DNA complexes were immunoprecipitated from crosslinked cells and p21 promoter levels were quantitated with Q-PCR. Non-specific binding was detected by parallel immunoprecipitations with IgG. VP16 served as a positive control. Standard error is depicted by the bars from one biological repeat with triplicate Q-PCR samples. The same trend was observed in subsequent biological repeats. Vehicle was PBS, VP16 was used at 10 μM, HU was used at 1.5 mM, PALA was used at 100 μM and DDATHF was used at 10 μM.

PALA, and VP16 were examined by loading an equivalent amount of p53 for all conditions on a gel and immunoblotting with phospho-specific peptide antibodies. VP16 caused robust phosphorylation at all the serine residues examined as was expected from previous literature for such a strong inducer of the DNA damage response. The phosphorylation profile of the p53 stabilized during HU treatment was very different to that of the p53 stabilized during PALA treatment. Interestingly, PALA treatment did not promote significant phosphorylation at serine 20 and induced only low levels of phosphorylation at serine 15, two of the most commonly phosphorylated serines on p53. HU promotes efficient phosphorylation of these residues. On the other hand serines 37, 46 and 392 were significantly phosphorylated during PALA treatment compared to that observed following HU treatment (Fig 2-8). The different pattern of post translational phosphorylations of p53 that resulted after PALA treatment and HU treatment suggested that the upstream regulators of p53 may differ as well was the cellular activities of the accumulated p53.

HU and PALA-treated cells undergo a prolonged cell cycle arrest in S-phase

The observation that p21 is not being robustly activated during HU and PALA treatment suggested that perhaps these two treatments are promoting cell cycle arrest in a different phase of the cell cycle other than the G_1/S or G_2/M checkpoint. G_1 synchronized HCT116 cells were released into drug-containing medium and cells were then stained with propidium iodide after 24 hours and analyzed by flow cytometry. Under these synchronization conditions, ~97% of the cell population was in G_1 immediately after release from synchrony with the remaining ~3% in G_2 (Fig 2-9). The VP16 control caused a G_2/M cell cycle arrest, which was expected from previous literature (Smith et al., 1994). Both HU and PALA treatment bypassed the G_1/S

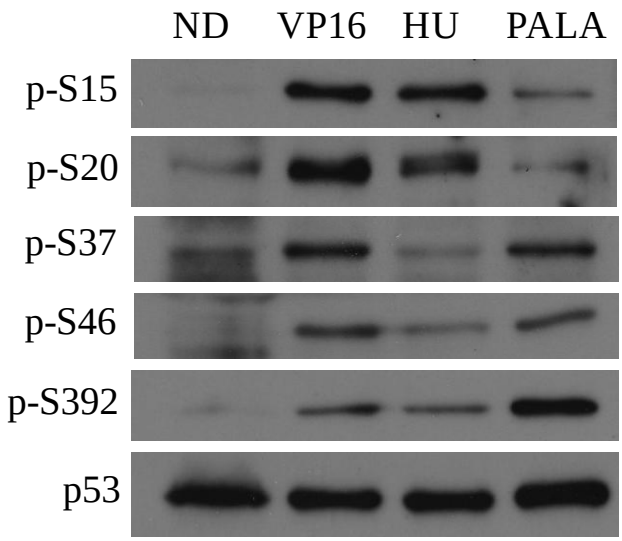

Figure 2-8. The post-translational modifications of the p53 that accumulate in HU- and PALA-treated cells are substantially different. This figure shows a western blot analysis of the post-translational modifications of p53 in asynchronous HCT116 cells after 24 hours of drug treatment. An initial western blot was performed with 25 μg of total protein to quantitate total p53 levels and then a second gel was run with differing volumes of lysates from the different conditions so that equivalent amounts of p53 were loaded and immunoblotted with antibodies specific for p53 phosphorylated at serine 15, 20, 37, 46, 392. Vehicle was PBS, HU was used at 1.5 mM, PALA was used at 100 μM and VP16 was used at 10 μM.

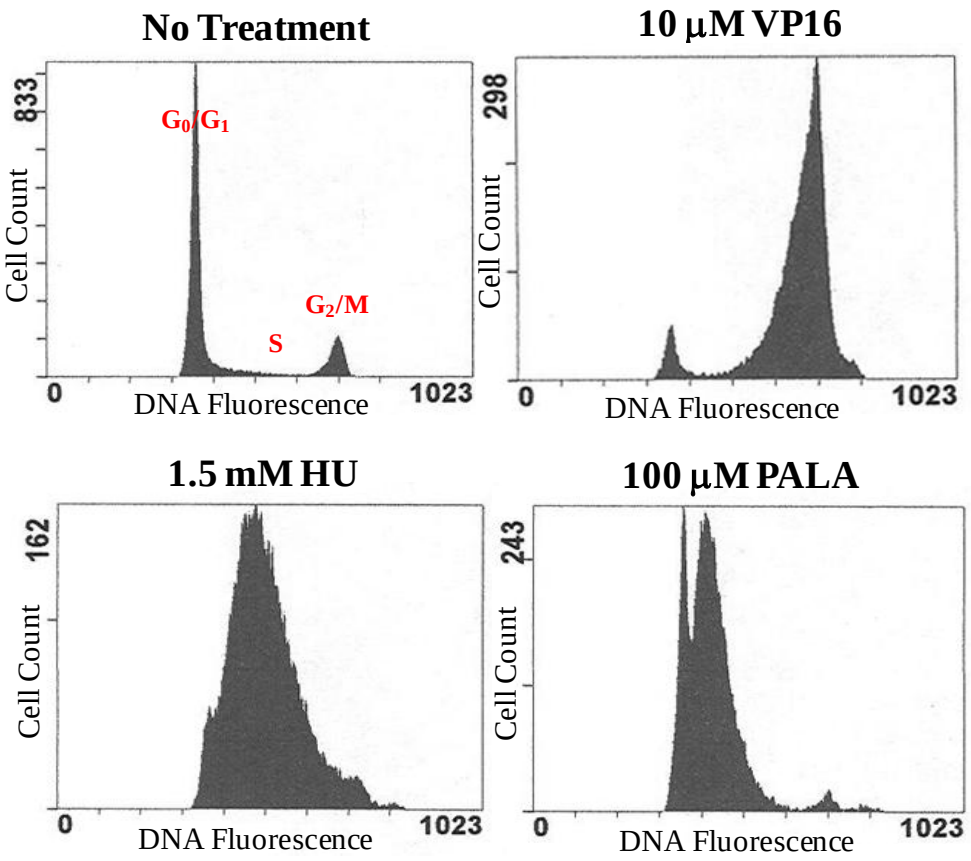

Figure 2-9. Synchronized HCT116 cells bypass the G_1 checkpoint and accumulate in S-phase upon nucleotide deficiencies. HCT11 cells were synchronized in G_0/G_1 by holding at confluence for 48 hours and released into drug containing medium at a low density for 24 hours. Cells were stained with PI and cell-cycle progression was monitored by flow cytometry.

checkpoint, an observation that was consistent with the low levels of p21 in these conditions, and accumulated in S-phase (Fig 2-9). This suggested that the low levels of p21 activated during PALA did not arrest the cells at the G_1/S border and that this checkpoint was not active. Compared to the vehicle, the HU and PALA treated cells moved through the cell cycle at a much slower rate and accumulated in early to mid S-phase.

S-phase Specific Events Resulting after Nucleotide Pool Imbalance

HU and PALA treatment promote a differentially phosphorylated Chk1

The phosphorylation of Chk1 is an event commonly used as definitive of the activation of the S-phase checkpoint (Lopez-Girona et al., 2001; Zhao and Piwnica-Worms, 2001). Since both HU and PALA treated cells arrested in S-phase, the phosphorylation status of Chk1 was investigated to determine if this checkpoint was being activated. VP16 and HU treatment resulted in a robust phosphorylation of Chk1 at serine 345, while PALA treatment did not (Fig 2-10). This was quite surprising. Minimal phosphorylation of Chk1 was observed following PALA treatment over that in the untreated control. A concentration-dependence study was performed to determine whether the Chk1 phosphorylation difference observed after HU and PALA was an artifact of the drug concentrations used. The concentration range for HU was 0.15 mM to 3 mM, 1.5 mM being the working concentration. Chk1 phosphorylation is detectable at 0.5 mM HU and was maximal at 3 mM (Fig 2-11). PALA concentrations from 10 μM to 500 μM did not cause appreciable Chk1 phosphorylation when compared with 1.5 mM HU or 10 μM VP16. Hence, substantial Chk1 phosphorylation following any reasonable dose of PALA was not occurring, while the phosphorylation occurring during HU treatment was robust (Fig 2-11).

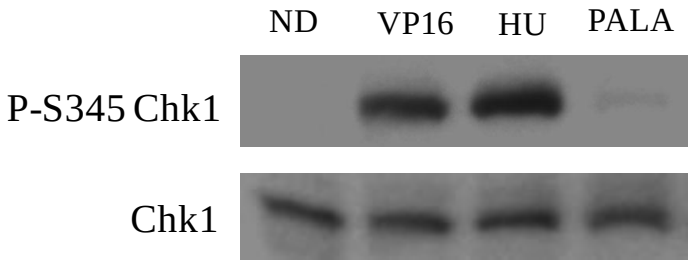

Figure 2-10. Chk1 is not phosphorylated at serine 345 upon PALA-induced pyrimidine deficiencies. This figure shows a western blot analysis of phosphorylated Chk1 at serine 345 and total Chk1 levels in asynchronous HCT116 cells exposed to 10 μM VP16, 1.5 mM HU or 100 μM PALA for 24 hours. Total cell lysate protein (25 μg) was subjected to SDS-PAGE and immunoblotted with antibodies against phospho-Chk1 serine 345 or total Chk1. HU was used as the positive control for stalled replication forks and VP16 served as a DNA-damage control.

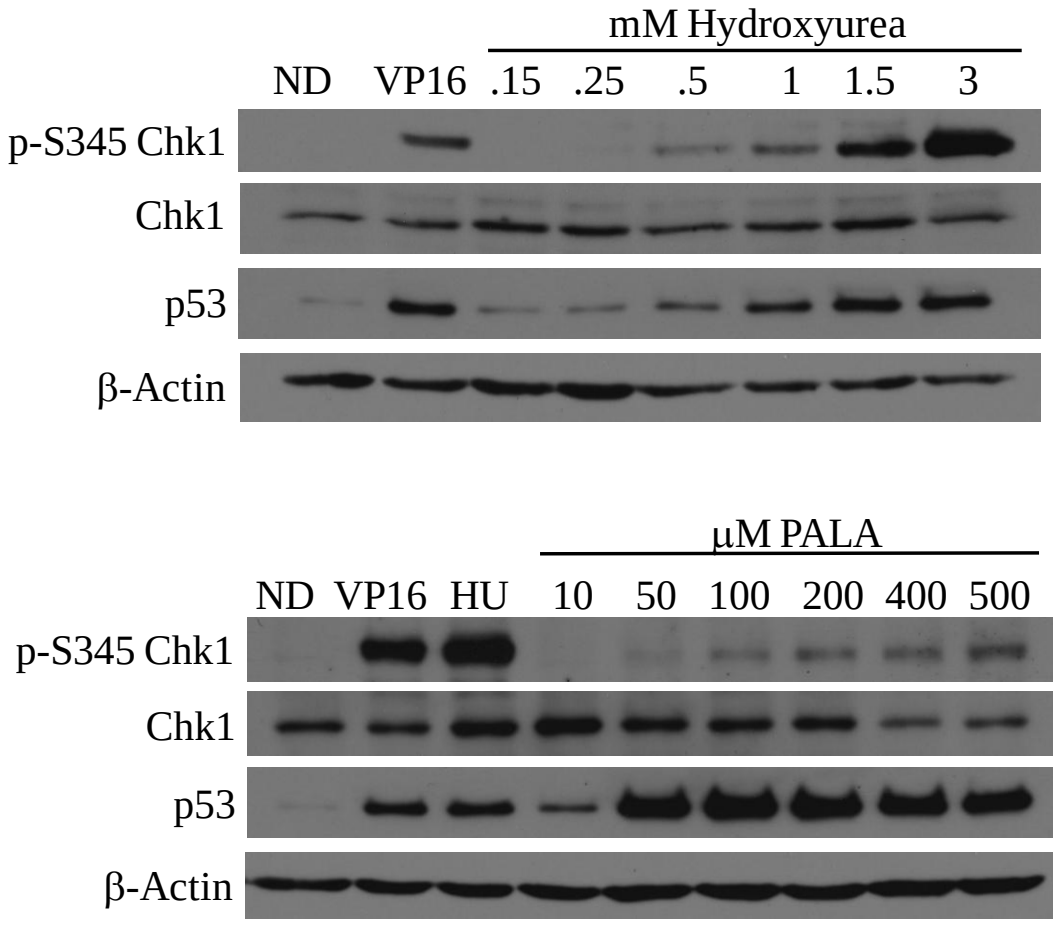

Figure 2-11. Concentration dependency of HU- or PALA-induced Chk1 phosphorylation and p53 accumulation. This figure shows a western blot analysis of levels of accumulated p53, total and phosphorylated Chk1 at serine 345 in asynchronous HCT116 cells treated with drug for 24 hours. Equal levels of total protein (25μg) were loaded in each lane. Vehicle was PBS, HU was used at 0.15 mM to 3 mM, PALA was used at 10 μM to 500 μM and VP16 was used at 10 μM. HU at 1.5 mM was used as a positive control for the concentration dependency of PALA treatment. Protein loading was assessed with β-Actin.

A time course was also performed to determine if the 24 hour time point used above possibly missed a transient Chk1 phosphorylation during PALA treatment. Cells were synchronized in G_1 and released into drug, then lysates were made at various time points to allow an enriched S-phase cellular population to be studied (Fig 2-12). Interestingly, a low level and transient phosphorylation of Chk1 was observed during PALA-induced pyrimidine imbalances. At 24 hours, Chk1 is heavily phosphorylated at serine 345 in HU and remained phosphorylated throughout the 48 hour time point (Fig 2-13). Throughout this period, the HU-treated cultures were found to be in a slowed S-phase by flow cytometry (Fig 2-12). The level of transient Chk1 phosphorylation observed during PALA treatment was much lower than that observed during HU treatment and, again, was observed only at time points corresponding to slow passage through S-phase (Figs 2-12, 2-13). Chk1 phosphorylation was detected as early as 12 hours after HU treatment while the low levels of Chk1 phosphorylation was first detected at 24 hours in PALA treated cells. Another interesting difference is the amount of accumulated p53 present during both of the drug treatments. During PALA treatment, p53 stabilization was detectable by 12 hours and was still substantial at 48 hours. During HU treatment, p53 stabilization was undetectable at 12 hours, a lower level of p53 had accumulated at 24 hours and this level decreased with time thereafter (Fig 2-13). The different levels of accumulated p53 that resulted from HU- and PALA-treatment suggested that p53 could be playing a role in the differential Chk1 phosphorylation. To address this question the p53 isogenic HCT116 cell lines were used to examine the possible p53 dependency of Chk1 phosphorylation. In HCT116 p53-/- cells, Chk1 phosphorylation at both serines 345 and 317 was partially restored during PALA treatment when compared to HCT116 p53 +/+ cells. The phosphorylation levels did not reach those observed during HU, but they were significantly higher than what was observed in the

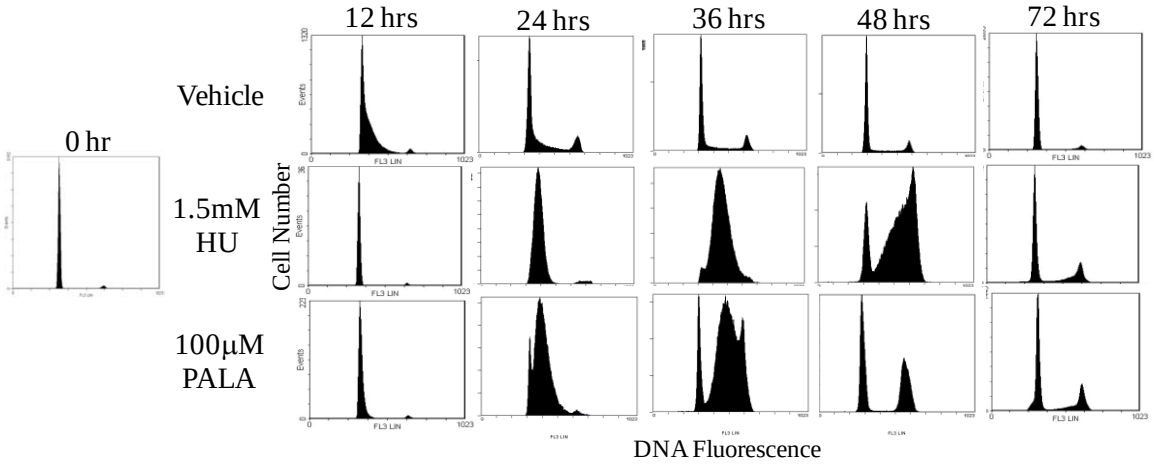

Figure 2-12. HU and PALA treatment slow S-phase progression. HCT116 cells were synchronized at G_0/G_1 and released into drug containing medium for the indicated times, stained with PI and their DNA content was analyzed by flow cytometry. Approximately 1 x 10^6 synchronized cells were collected and saved for the 0 hr time point prior to releasing the remainder into drug. Vehicle was PBS, HU was used at 1.5 mM, PALA was used at 100 μM.

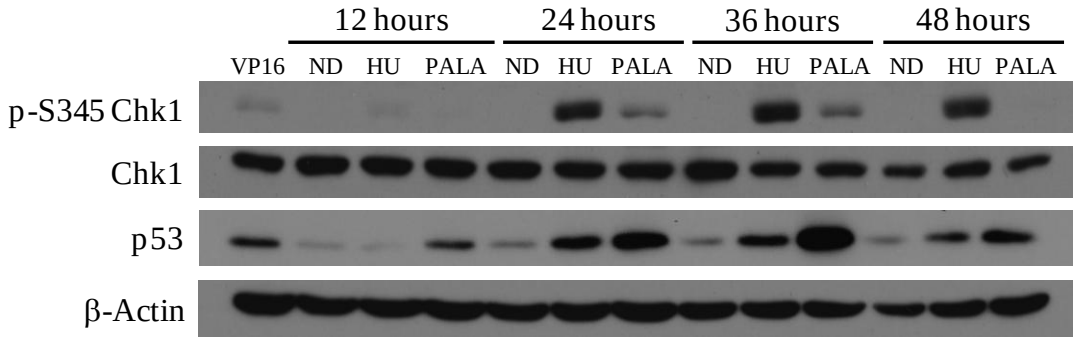

Figure 2-13. The time course of Chk1 phosphorylation and p53 accumulation after HU- or PALA-induced nucleotide deficiencies. This figure shows a western blot analysis of total and phosphorylated Chk1 at serine 345 in G_0/G_1 synchronized HCT116 cells released into drug for the indicated times. Equal levels of total protein (25 μg) were loaded in each lane. Vehicle was PBS, HU was used at 1.5 mM, PALA was used at 100 μM and the VP16 control was used at 10 μM for 24 hours. Protein loading was assessed with β-Actin.

presence of p53, suggesting that the presence of p53 is preventing the phosphorylation of Chk1 (Fig 2-14). HU inhibits the synthesis of both purine and pyrimidine deoxyribonucleotides and PALA solely inhibits the synthesis of pyrimidines. The Chk1 phosphorylation deficiency observed during PALA treatment may be a result of the fact that the pyrimidine pools are being affected with no effect on purines while HU is causing an overall deficiency in all of the deoxyribonucleotide pools. To indirectly determine if the Chk1 phosphorylation deficiency in PALA was due to the asymmetric effect on purine and pyrimidine nucleotide pools, HU treated cells were supplemented with 2-deoxyadenosine (AdR) and 2-deoxyguanosine (GdR), precursors of purine nucleotides. Prior to the supplementation, studies were performed with the purine inhibitor DDATHF, and the purine deoxynucleotides, to optimize the concentrations required to fully rescue the purine synthesis inhibition. The salvage metabolite inosine was used as a positive control for full rescue of DDATHF treatment. DDATHF treatment alone resulted in a 90% suppression of the growth of HCT116 cells compared to the no drug control. Supplementation of medium with 100 μM inosine or by addition of both 100 μM AdR and GdR rescued the cell growth caused by 10 μM DDATHF treatment (Fig 2-15A). Hence, these concentrations of extracellular AdR and GdR allowed support for growth by salvage and they were used to study the effect of HU suppression of deoxypyrimidine pools in the presence of exogenously supplied deoxypurines. The level of Chk1 phosphorylation did not decrease during HU treatment in the presence of purine deoxynucleotides, suggesting that the deficiency in Chk1 phosphorylation during PALA treatment is not due to deoxypurine/pyrimidine pool imbalances (Fig 2-15B).

HU and PALA treatment slows S-phase progression

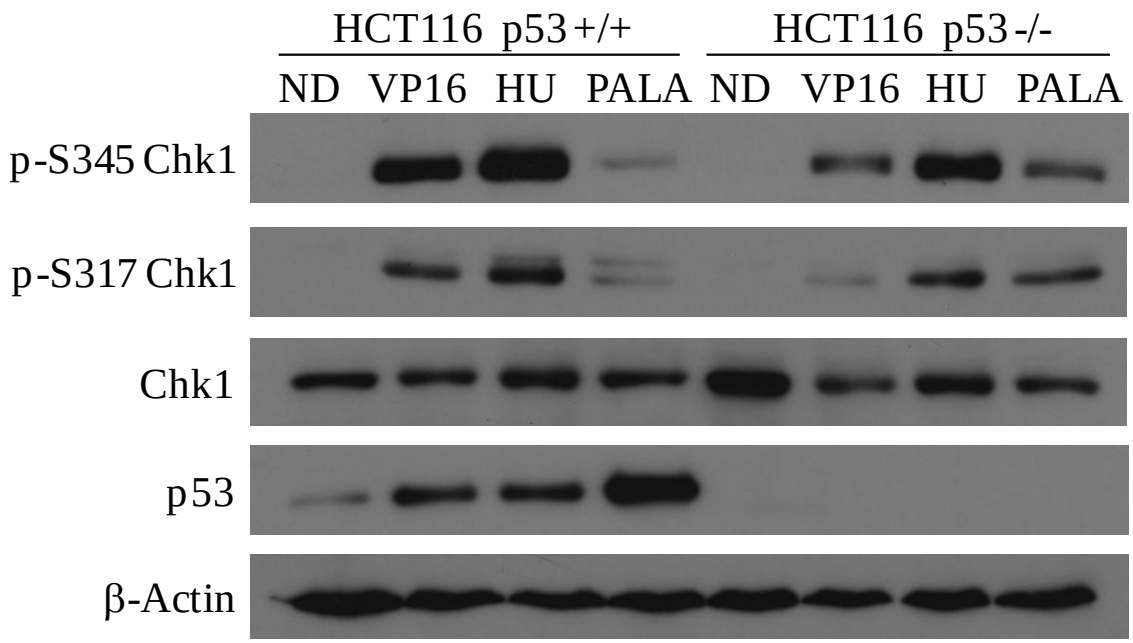

Figure 2-14. p53 dependency of Chk1 phosphorylation. This figure shows a western blot analysis of total and phosphorylated Chk1 at serines 317 and 345 and accumulated p53 in asynchronous HCT116 p53 +/+ and HCT116 p53 -/- cells exposed to drug for 24 hours. Equal levels of total protein (25 μg) were loaded in each lane. Vehicle was PBS, HU was used at 1.5 mM, PALA was used at 100 μM and the VP16 control was used at 10 μM. Protein loading was assessed with β-Actin

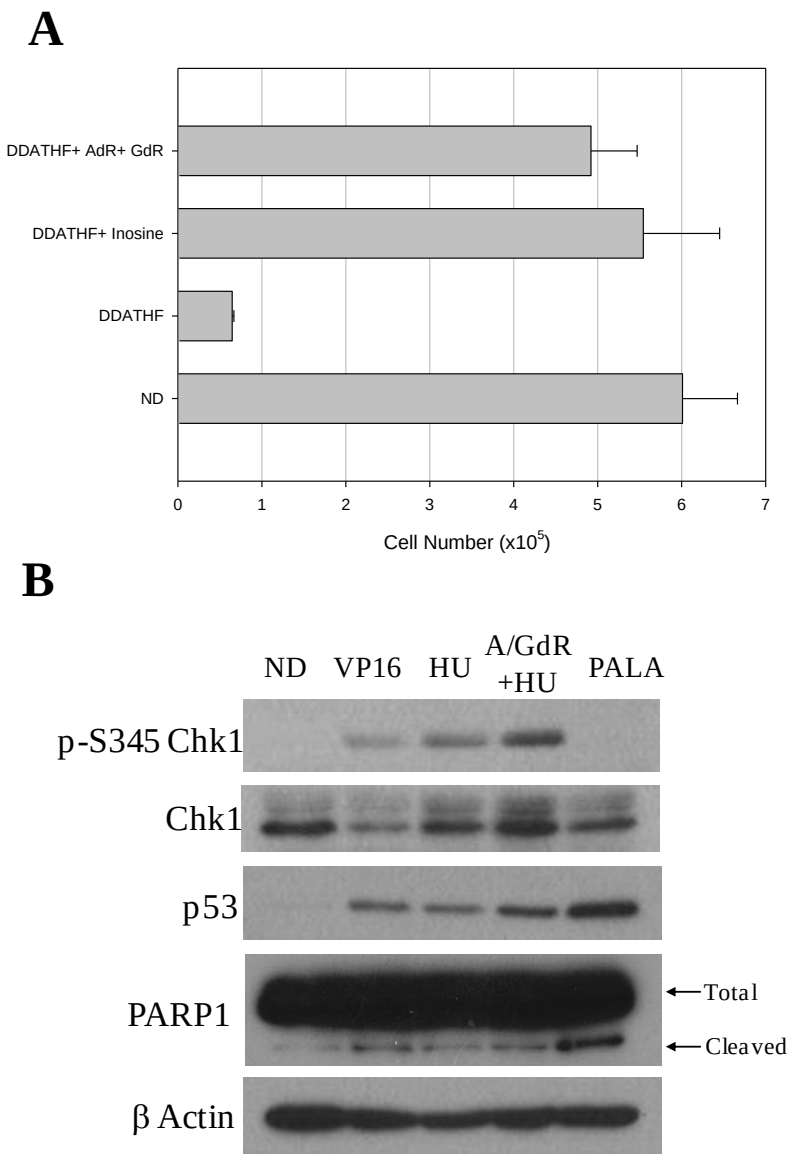

Figure 2-15. Differences in Chk1 phosphorylation is not due to the pool of nucleotides being inhibited. A, Growth rescue of DDATHF treatment with deoxyribonucleotides or inosine to determine concentrations for partial rescue of purine deoxyribonucleotides during HU treatment. HCT116 cells were treated with 10 μM DDATHF alone or supplemented with either 100 μM inosine or 100 μM AdR and 100 μM GdR for 72 hours. Cells were trypsinized and counted with the Beckman Coulter Z1 Coulter Particle Counter. Each bar indicates the mean of three plates within a single experiment, and standard deviation is shown. B, Western blot analysis of total, phosphorylated Chk1 at serine 345, accumulated p53, and cleaved PARP1 in asynchronous HCT116 cells exposed to drug for 24 hours. Purine deoxyribonucleotides were rescued during HU treatment by supplementation with 100 μM AdR and 100 μM GdR. Equal levels of total protein (25 μg) were loaded in each lane. Vehicle was PBS, HU was used at 1.5 mM, PALA was used at 100 μM and the VP16 control was used at 10 μM. Protein loading was assessed with β-actin.

The differences in the time course and degree of Chk1 phosphorylation in HU and PALA suggested that fundamentally different cellular processes were occurring during the two drug treatments (Fig 2-13). The flow cytometry performed on the treated cells after 24 hours was expanded to a full time course. G_1-synchronized cells were immediately released into drug and the adherent cells were collected after different time points and stained with propidium iodide. Neither HU nor PALA-treated cell populations were blocked at the G_1 checkpoint and the majority of both populations progressed into S-phase at a slower rate than the untreated cells. Both populations progressed into S-phase very slowly, but eventually completed transit through S-phase. Starting at 12 hours the cells began to enter S-phase and by 48 hours they were almost completely out of S-phase, whereas untreated HCT116 cells appeared to progress at a much faster rate, transiting through one or more S-phases within 24 hours. PALA-treated cells progressed through S-phase at a somewhat faster rate, approximately 12 hours ahead of HU treated cells. At the 48 hour time point, they are completely out of S-phase while HU cells are in the latter half of S-phase. There was a noticeable accumulation of cells in G_2/M in both drug treatments that was not observed in untreated cell populations. By 72 hours the cells are asynchronous and the flow cytometry cell cycle histograms appeared identical (Fig 2-12).

p53 Binds to BLM during Both HU and PALA treatment

Because Chk1 phosphorylation was not observed during PALA treatment, other S-phase specific events were investigated to define the scope of the difference in the cellular responses to HU and PALA. Previous studies have demonstrated the interaction of BLM and p53 during the S-phase checkpoint (Sengupta et al., 2003; Yang et al., 2002). BLM was immunoprecipitated from HCT116 cells that were treated with either HU or PALA for 24 hours. This

immunoprecipitate was analyzed by western blot to determine if p53 was interacting with BLM. Both HU and PALA treatment stimulated the binding of p53 to BLM (Fig 2-16). Equivalent amounts of BLM were immunoprecipitated from both drug treated lysates, but slightly more p53 was found associated with BLM during PALA treatment, consistent with the higher levels of p53 in PALA-treated cells (see input lanes, Fig 2-16). Minimal BLM was pulled down in the untreated lysates, but p53 was still found in this pellet, suggesting that BLM and p53 associate in unstressed cells as well as in cells depleted of nucleotides. Only a small fraction of total cellular p53 immunoprecipitated with BLM under the experimental conditions, suggesting that the stabilized p53 has other roles besides modulating BLM function, in the cellular response to HU and PALA treatment (Fig 2-16).

Enrichment of p53 at the Rad51 promoter is stimulated by PALA treatment

p53 has been shown to bind to the Rad51 promoter inhibiting the transcription of this pro-recombinogenic protein during the S-phase checkpoint (Arias-Lopez et al., 2006). The observation that only a small fraction of total cellular p53 was binding to BLM suggested that p53 was involved in other cellular processes, and therefore the residence of p53 at the p53RE in the Rad51 promoter after 24 hours of HU and PALA treatment was measured by ChIP. PALA treatment caused more than a threefold enrichment of p53 at this promoter over the no drug treatment. HU treatment did not elevate the levels of p53 at the Rad51 promoter (Fig 2-17). Thus, HU-stabilized p53 is not inhibiting the transcription of Rad51 while p53 that is accumulated during PALA treatment is bound at the promoter suggesting that it is negatively regulating the transcription of Rad51. It has been suggested that induction of apoptosis in cells

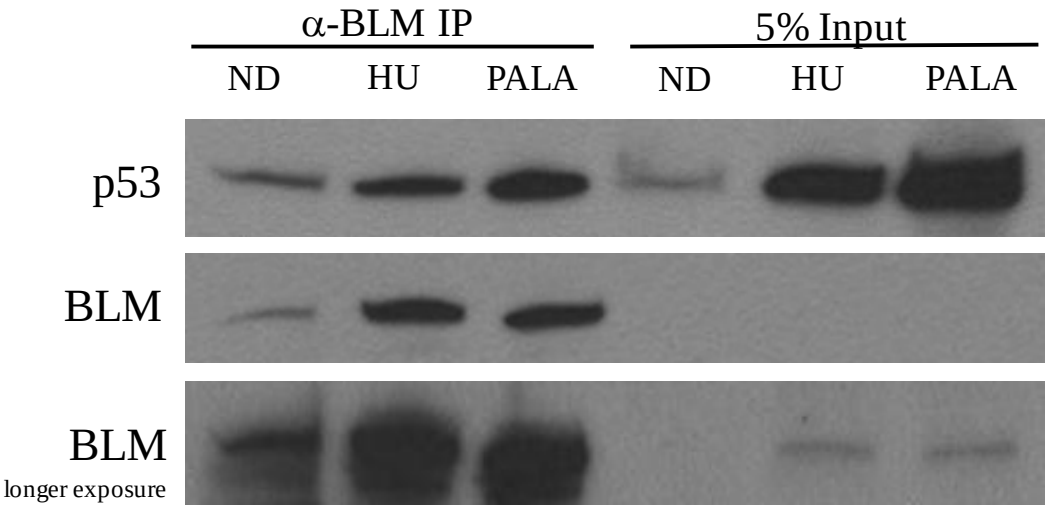

Figure 2-16. BLM and p53 interact during HU- or PALA-induced nucleotide deficiencies. This figure shows a western blot analysis of the interaction between p53 and BLM after 24 hours of HU- or PALA- induced nucleotide pool deficiencies in asynchronous HCT116 cells. BLM was immunoprecipitated from 750 μg protein from whole cell lysates with the p53 antibody (DO-1); p53 was detected in the BLM immunoprecipitate by western blotting. Input indicated 5% of the lysates used for the IP and the efficiency of the IP was verified with the BLM antibody. PBS was added to the no drug treatment, HU was used at 1.5 mM and PALA was used at 100 μM.

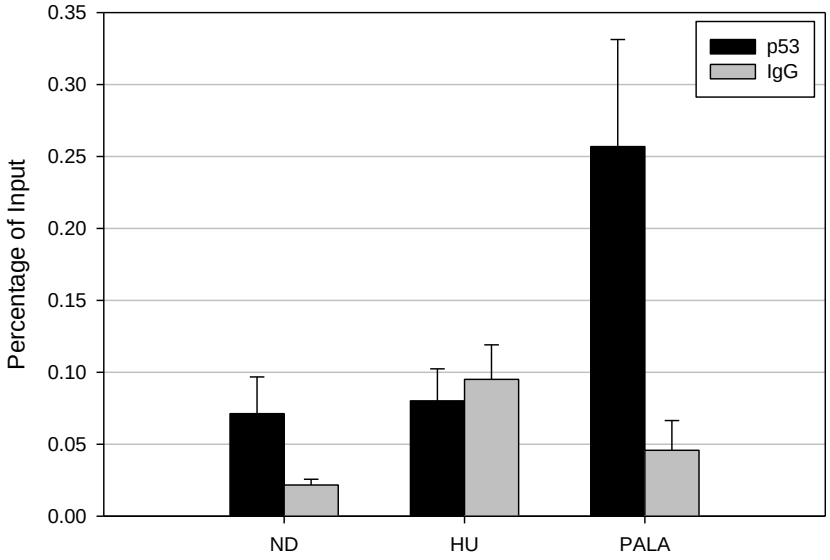

Figure 2-17. PALA treatment induces p53 binding at the Rad51 promoter. ChIP analysis of p53 enrichment at the Rad51 promoter in asynchronous HCT116 cells after 24 hours of drug treatment. p53-DNA complexes were immunoprecipitated from crosslinked cells and Rad51 promoter levels in the immunoprecipitate were quantitated with Q-PCR. Non-specific binding was immunoprecipitated with IgG. Standard error is depicted by the bars from two biological repeat with triplicate Q-PCR samples. Vehicle was PBS, HU was used at 1.5 mM and PALA was used at 100 μM.

containing abundant DNA damage may require the repression of homologous recombination (Ivanov et al., 2003). If this is true, it could explain that the enrichment of p53 at the Rad51 promoter is repressing transcription of the homologous recombination protein Rad51 in order to induce apoptosis.

Mechanism of the failure of PALA to induce Chk1 phosphorylation

PALA treatment activates the transcription of the Wip1 phosphatase

Although HU and PALA treatment slowed S-phase progression, the activities of the S-phase checkpoint were found to be conflicting. That is, HU-treatment resulted in Chk1 phosphorylation and p53 interaction with BLM, while Chk1 was not phosphorylated after PALA-treatment, yet p53 associated with BLM and regulated Rad51 transcription. In order to clarify the complexity of the cellular responses, we focused on the transient nature of Chk1 phosphorylation during PALA treatment. The increase in Chk1 phosphorylation in the absence of p53 in PALA-treated HCT116 p53-/- cells suggested that p53 was preventing Chk1 phosphorylation (Fig 2-14). In combination with the p53 dependency and the transient nature of Chk1 phosphorylation during PALA treatment, we hypothesized that the p53-dependent gene, Wip1, was dephosphorylating Chk1. The presence of p53 at the Wip1 promoter after 24 hours of drug treatment was investigated using ChIP. There was a massive (> eight fold) enrichment of p53 binding to the Wip1 promoter after PALA treatment that was not observed after HU treatment (Fig 2-18A). RT-QPCR demonstrated that the high occupancy of p53 at the Wip1 promoter after PALA treatment was strongly activating transcription as is seen by a 12-fold increase in Wip1 transcript levels. There was about a four-fold increase in Wip1 transcript after HU treatment. The Wip1 transcriptional activation was p53 dependent: in HCT116 cells that are

A

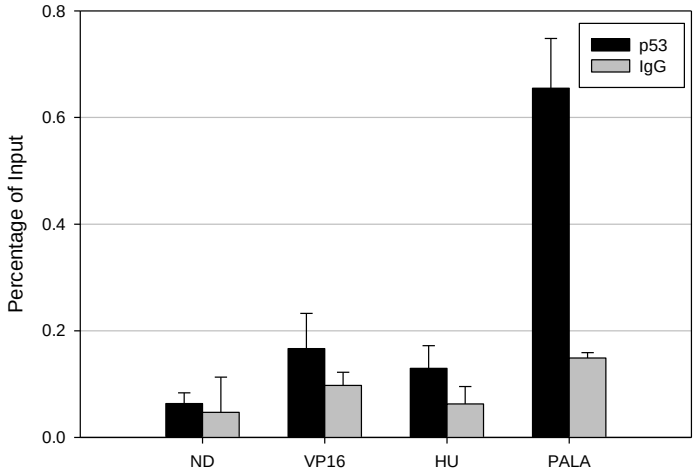
0.8
0.6
0.4
0.2
0.0
Percentage of Input
p53
IgG
ND
VP16
HU
PALA

B

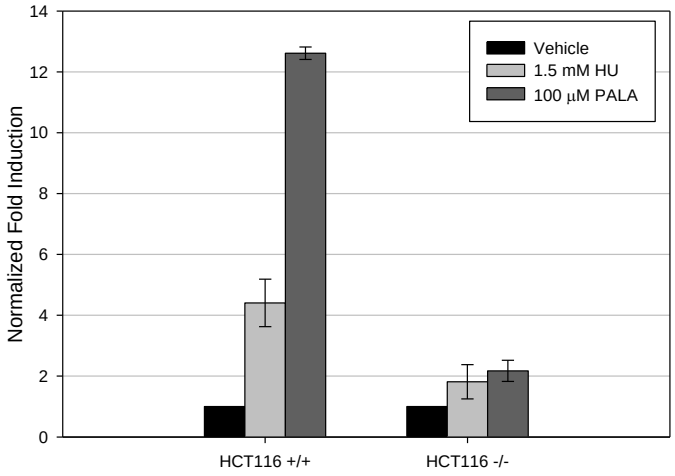
14
12
10
8
6
4
2
0
Normalized Fold Induction
Vehicle
1.5 mM HU
100 μM PALA
HCT116 +/+
HCT116 -/-

C

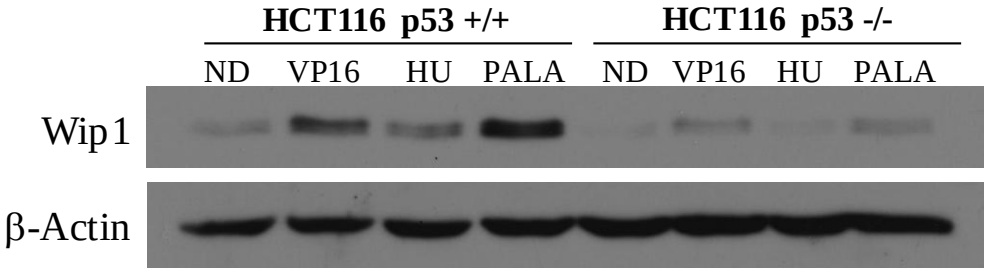
HCT116 p53 +/+
HCT116 p53 -/-
ND
VP16
HU
PALA
ND
VP16
HU
PALA
Wip1
β-Actin

Figure 2-18. PALA treatment activates Wip1 transcription. A, ChIP analysis of p53 enrichment at the Wip1 promoter in asynchronous HCT116 cells after 24 hours of drug treatment. p53-DNA complexes were immunoprecipitated from crosslinked cells and Wip1 promoter levels present in the immunoprecipitate were quantitated with Q-PCR. Non-specific binding was assessed by a parallel immunoprecipitate with IgG. Standard error is depicted by the bars from one biological repeats with triplicate Q-PCR samples. The same trend was observed in subsequent biological repeats. B, Wip1 transcript levels quantitated using RT-Q-PCR in asynchronous HCT116 p53 +/+ and HCT116 p53 -/- cells treated with drug for 24 hours. Transcript levels were normalized to β-actin. Standard error is depicted by the bars from two biological repeat with triplicate Q-PCR samples. C, Western blot analysis of the p53-dependent activation of Wip1 in asynchronous HCT116 p53 +/+ and HCT116 p53 -/- cells exposed to drug for 24 hours. Equal levels of total protein (25 μg) were loaded in each lane. Vehicle was PBS, HU was used at 1.5 mM, PALA was used at 100 μM and VP16 was used at 10 μM. Protein loading was assessed with β-Actin.

null for p53, the Wip1 transcript levels are down to basal (Fig 2-18B). Wip1 protein levels correlated with the transcript levels; there is a large induction of Wip1 protein after PALA treatment and only a small, if any, induction of Wip1 protein after HU treatment. There was no significant Wip1 protein in HCT116 p53 null cells (Fig 2-18C).

In order to determine the functional significance of the enhanced Wip1 levels found in PALA-treated cells, Wip1 was knocked down with pools of siRNA and the phosphorylation status of Chk1 was investigated to determine the role of Wip1 in preventing Chk1 phosphorylation during PALA treatment. Drug treatment began 48 hours after transfection of the Wip1 siRNA. Lysates were made 72 hours after transfection. Wip1 knock-down was remarkably efficient; Wip1 protein was undetectable in all samples following siRNA treatment. Chk1 phosphorylation was not restored during PALA treatment in the absence of Wip1 (Fig 2-19). The amount of Wip1 knockdown effectively abolished phosphatase activity as is observed by the increase in phosphorylation at serine 15 of p53, a residue that Wip1 is known to dephosphorylate. This suggests that Wip1 was playing a minor role in the failure to activate Chk1 following PALA treatment and, hence, in assembling the S-phase checkpoint. Interestingly, there was a substantial increase in the level of phosphorylation of p53 at serine 15 in all siRNA treated samples, an indication of the role of Wip1 in control of the steady-state levels of this phosphorylation.

The protein phosphatase 2A (PP2A) has been shown to dephosphorylate Chk1 at serine 345 maintaining a hypophosphorylated Chk1 during unperturbed S-phases (Leung-Pineda et al., 2006). To rule out the possibility that PP2A was compensating for the loss of Wip1 phosphatase activity during these knock down experiments okadaic acid was used as a pharmacological

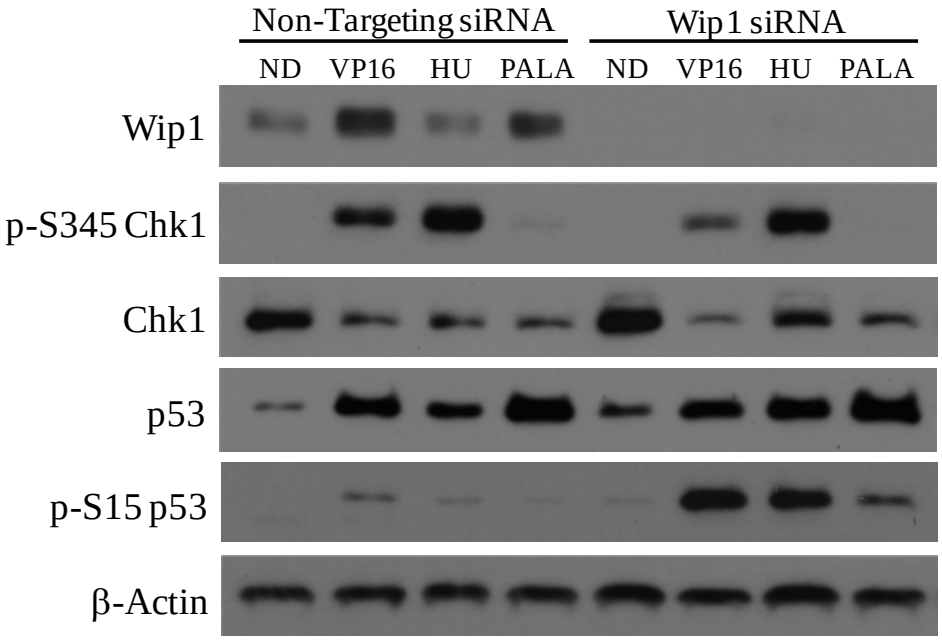

Figure 2-19. Wip1 does not dephosphorylate Chk1 during PALA treatment. This figure shows a western blot analysis of Wip1, total and phosphorylated Chk1 at serine 345 and total and phosphorylated p53 at serine 15 in asynchronous HCT116 cells transiently transfected with Wip1 siRNA pools. Cells were exposed to drug 48 hours post transfection for 24 hours. Non-targeting siRNA pools were used as a control. Equal levels of total protein (25 μg) were loaded in each lane. Vehicle was PBS, HU was used at 1.5 mM, PALA was used at 100 μM and VP16 was used at 10 μM.

inhibitor of the PP2A. Treatment of HCT116 cells prior to knocking down Wip1 with 50 nM okadaic acid alone or in combination with PALA did not change Chk1 phosphorylation levels; they were similar to what was observed with PALA treatment (Fig 2-20). In HCT116 cells in which Wip1 was knocked down, okadaic acid treatment did not restore Chk1 phosphorylation following PALA treatment. The phosphorylation of Chk1 was not detectable during okadaic acid and PALA treatment suggesting PP2A is not responsible for the lack of Chk1 phosphorylation in the absence of Wip1 (Fig 2-20B).

PALA treatment fails to recruit ATR to the chromatin

The other explanation for the lack of Chk1 phosphorylation during PALA treatment could be that ATR is not activated by recruitment to replication forks during the slowed S-phase progression. If ATR is not present at stalled replication forks, Chk1 will not become phosphorylated and activated and, as a result, the S-phase checkpoint will not be intact. This question of the recruitment of ATR to nucleotide deficiency-induced stalled replication forks was addressed by fractionating chromatin away from the soluble nuclear proteins in synchronized HCT116 cells and determining whether ATR was bound to chromatin in HU and PALA treatment. The fractions were blotted for the presence of ATR. In whole cell and soluble nuclear fractions the levels of ATR are relatively consistent over the treatments, ruling out transcriptional or post-transcription effects on total cellular levels of ATR by PALA. Yet, there is no detectable ATR accumulating in the chromatin-bound fraction during PALA treatment, while there is a significant level of ATR recruited to the chromatin after HU treatment, indicating that Chk1 is not phosphorylated during PALA due to the lack of ATR chromatin recruitment (Fig 2-21). Interestingly, the S-phase checkpoint proteins phosphorylated Chk1 and BLM were also not recruited to the chromatin during PALA treatment, yet there were equivalent levels of p53 at the chromatin during HU and PALA treatment (Fig 2-21). The lack of S-phase proteins at the chromatin during PALA

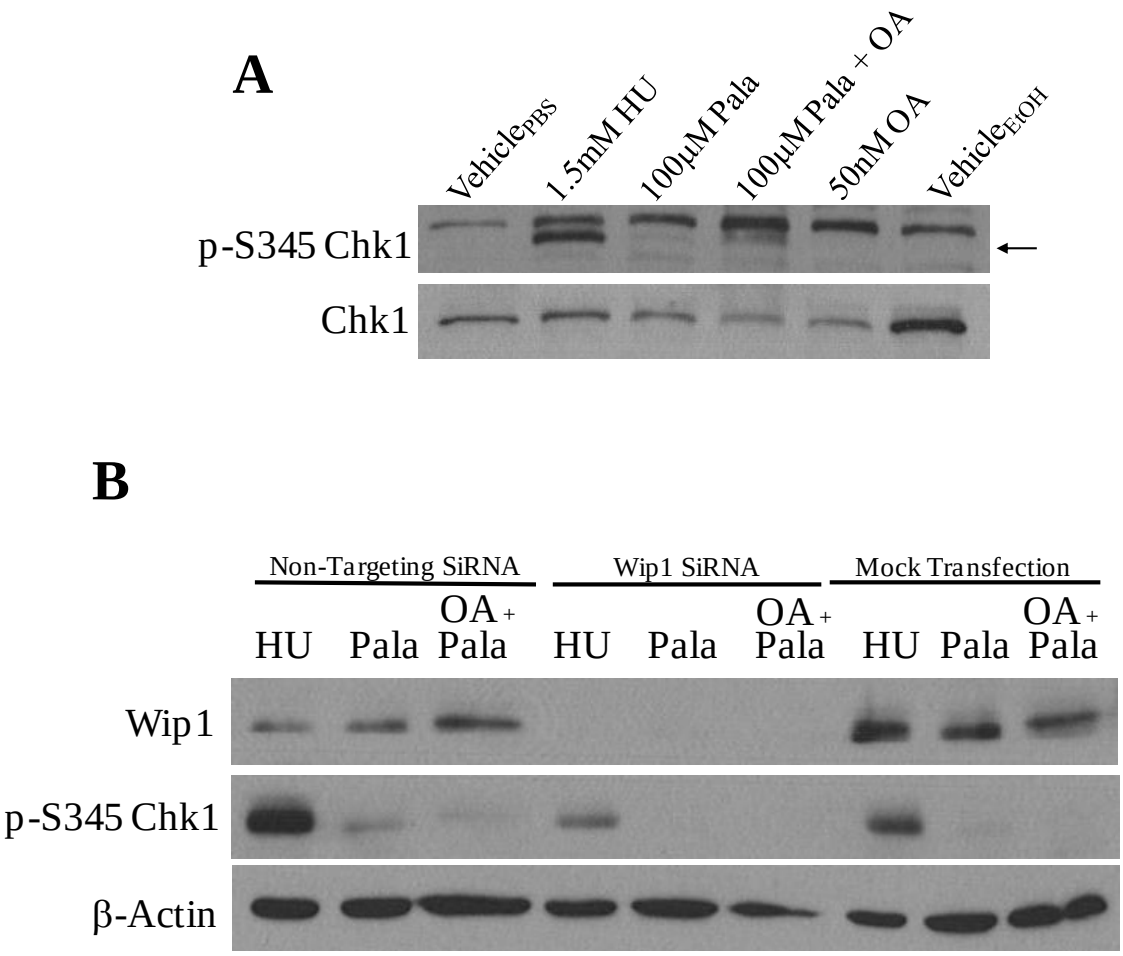

Figure 2-20. PP2A does not compensate for the absence of Wip1. A, This figure shows a western blot analysis of total and phosphorylated Chk1 at serine 345 in asynchronous HCT116 cells. The arrow indicates the band specific for phosphorylated Chk1. The PBS vehicle corresponds to the HU and PALA samples and the EtOH vehicle corresponds to the PALA with OA and OA alone samples. B, This figure shows a western blot analysis of Wip1 and phosphorylated Chk1 in asynchronous HCT116 cells transiently transfected with Wip1 siRNA pools. Cells were exposed to drug 48 hours post transfection for 24 hours. Non-targeting siRNA pools and a mock transfection were used as a control. HU was used at 1.5 mM, PALA was used at 100 μM and OA at 50 nM.

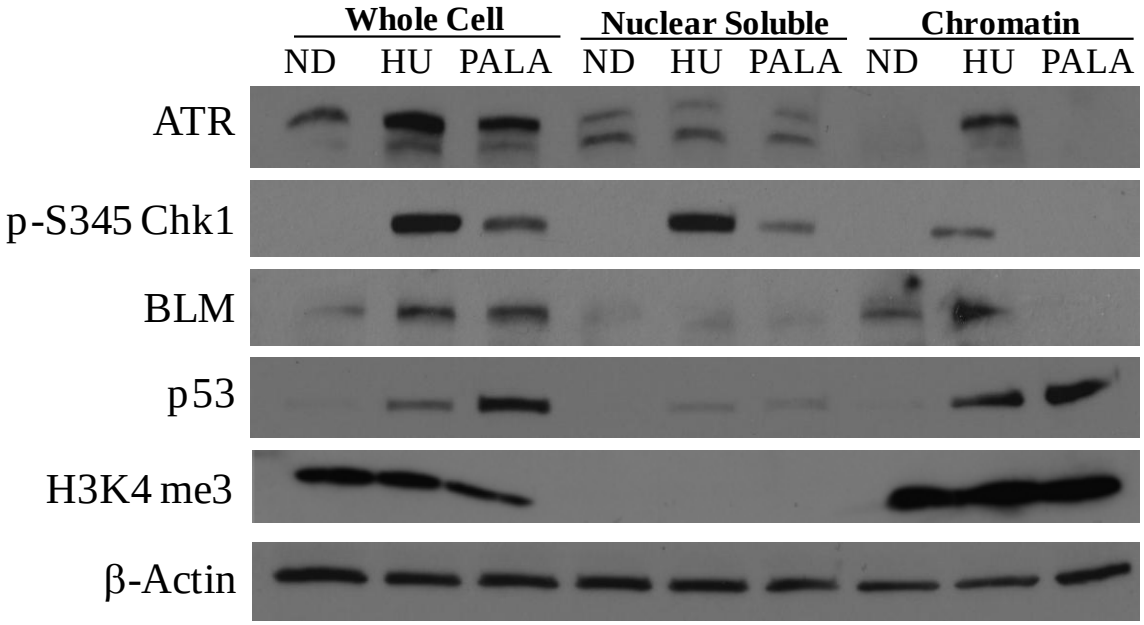

Figure 2-21. S-phase checkpoint proteins are not recruited to the chromatin after PALA treatment. This figure shows a western blot analysis of the assembly of S-phase checkpoint proteins on chromatin. G_0/G_1 synchronized HCT116 cells were released into drug containing medium for 24 hours and the chromatin was fractionated from whole cell lysates as described by (Mendez and Stillman, 2000). Equal protein levels (25 μg) of whole cell, nuclear soluble and chromatin fractions were analyzed by western blot for ATR, phospho Chk1, BLM and p53. H3K4 me3 was used to demonstrate the purity of the fractions. Vehicle was PBS, HU was used at 1.5 mM and PALA was used at 100 μM.

treatment suggests that, due to the failure of ATR recruitment, the S-phase checkpoint is not activated and therefore, these proteins were not being actively recruited to stalled replication forks. The equivalent levels of chromatin-bound p53 observed during the two treatments suggests that, during PALA treatment, p53 is involved in other cellular processes occurring at the chromatin, possibly at the level of transcription, i.e. binding at p53RES in promoters.

The Cellular Consequences of the Differential Chk1 Phosphorylation

PALA treatment is cytotoxic while HU treatment is cytoprotective

Colony formation assays were used to test the ability of cells to recover and survive after HU and PALA treatment. A classical colony formation assay was performed, allowing cells to adhere for five hours and then replacing the growth medium with medium containing increasing concentrations of drugs for 24 hours. Both HCT116 p53 +/+ and HCT116 -/- cells lines were used in this assay. PALA treatment had a steeper decline in cell survival over the range of concentrations tested; this trend was observed in both cell lines. HU treatment did not decrease cell survival as steeply as did PALA treatment, but at concentrations ≥ 3mM HU, cell survival decreased in both cell lines. In both treatments, cells were unable to survive at a higher drug concentration and cells without p53 were less sensitive to the cytotoxicity of both drugs. However, the most important aspect of this analysis is that, at concentrations of HU that were markedly inhibitory to cell progression through S-phase, i.e. 1.5 mM, HU was without cytotoxicity whereas a concentration of PALA that impeded S-phase progression (100 μM) was grossly cytotoxic (Fig 2-22).

To determine the time course of commitment to cell death, synchronized cells were released into either HU or PALA for various lengths of time. At each time point, adherent and

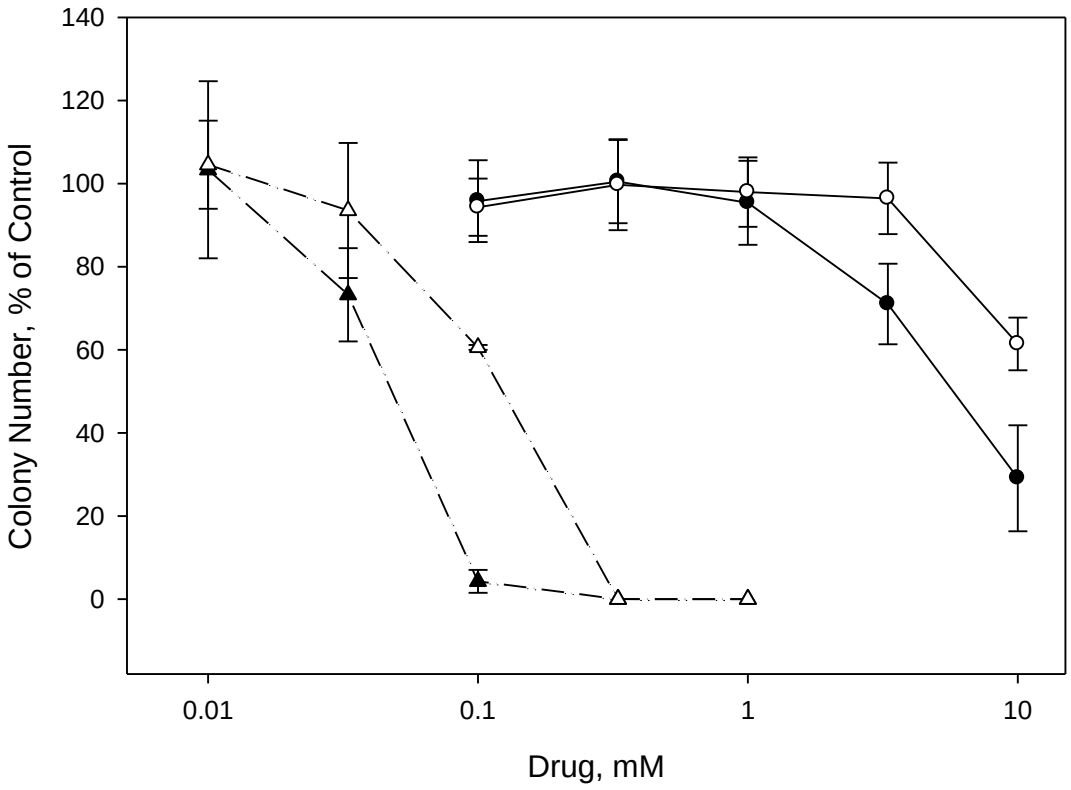

Figure 2-22. HCT116 cells containing wild-type p53 are more sensitive to cell kill induced by HU or PALA treatment than HCT116 null of p53. HCT116 p53 +/+ (solid symbols) and HCT p53 -/- (open symbols) were plated and allowed to adhere for 5 hours. Medium containing 10% dFBS and various concentrations of HU (circles) or PALA (triangles) were added for 24 hours. Cells were maintained in drug free medium after the exposure for an additional 8 days and colonies were stained and counted and plotted as survival of drug treated cells compared to vehicle treated cells. Points indicate the mean of three plates within a single experiment and standard error is depicted by the bars.

floating cells were collected and counted. Both ND and HU treated cells were plated in fresh drug-free medium at 150 cells/60 mm^2 dish while PALA treated cells were plated at 150, 1,500 and 15,000 cells/60 mm^2 dish and allowed to attach and grow for 7 days. HU-treated cells were protected from nucleotide deficiencies for 36 hours, after 48 hours of drug treatment cell survival decreased slightly. However, the cell survival observed during HU treatment never decreased below 10% survival throughout the 72 hour time course (Fig 2-23). Conversely, the cytotoxicity of PALA treatment was observed within 6 hours of treatment; cell survival decreased to ~10% and continued to decrease with time. By 48 hours, PALA treatment was cytotoxic with $\leq 0.1\%$ cell survival (Fig 2-23). The cytotoxicity of PALA treatment can easily be seen in Fig 2-23A; very few colonies out of the total of 15,000 plated cells survived after 12 hours of PALA treatment, while HU and untreated cells contained a similar number of colonies at 12 hours (Fig 2-23A). The S-phase checkpoint appeared to be protecting HU-treated cells from cytotoxicity while the lack of S-phase checkpoint resulted in cytotoxicity within 6 hours of PALA treatment.

PALA treatment promotes a p53-dependent apoptosis

The post-translational phosphorylation of p53 during PALA treatment at serine 46 suggested that these cells may be undergoing p53 dependent apoptosis (Mayo et al., 2005). This proved to be the case: after 24 hours, PALA-treatment resulted in apoptosis as observed by cleaved caspases 7 and 9, as well as by PARP1 (Fig 2-24). Treatment with HU did not cause cleavage of any of these proteins crucial to the apoptotic response. The PARP1 cleavage during PALA treatment was shown to be dependent on p53, in concordance with the data in Fig 2-14.

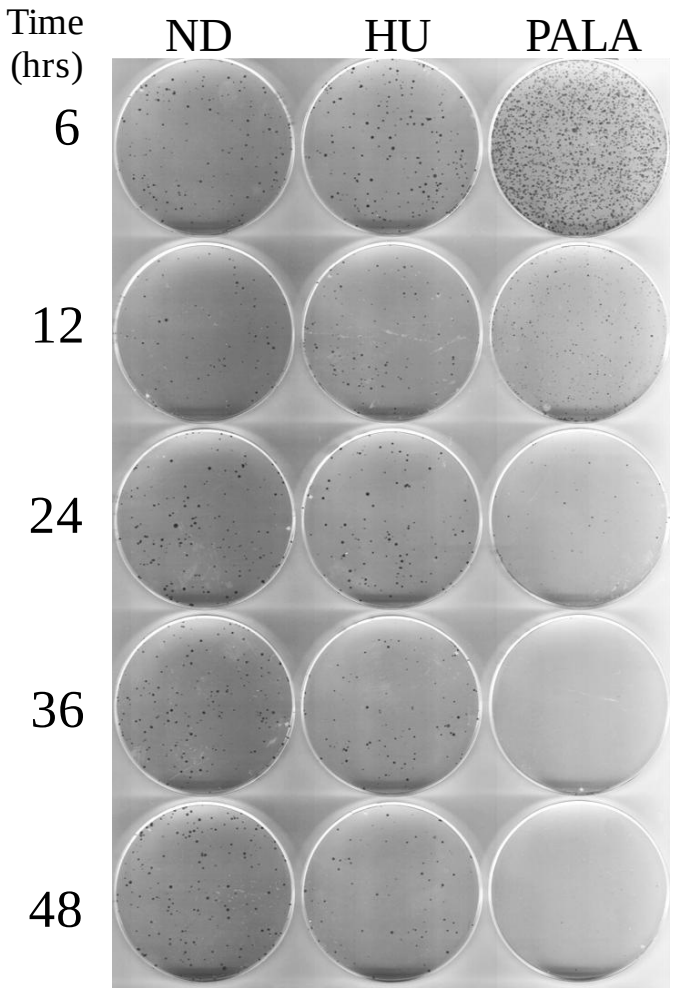
Time (hrs)
ND
HU
PALA
6
12
24
36
48

B

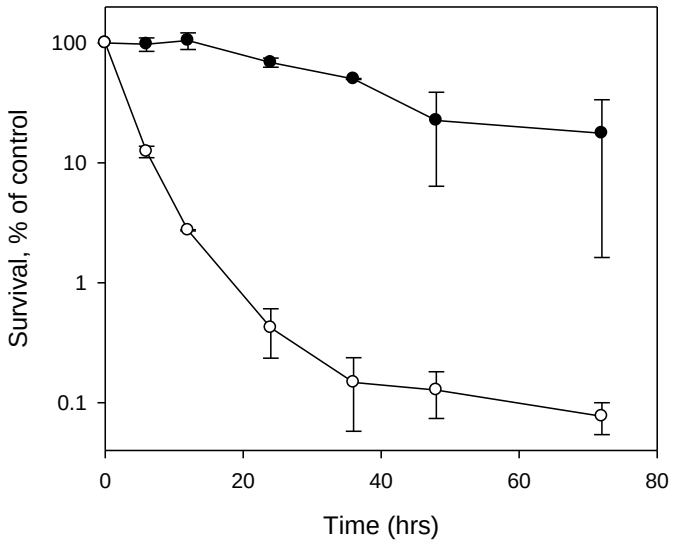
Survival, % of control
100
10
1
0.1
0
20
40
60
80
Time (hrs)

Figure 2.23. The imposition of an S-phase checkpoint by HU protects HCT116 cells from cytotoxicity for an extensive period, whereas PALA exposure is rapidly cytotoxic. G_0/G_1 synchronized HCT116 cells were released into drug-containing medium for the indicated times and adherent and non-adherent cells were re-plated at 150 cells/plate in drug free medium allowing for colony formation. B, Quantitation of the colony formation assay in HCT116 cells after treatment with HU or PALA at the indicated times. Points indicate the mean of two biological repeats containing two plates within a single experiment and standard error is depicted by the bars. Colony number was plotted as survival of drug- treated cells compared to vehicle-treated cells. Vehicle was PBS, HU was used at 1.5 mM, PALA was used at 100 μM.

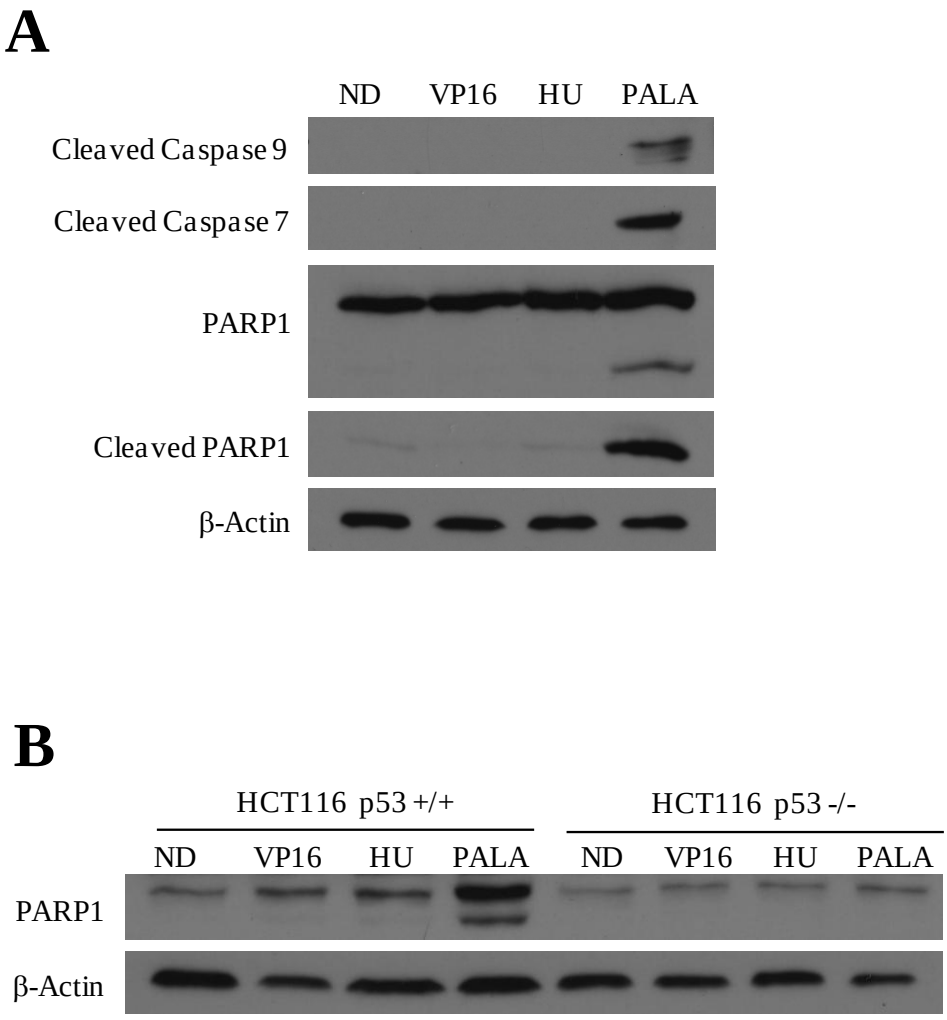

Figure 2-24. PALA treatment induced p53 dependent apoptosis while the HU-induced S-phase checkpoint protects cells from apoptosis. This figure shows a western blot analysis of cleaved caspases 7 and 9, PARP1 and cleaved PARP1 in asynchronous HCT116 cells treated with drug for 24 hours. B, Lysates from asynchronous HCT116 p53 +/+ and HCT116 p53 -/- cells were probed for PARP1 to determine the p53 dependency of apoptosis. Equal levels of total protein (25 μg) were loaded in each lane. Vehicle was PBS, HU was used at 1.5 mM, PALA was used at 100 μM and VP16 was used at 10μM.

Using the p53 HCT116 isogenic cell lines, PARP1 cleavage was not observed after PALA treatment in the absence of p53. The p53 dependency of this apoptosis was further investigated by examining the presence of p53 at a panel of known p53-dependent pro-apoptotic promoters after 24 hours in drug. Five promoters were chosen based on their known p53RE affinities for p53. The p53RE in the BAX, PIG3, and AIP1 promoters are known to have weaker p53 binding affinities while that in the PUMA and FAS promoters have higher p53 promoter affinity (Inga et al., 2002; Kaeser and Iggo, 2002; Weinberg et al., 2005). PALA treatment promoted enhanced binding of p53 at all of these promoters at or exceeding levels seen with the highly cytotoxic dose of VP16 used as the control, indicating that after 24 hours in drug, PALA treatment facilitated p53 binding to pro-apoptotic promoters (Fig 2-25). This is in agreement with the apoptosis observed by the cleavages of caspases 7, 9 and PARP1 and the cytotoxicity measured by colony formation assays. The species of p53 accumulating in HU-treated cells was apparently much less active at entering the nucleus and binding at either high- or low-affinity p53REs.

γH2AX formation is a rapid cellular response for DNA double strand breaks and therefore to determine if apoptosis resulting from PALA treatment was due to DNA damage, levels of γH2AX were measured (Rogakou et al., 1998). There were no significant differences in the levels of γH2AX between HU and PALA treatment and both were less than the positive control for DNA damage, VP16 (Fig 2-26).

Another hypothesis was tested in the experiments that investigated rescue of HU treatment with the addition of 2-deoxyadenosine (AdR) and 2-deoxyguanosine (GdR), the purine deoxyribonucleotides discussed above. The apoptosome formed by the intrinsic apoptotic pathway responsible for cleavage of caspase 9 and initiating the downstream signaling has been

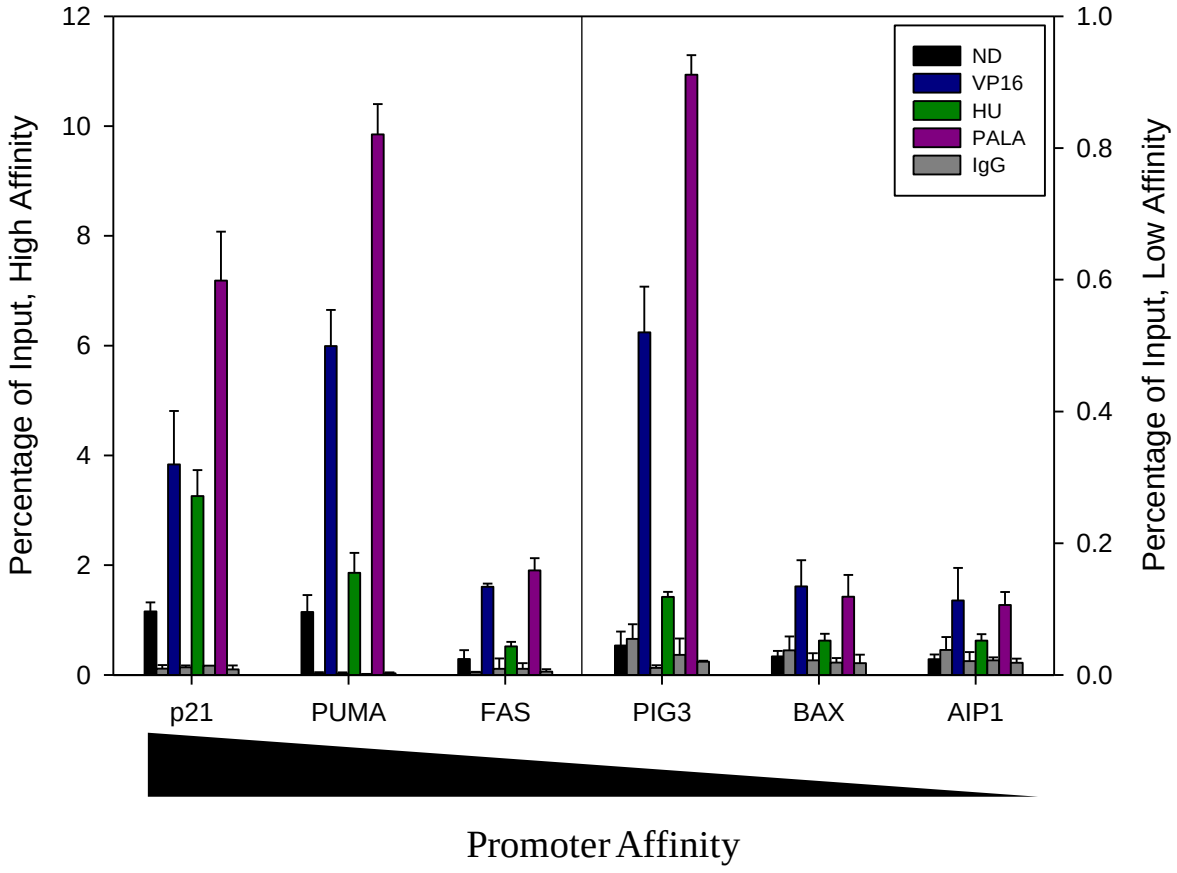

Figure 2-25. PALA treatment induces p53 binding at promoters of pro-apoptotic proteins. ChIP analysis of p53 enrichment at pro-apoptotic promoters in asynchronous HCT116 cells after 24 hours of drug treatment. p53-DNA complexes were immunoprecipitated from crosslinked cells and PUMA, FAS, PIG3, BAX, AIP1 promoter levels were quantitated with Q-PCR. Non-specific binding was immunoprecipitated with IgG. PUMA and FAS promoters correspond to the left ordinate while PIG3, BAX and AIP1 promoters correspond to the right ordinate. Standard error is depicted by the bars from one biological repeat with triplicate Q-PCR samples. The same trend was observed in subsequent biological repeats. Vehicle was PBS, VP16 was used at 10 μM, HU was used at 1.5 mM and PALA was used at 100 μM.

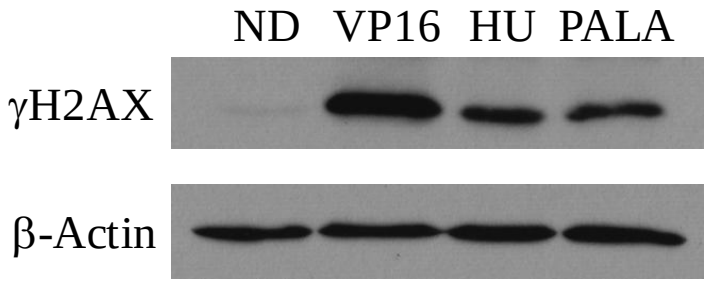

Figure 2-26. HU and PALA-treatment induce the same level of γH2AX in asynchronous HCT116 cells. This figure shows a western blot analysis of levels of γH2AX after exposure to 10 μM VP16, 1.5 mM HU or 100 μM PALA for 24 hours. Total cell lysate protein (25 μg) was subjected to SDS-PAGE and immunoblotted with antibodies against γH2AX and β-Actin. VP16 was used as the positive control. Protein loading was assessed with β-Actin.

shown to be dependent on cytochrome c and dATP (Zou et al., 1999). Since HU depletes all dNTPS (Bianchi et al., 1986; Rosenthal et al., 1928), it was hypothesized that HU treatment cannot promote apoptosis due to the lack of availability of dATP for apoptosome assembly. PARP1 cleavage was immunoblotted for in these samples. There was no change in cleavage between the HU sample alone and the HU supplemented with AdR and GdR. Therefore, the depletion of dATP is not preventing apoptosis in HU treatment (Fig 2-15 B). Ultimately, the supplementation experiments with AdR and GdR did not explain the differences in the cellular responses between HU and PALA treatment.

Discussion

We have found that HCT116 cells respond very differently to two drugs that both cause an inhibition of nucleotide synthesis pathways and a subsequent slowed progression of S-phase and stalling of replication forks. The ribonucleotide reductase inhibitor HU activates the S-phase checkpoint through ATR recruitment to the chromatin and Chk1 phosphorylation and is not appreciably cytotoxic for several generation times. PALA, an inhibitor of aspartate transcarbamylase in the de novo pyrimidine synthesis pathway, fails to activate the S-phase checkpoint resulting in commitment to a p53-dependent apoptosis without a lag time. One would hypothesize that these two drugs essentially stress the cells in the same manner, by causing an imbalance of nucleotides, and would be expected to result in similar cellular responses. This is clearly not the case in HCT116 colon carcinoma cells.

Why does HU induce the S-phase Checkpoint and PALA does not?

Flow cytometry analysis of G_1 synchronized cells released into HU and PALA demonstrated that the cells are slowly progressing though the S-phase (Fig 2-12). The nearly comparable rates of S-phase progression suggested that the two drug treatments were causing similar cell cycle signaling; this was shown to not be true. The S-phase checkpoint effector kinase Chk1 was phosphorylated during HU treatment indicating an activated S-phase checkpoint, while PALA treatment resulted in minimal phosphorylation of Chk1 (Fig 2-13). The differential Chk1 phosphorylation was found to be due to the levels of ATR recruited to the chromatin (Fig 2-21). PALA treatment did not cause ATR recruitment to the chromatin, explaining the lack of Chk1 phosphorylation; the upstream kinase was not recruited and therefore, Chk1 could not become phosphorylated and activated. Interestingly, another S-phase checkpoint protein, BLM, was also not at the chromatin after PALA treatment, while HU treatment resulted in BLM recruitment. It is clear that PALA treatment did not activate the signaling pathway involved in the S-phase checkpoint (Fig 2-5), but the question remains as to why there is such a disparity between HU and PALA treatment? Why is ATR recruited to the chromatin only after HU treatment? ATR recruitment was shown to be dependent on ATRIP loading onto RPA coated ssDNA and that the long stretches of RPA-coated ssDNA is the molecular trigger initiating the S-phase checkpoint (Zou and Elledge, 2003). It is possible that PALA treatment does not result in long stretches of exposed ssDNA at replication forks. Since the recruitment of ATRIP and ATR depends on RPA bound ssDNA, if this event is not occurring, then the differences in ATR recruitment between HU and PALA treatment could be explained be examining the RPA levels at stalled replication forks.

Why is PALA cytotoxic and HU is not?

Cell kill was obvious early studies of PALA treatment. After cells were treated with PALA for extended lengths of time (> 24 hours) the majority of the cells were falling off the tissue culture dish and floating. Throughout the time course studies, it was difficult to obtain enough cells at the later time points for flow cytometry or western blot analysis. The answer became clear when I discovered that the HCT116 cell death after PALA was apoptotic (Fig 2-24). PALA induces apoptosis and HU does not at equivalent functional effects on S-phase traverse. Interestingly, there appeared to be no lag time in the observed apoptosis. Within 6 hours of PALA treatment, 90% of the cells were unable to survive and by 36 hours no significant cell survival was observed (Fig 2-23). This was not true for HU-treated cells; almost all plated cells were still able to survive and form visible colonies after 48 hours of HU treatment. When the dependency of cell survival on p53 was investigated, it was shown that at the working concentration of PALA (100 μM), 50% of HCT116 cells null for p53 could survive while cells wild-type for p53 could not (Fig 2-22).

The mode of cell death was first suggested by analysis of the PTMs of p53 after HU and PALA treatment. The PTMs of the accumulated p53 were completely opposite following HU or PALA treatment (Fig 2-8). During HU treatment serines 15 and 20 were phosphorylated. ATR is known to phosphorylate p53 at serine 15 and Chk1 is known to phosphorylate p53 at serine 20 (Shieh et al., 2000; Tibbetts et al., 1999); therefore these modifications correlate with the observed activation of the S-phase checkpoint in HU but not in PALA. The modifications on serines 37, 46 and 392 during PALA treatment are informative of the cellular activities of p53: phosphorylation of serine 46 has been shown to favor p53-dependent apoptosis (Mayo et al., 2005), serine 392 phosphorylation enhances p53 tetramerization and subsequent DNA binding (Hupp et al., 1992; Keller et al., 2001; Sakaguchi et al., 1997), and phosphorylation of serine 37

promotes sequence-specific DNA binding of p53 (Sakaguchi et al., 1998). During HU treatment none of these sites were phosphorylated to the extent observed during PALA treatment, suggesting that the p53 accumulated during PALA treatment was activated to bind to DNA and promote apoptosis whereas the p53 in HU-treated cells was not. This was found to be true; PALA-stabilized p53 was bound to all investigated pro-apoptotic promoters at levels greater than that of the HU-stabilized p53 (Fig 2-25). It was later discovered that PALA induces apoptosis which is dependent on p53; cleavage of PARP1 was not observed after PALA treatment in HCT116 cells null for p53 (Fig 2-24). The dependency on p53 for inducing apoptosis after PALA treatment and the fact that HCT116 cells null for p53 are able to survive after 24 hours of PALA treatment while HCT116 cells wild-type for p53 are not, indicated that the key factor in this decision for apoptotic cell death appeared to be p53.

Does p53 determine cellular fate?

It appears that p53 is involved in the differing cellular responses to HU and PALA. The total amount of accumulated p53 between the two treatments is significantly different and the post-translational modifications of the accumulated p53 are completely opposite when comparing drug treatments. Secondly, the apoptotic response was found to be p53-dependent and the colony formation assays demonstrated that p53 null cells are better able to survive after PALA treatment, all implicating the involvement of p53.

It was consistently observed that PALA treatment resulted in the accumulation of twice as much p53 than seen after HU treatment (Figs 2-11, 2-13, 2-14, 2-15). This was observed in synchronous cells, asynchronous cells and over a range of time points. Why is there a difference in the p53 levels accumulated after HU and PALA treatment? It has been shown that the nuclear

export sequence (NES) that is located at amino acids 340-351 within the oligomerization domain is masked by p53 tetramerization resulting in nuclear retention of p53 (Stommel et al., 1999). The PTMs of p53 after PALA treatment, specifically phosphorylation of serine 392, suggested that after PALA treatment, the accumulated p53 forms tetramers more readily than the HU-stabilized p53. If this is found to be true, then during PALA treatment the tetramerization of p53 may be masking the NES and therefore trapping p53 in the nucleus and protecting it from degradation, while the p53 accumulated during HU treatment is not**.**

How do the differing levels of accumulated p53 ultimately determine the cellular fate of PALA-treated cells?

Although the exact answer to this question remains to be elucidated, the experiments presented throughout this chapter have led to some interesting hypotheses. The role of p53 in the S-phase checkpoint is complex and there is no known required transcriptional role for p53 in the S-phase checkpoint. It is thought that p53 interacts with BLM and Rad51, enhancing their recruitment to stalled replication forks independent of transcriptional activation. Previous literature has suggested that the p53 stabilized during HU treatment has decreased transcriptional activity when compared to IR-stabilized p53 as determined by northern blot analyses of RNA levels of several p53 dependent genes including, p21, gadd45, hdm2 and cyclin G (Gottifredi et al., 2001). In this chapter, we showed that HU treatment activates a functional S-phase checkpoint as shown by ATR recruitment to the chromatin and phosphorylation of Chk1. This would suggest that the transactivating ability of p53 is dispensable for a functional S-phase checkpoint. Furthermore, it appears that, during PALA treatment, promoters are enriched with p53 to a greater extent than during HU treatment. In the ChIP assays described throughout this

chapter, PALA-stabilized p53 was found to bind to large range of promoters, as observed in the panel of pro-apoptotic promoters and the p21 promoter (Fig 2-7 & Fig 2-25). Conversely, during HU treatment the upstream binding site of the p21 promoter, which is known to have the highest affinity for p53 (Inga et al., 2002; Kaeser and Iggo, 2002; Weinberg et al., 2005), was the only promoter that had significant levels of p53 enrichment. These data suggest that the PALA-stabilized p53 is able to bind p53RE within promoters better than that of the HU-stabilized p53. The PALA-stabilized p53 is capable of transactivating genes, as is evident from the robust stimulation of Wip1 transcription (Fig 2-18). Therefore, these data raise the possibility that a stabilized p53 that is able to bind and transactivate genes is capable of inducing apoptosis while the p53 accumulated during HU treatment is not capable of activating the genes required for apoptosis. However, stabilization of p53 caused by HU treatment may enhance the recruitment of BLM and Rad51 to stalled replication forks in the S-phase checkpoint.

Is p53 differentially recruited to replication forks in HU and PALA treatment?

Although the levels of p53 recruited to the chromatin during HU and PALA treatment appeared to be similar (Fig 2-21), the chromatin fractionation isolated all nuclear chromatin. Replication forks as well as promoters of p53-dependent genes were both included in this chromatin fraction, making it difficult to differentiate the levels of p53 recruited to the chromatin from that of p53 bound to p53REs in promoters. The p53 accumulated after PALA treatment was shown to be more capable of binding to promoters than the HU-stabilized p53 (Fig 2-25), so it is logical to hypothesize that a large majority of the chromatin bound p53 is indeed p53 bound to promoters, not p53 at replication forks. To determine if HU and PALA treatment differentially recruit p53 to replication forks, colocalization studies of p53 and BrdU in HU and PALA treated cells could be performed. Treating cells with DNase after a brief pulse with BrdU

has been shown to lead to BrdU incorporation at stalled replication forks (Kennedy et al., 2000). This methodology would allow the identification of stalled replication forks by immunofluorescence and colocalization of p53 with the replication forks could then be determined.

Is the S-phase checkpoint activated by HU treatment cytoprotective?

It was clear that PALA treatment resulted in marked cytotoxicity, but did the S-phase checkpoint activated by HU treatment protect the cells from nucleotide deficiencies? The data presented within this chapter centrally proves that HCT116 cells are protected from cytotoxicity during HU treatment. After 36 hours of HU treatment, cells were able to survive as well as the untreated control and even after 72 hours of HU treatment, cells showed some toxicity but a small percentage (~17%) of them still were able to survive and form colonies (Fig 2-23). Interestingly, HCT116 cells null for p53 and HCT116 wild-type for p53, were able to survive to the same extent when treated with HU at the working concentration of 1.5 mM for 24 hours (Fig 2-22). The p53 dependency of Chk1 phosphorylation during HU treatment also demonstrated that Chk1 was phosphorylated at serine 345 and 317 in HCT116 p53 -/- cells to the same extent as HCT116 cells containing wild-type p53 (Fig 2-14). Both observations suggest that p53 is not required for a functional checkpoint and the resulting cytoprotectivity that the S-phase checkpoint provides during HU treatment. The exact role of p53 during the S-phase checkpoint activated by HU treatment remains to be elucidated and the cell line, which will be described in the next section was generated to address this question.

Chapter 3: Development and Characterization of an Endogenously TAP-tagged p53 Locus

Introduction

The p53 tumor suppressor is known to be involved in several cellular pathways that are in place to protect the cell from tumorigenesis. p53 is one of the main regulators in cell cycle control and apoptosis pathways yet it is mutated in half of all human cancers resulting in dysregulation of the cell cycle and of apoptosis. For this reason, the cellular and molecular functions of p53 have been thoroughly investigated to understand its cellular roles and to better comprehend the changes that cancer cells undergo following mutation of p53.

p53 exerts its tumor suppressor activity through two main functions; by binding to gene promoters recruiting transcriptional machinery activating (or repressing) transcription, and by directly binding to and modulating protein functions. The transcriptional regulation activity of p53 has been extensively investigated while the modulation of protein functions by p53 is less well characterized. There are examples in both cell cycle regulation and apoptosis pathways where p53 exerts its tumor suppressor activity by both mechanisms.

p53 was first implicated in homologous recombination when p53 null mammalian cells were shown to have elevated levels of spontaneous homologous recombination (Mekeel et al., 1997). Since then, the proteins involved in homologous recombination have been identified and the role of p53 in this pathway has been further elucidated. Rad51 is induced in late S-phase and G_2 and binds to single stranded DNA during the initial steps of homologous recombination (Benson et al., 1994; Flygare et al., 1996). Rad51 possesses DNA-dependent ATPase activity

which supplies the energy needed for the homologous pairing and strand exchange steps during homologous recombination (Baumann et al., 1996). p53 was shown to inhibit homologous recombination through binding to and modulating the function of Rad51 (Linke et al., 2003; Sturzbecher et al., 1996). Rad51 and p53 co-localize to stalled replication forks induced by HU and their interaction stabilizes the replication fork through inhibition of the Rad51-driven branch migration (Sengupta et al., 2003; Yoon et al., 2004). During VP16-induced DNA damage, p53 binds to the Rad51 promoter inhibiting the transcription of this gene. Therefore, p53 controls homologous recombination at two levels when the genome integrity is compromised; through protein-protein interactions and through transcriptional repression (Arias-Lopez et al., 2006).

This duality of p53 in control of a cellular process also occurs during apoptosis. It was shown that p53 had a role in apoptosis when p53 null tumor cells underwent spontaneous cell death after the introduction of wild-type p53 (Yonish-Rouach et al., 1991). Bax has been well-defined as an apoptotic protein that inserts into the outer mitochondrial membrane to form a pore, releasing cytochrome c and activating cytosolic events in the apoptotic pathway (Rosse et al., 1998). The restoration of p53 in murine leukemia cells caused an increase of Bax mRNA and protein levels (Selvakumaran et al., 1994). Bax was found to be a direct transcriptional target of p53 and it was the first example of a proapoptotic gene that is directly regulated by p53 (Miyashita and Reed, 1995). Almost ten years after the discovery of the transcription activation of Bax by p53, p53 was found to bind to Bax directly, promoting mitochondrial permeabilization, a characteristic of apoptosis (Chipuk et al., 2004). Homologous recombination and apoptosis are two examples of very different cellular processes in which p53 exerts tumor suppressor activity through effects at both the level of transcriptional control and at the level of protein-interactions.

There are several examples where p53 exerts only one level of control by binding to and modulating protein functions. One such example is the control of the function of the RecQ helicase, BLM, the product of the gene responsible for causing Bloom's syndrome when mutated. Cells from Bloom Syndrome patients exhibit chromosomal instability due to an elevated rate of sister-chromatid exchange, suggesting that a protein involved in recombination is mutated in these cells (Chaganti et al., 1974). The sequence of BLM has high homology with the RecQ family of helicases and was shown to have 3′-5′ helicase activity (Ellis et al., 1995; Karow et al., 1997). BLM selectively recognizes Holliday junctions and promotes the branch migration of these junctions, preventing homologous recombination events from occurring (Karow et al., 2000). It has been hypothesized that when replication forks stall, Holliday junctions arise and that resolution of these structures would result in a double-strand DNA break (Sharples et al., 1999). p53 has been shown to bind directly to BLM, modulating the helicase activity. By inhibiting the resolution of the Holliday junctions at stalled replication forks, modulation of BLM by p53 prevents the collapse of replication forks, as well as further DNA damage and the threat of tumorigenesis (Yang et al., 2002).

The problem addressed in this chapter

With the myriad mechanisms of action of p53 that occur, the question arises of how to suitably study the binding of p53 to various proteins and promoters in the cell while also conserving the ability to determine whether various PTMs drive p53 to these various nuclear, cytosolic and mitochondrial compartments. Specifically, the role of p53 in the S-phase checkpoint has been recently proposed and the question arises whether p53 is binding to other checkpoint proteins. In order to address this question, p53 has to be isolated at endogenous

levels with all interacting proteins during nucleotide deficiencies to determine what proteins bind p53. To address these questions, we have designed and created a HCT116 cell line in which a tandem affinity purification tag has been inserted into one of the endogenous p53 alleles by homologous recombination.

The use of TAP tag to study protein-protein interactions

Until recently, the methodology to ask non-biased questions about protein interactions within mammalian cells has been limited. Co-immunoprecipitation experiments only provide data answering specific questions such as, 'does protein x interact with protein y?' and usually are confined to analysis of such events in whole cell lysates. The ability to ask 'what are all of the proteins that interact with protein x?' has not been easily feasible until the introduction of the tandem affinity purification (TAP) tag technology combined with mass spectrometry. This tag was designed to allow the target protein to be purified with all interacting proteins using mild, non-denaturing, purification conditions. The two step purification tag consists of a protein A tag and a calmodulin binding peptide separated by a tobacco etch virus (TEV) protease cleavage site (Fig 3-1) (Rigaut et al., 1999). This cleavage site was found to be advantageous over others because the TEV nuclear inclusion A protein encoded by the tobacco etch virus is stable and active over a range of pH, ionic strengths and temperatures and recognized a short peptide sequence rarely found in mammalian tissues. The proteinase has stringent sequence specificity for the TEV cleavage site, decreasing proteolysis of cryptic sites within mammalian proteins (Parks et al., 1994). IgG beads are used as the first affinity adsorption matrix to select any protein bearing the protein A tag. The complex is removed from the beads by cleavage with the

TEV protease. The complex is then subjected to the second affinity matrix absorption onto beads covalently attached to calmodulin in the presence of Ca^{2+} which selectively binds to the calmodulin binding peptide. The protein complex is eluted and isolated through chelation of the Ca^{2+} with EGTA (See Figure 3-1) (Rigaut et al., 1999). The tandem purification approach is superior to single purification tags for two reasons; the two purification steps allow for a purer isolated product with less contaminants, and the design of the TAP tag allows for stringent, non-denaturing purification conditions making it possible to isolate protein binding partners.

Gene Targeting Allows Protein Interactions to be studied at endogenous levels

Protein interactions are driven by association constants (Ka) and therefore protein-protein interactions should be studied at endogenous levels to rule out any false positives resulting from the over expression of the target protein of interest. With the use of the TAP tag, isolation of these interactions are now possible, and in combination with gene targeting, the TAP tag sequence can be inserted by homologous recombination at the end of the endogenous gene locus coding the protein of interest. This would result in the transcription and translation of the target gene and the incorporated TAP tag in one contiguous transcript, allowing protein interactions to be studied at natural endogenous levels. This was first achieved in yeast in 1999 and, in 2002, Seraphin's group used the TAP tag to identify 234 multiprotein complexes and proposed new roles for 344 of the proteins, 231 of which had no previously known function. Function could be assigned for most of these unassigned open reading frame proteins by a "guilt-by-association" logic, demonstrating the power of this technology (Gavin et al., 2002; Rigaut et al., 1999).

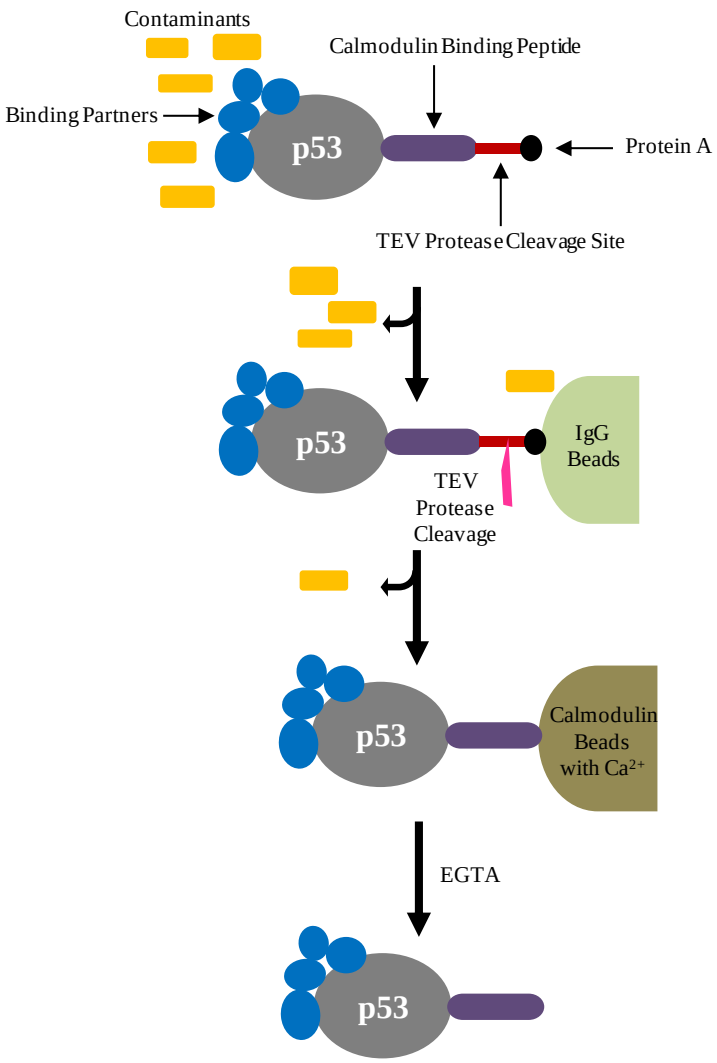

Figure 3-1. Overview of Tandem Affinity Purification Procedure. Cellular lysates are incubated with IgG beads that bind to protein A in the TAP tag. The target protein and binding partners are eluted from the IgG beads with TEV protease. The eluate is then bound to calmodulin beads in the presence of $CaCl_2$, which will bind to the calmodulin binding peptide. The target protein and binding partners are eluted by chelating the $CaCl_2$ with EGTA.

rAAV as the mode for gene delivery

For successful gene targeting events to occur, the targeting vector must pair up with the homologous sequence in the chromosome. Considering that the human genome is three million base pairs, the frequency of this occurring is exceptionally low (Vasileva and Jessberger, 2005). Previous methodologies to introduce targeting vectors into mammalian somatic cells consisted of lipid based transfections or electroporation of double-stranded DNA plasmid, which resulted in frequencies of one cell out of a million transfected cells incorporating the targeting sequence into their genomes by homologous recombination, but substantial frequencies of incorporation at random locations within the genome occurred (Sedivy and Sharp, 1989). This low frequency of correct insertion against a very high background made manipulating the endogenous genetic locus of mammalian cells difficult, and required screening tens of thousands of cell clones to find one clone in which correct sequence-specific integration had occurred. The introduction of recombinant adeno-associated viruses (rAAV) as the mode of gene delivery greatly improved these frequencies (Kohli et al., 2004). AAV were first used in the early 2000's as a method to introduce genetic modifications into homologous human chromosomes. Vectors containing 1.5 kb of homologous sequence could be inserted into the correct location of the targeted gene at a frequency of 1%, a vast improvement from previous methodologies (Hirata et al., 2002).

AAV is a single-stranded linear DNA virus with a 4.7 kb genome containing a *rep* gene and a *cap* gene encoding proteins required for viral replication and encapsidation of the viral genome. Inverted terminal repeats (ITR) are also required for replication. The ITR sequences are 145 bp palindromic sequences which allow the virus to fold into a hairpin, these sequences are required for integration into the host genome and viral replication. In recombinant rAAVs, the *rep* and *cap* genes are replaced with homologous sequence to the gene to be targeted and the

viral genes are supplied in *trans* through helper vectors during the viral packaging step. The packaging limit of AAV is approximately 4.9 kbs and the ITR sequence is the only viral sequence required to be provided in *cis*, providing space for 4.4 kb homologous sequence to be cloned into the vector. These longer stretches of homologous sequences increase the frequency of homologous recombination with the targeted genome (Reviewed in (Carter, 1992)).

It is not well understood why rAAV yield higher frequencies of gene targeting than previous methodologies, but there are several hypotheses. Since a large number of intact viral vectors are delivered to each cell, this increases the probability of homologous recombination occurring. In addition, the single stranded viral genome is highly recombinogenic and is thought to promote homologous pairing better than double stranded substrates similarly to homologous recombination frequently seen with stretches of single-stranded DNA at replication forks and, lastly, the hairpin structure of the genome may decrease random integration (Russell and Hirata, 1998).

Steps involved in generating human somatic knock-ins

Generating human somatic knock-ins consists of four steps: (i) designing and creating a targeting vector containing homologous sequence to the gene to be targeted, (ii) delivery of the targeting vector by rAAV to the cells, (iii) selecting for cells which underwent homologous recombination with the targeting vector and (iv) screening cell clones for gene knock-in at the correct location in the genome. Although this process is laborious, when compared to creating cell lines where the sequence transfected randomly integrates into the genome, the advantages of studying endogenously altered genes far outweighs the time involved in the creation of the cell line.

To understand the function of p53 at the replication fork during nucleotide deficiencies we have inserted a TAP tag into the p53 genomic locus at the C-terminus in human colon cancer HCT116 cells. The protein product of this allele appears to be fully functional in comparison with the wild-type p53 protein translated from the unaltered allele. We have used this cell line to isolate p53 with its binding partners under the cellular stress of DNA damage induced by VP16 and nucleotide imbalances induced by HU and PALA. This cell line is a powerful tool for studying p53 in various cellular compartments, when combined with physical subfractionation of the cell and/or immuno-selection of megacomplexes, as well as in studying the protein-protein interactions of p53 during any form of cellular stress.

Materials & Methods

Prior to deciding to use the rAAV as the method of delivery of the TAP tag sequence into the HCT116 cells, the sequence encoding the TAP tag and 3kb of the p53 coding sequence directly upstream from the stop codon were cloned into the pIRES-neo2 vector. The cloning of this vector will be explained first (Fig 3-2), and then the use of this vector as the template for PCR in cloning the vector which was ultimately used in the gene targeting by rAAV will be described. The final vector used for inserting the TAP tag sequence into the p53 genomic locus was named pAAV-MCS p53 TAP (Fig 3-3).

Generating the template sequences used to clone the pAAV-MCS p53 TAP

Amplifying the TAP tag sequence and the 3 kb p53 coding sequence

The sequence encoding the calmodulin peptide, TEV cleavage site and protein A of the TAP tag was amplified from the p-Zome-1-C plasmid using TAP tag pZome sense primer

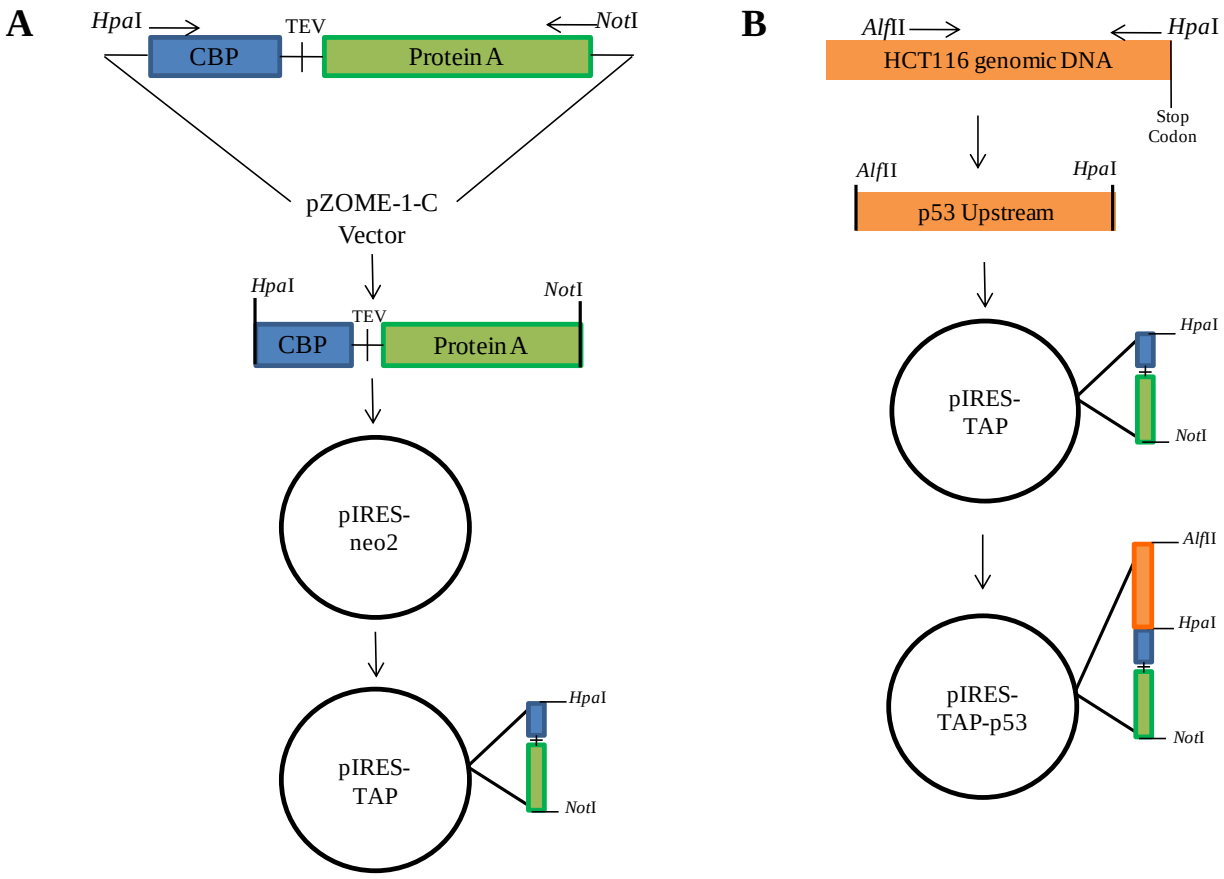

Figure 3-2. Overview of cloning the pIRES-TAP-p53 vector. A, The sequence encoding the TAP tag peptide was amplified from the pZOME-1-C vector with a sense primer with a 5′- *Hpa*I restriction site and an antisense primer with a 3′-*Not*I restriction site. The amplified TAP tag PCR product and the pIRES-neo2 vector were digested with *Hpa*I and *Not*I and ligated, generating the pIRES-TAP vector. B, The p53 coding sequence upstream from the stop codon was amplified from genomic HCT116 DNA with a sense primer containing a 5′- *Alf*II site and an antisense primer containing a *Hpa*I site. The amplified p53 upstream PCR product and the pIRES-TAP vector were digested with *Alf*II and *Hpa*I and ligated generating the pIRES-TAP-p53 vector. This vector was used as the PCR template in amplifying the left homology arm required for the cloning of the vector required for rAAV gene targeting.

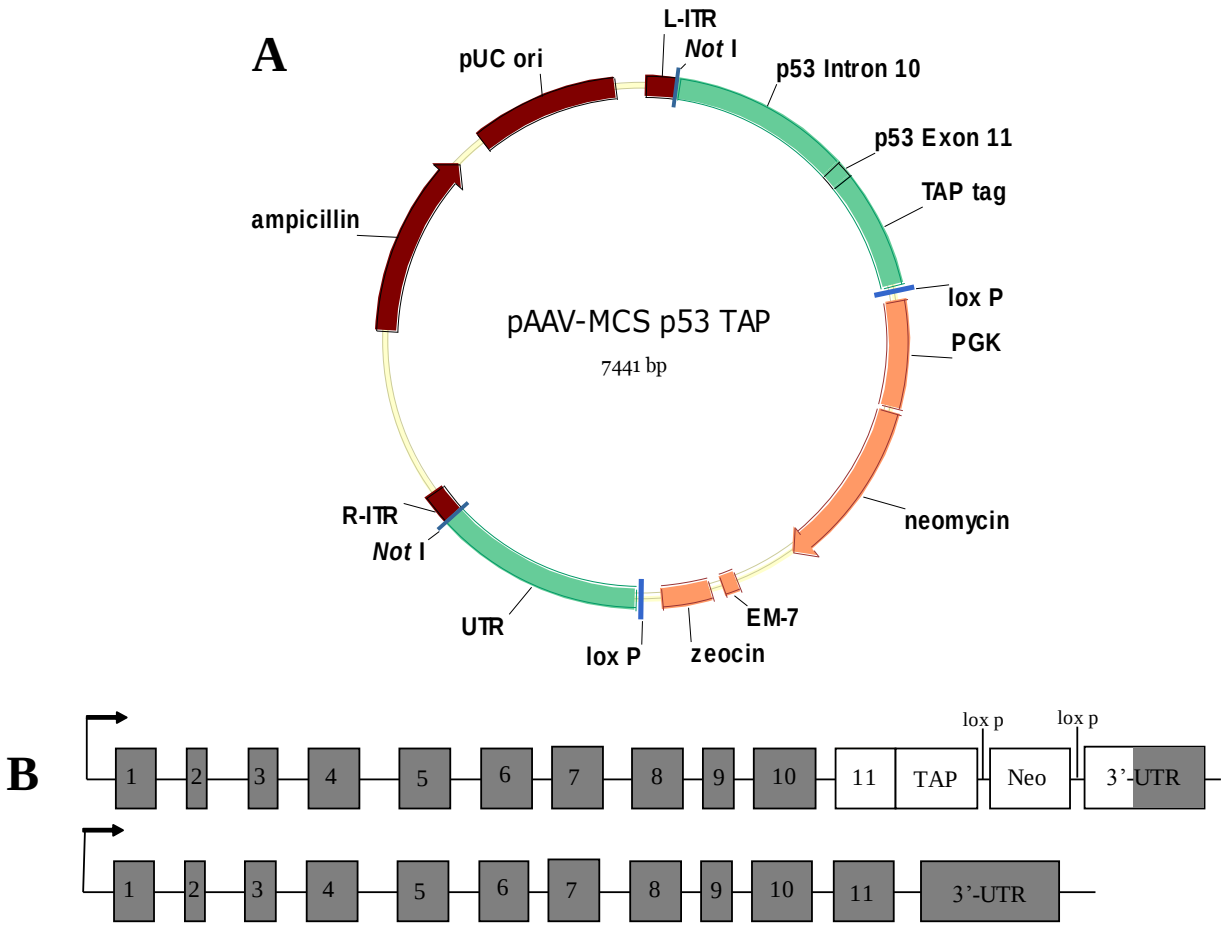

Figure 3-3. Overview of the insertion of a TAP tag into the endogenous p53 locus by homologous recombination. A, This figure shows the vector designed, cloned and transfected in the generation of the cell line. The plasmid backbone is in rust, the right and left homology sequences required for homologous recombination are in turquoise and the resistance cassettes are in peach. B, The two p53 genomic loci after homologous recombination with the transducing vector. Grey boxes indicate the endogenous exons and white indicates the exogenous sequence inserted through homologous recombination.

containing a *Hpa*I restriction site and TAP tag pZome antisense primer containing a *Not*I restriction site (Table 3-1, Fig. 3-2A) (Euroscarf, Frankfurt Germany). The 25 μL PCR reaction contained 20 mM Tris-HCl, 50 mM KCl (pH 8.4; $MgCl_2$ Free 10x PCR Reaction Buffer), 200 μM deoxynucleotides, 1.5 mM $MgCl_2$, 0.6 μM of each primer, 1 U Taq DNA Polymerase, 0.25 U PfuTurbo DNA Polymerase, 5% DMSO and 100 ng of p-Zome-1-C. The PCR program consisted of a 10 minute incubation at 94ºC, followed by 35 cycles of 94ºC for 45 second, a range of temperatures from 45ºC-42ºC to determine the optimal annealing temperature of the primers for 45 seconds, and 72ºC for 3 minutes, and finished with a final extension at 72ºC for 5 minutes. PCR products were run on a 1% agarose gel with ethidium bromide and the 600 bp product was extracted and purified using the Promega Wizard SV gel and PCR Clean-Up System. The concentration of the purified product was determined by sample absorbance at 260 nm and the sequence of the purified product was checked.

A 3 kb fragment of the genomic p53 coding sequence was amplified from 50 ng genomic DNA isolated from HCT116 cells by Fiona Turner with the Upstream p53 sense primer containing a *Alf*II restriction site and the Upstream p53 antisense primer containing a *Hpa*I restriction site (Table 3-1). The 25 μL PCR reaction contained 12.5 μL Hot StartTaq Master Mix, 0.5 U PfuTurbo DNA Polymerase and 0.3μM of each primer. The PCR program started with a 15 minute incubation at 95ºC followed by a 10 cycles of 94ºC for 45 seconds, a range of temperature from 70ºC -60ºC for 45 seconds to optimize the annealing temperature of the primers and 72ºC for 3 minutes. This was followed with an additional 35 cycles of 94ºC for 45 seconds, 59.3ºC for 45 seconds and 72ºC for 3 minutes, and finished with an extension for 15 minutes at 72ºC (Fig 3-2B). The 3 kb band was purified as stated above and the sequence was checked.

Primer	Sequence
TAP tag pZome sense	5′-AGTCTAGTTAACATGGAAAAGAGAAGATGG-3′
TAP tag pZome antisense	5′- TATTATGCGGCCGCATAACTTCGTATAATGTATGCTATACGAA GTTATCTAATTAGCGTCTACTT-3′
Upstream p53 sense	5′-CACTACTTAAGTCCCAAGTTGCTTCAACTACAGGC-3′
Upstream p53 antisense	5′-TAGATAGTTAACGTCTGAGTCAGGCCCTTCTGTC-3′
Downstream p53 sense	5′-TAACTAGTCGACATAACTTCGTATAGCATACATTATACGAAGTT ATCATTCTCCACTTCTTGTTCCCCACTG-3′
Downstream p53 antisense	5′-GTCAATCAGCTGCTGAAGCCATGAGGAAATTGGG-3′
Left homology arm sense	5′-ATACATACGCGGCCGCCATGGTCAAAGGCAGCTG-3′
Left homol arm antisense	5′-GCTCCAGCTTTTGTTCCCTTTAGCTAATTAGCGTCTACTTT-3′
Right homology arm Sense	5′-CGCCCTATAGTGAGTCGTATTACCATTCTCCACTTCTTGTTC-3′
Right homol arm antisense	5′-ATACATACGCGGCCGCTTGGCTGGCCATGGTGGCATGA-3′
Left homol-Neo sense	5′-ATACATACGCGGCCGCCATGGTCAAAGGCAGCTG-3′
Left homol-Neo antisense	5′-GCGTAATACGACTCACTATAGGGCGAATTGGGTACC-3′
Neo-right homol sense	5′-CTAAAGGGAACAAAAGCTGGAGCTCCACCGCGG-3′
Neo-right homol antisense	5′-ATACATACGCGGCCGCTTGGCTGGCCATGGTGGCATGA-3′
Exon 10 screening sense	5′-AGA GCTGAATGAGGCCTTGGAACT-3′
TAP screen antisense	5′-TAGCGCTTTGGCTTGGGTCATCTT-3′
3′-screening sense	5′-AGTCTAGTTAACATGGAAAAGAGAAGATGG-3′
3′-screening antisense	5′-CTTCCCAGCACCTCCTCACTCACCCCTG-3′

Table 3-1. The primers used in cloning the pAAV-MCS p53 TAP vector and in screening for the correct insertion of the TAP tag into the p53 genomic locus by homologous recombination.

Cloning the sequence encoding the TAP tag and p53 sequence into the pIRES-neo2 vector

The TAP tag PCR product and pIRES-neo2 vector (Clontech) were digested with *Hpa*I and *Not*I at 37ºC for 1 hour in a 20 μL reaction containing 50 mM NaCl 10 mM Tris-HCl, 10 mM $MgCl_2$, 1 mM dithiothreitol (pH 7.9), 0.1 μg/μL BSA, 10 U of *Not*I and 10 U *Hpa*I (Fig 3-2A). Following the digestion the products were electrophoresed, purified and their concentrations were determined as stated above. Ligation of 25 ng of the pIRES-neo2 vector with 9.9 ng of the TAP tag PCR product (a 3:1 molar ratio) was carried out at 16ºC for 16 hours in a 10 μL volume reaction containing 66 mM Tris-HCl, 5 mM $MgCl_2$, 1 mM dithiothreitol, 1 mM ATP (pH 7.5) and 1 U T_4 DNA ligase.

TOP10 chemically competent *E. coli* cells were transformed with the ligation product. TOP10 cells were removed from the -80ºC and thawed on ice; 4 μL of the ligation reaction was added to the TOP10 cells and mixed gently. This mixture was incubated on ice for 15-30 minutes and then heat shocked at 42ºC for 30 seconds. S.O.C. medium (2% tryptone, 0.5 % yeast extract, 10 mM NaCl, 2.5 mM KCl, 10 mM $MgCl_2$, 10 mM $MgSO_4$ and 20 mM glucose) was warmed to 25ºC and 250 μL was added to the tubes and the tubes were shaken vertically at 225 rpm at 37ºC for 1 hour in an orbital shaker. The transformed TOP10 cells were plated on Luria-Bertani (LB) plates with 100 μg/ml carbenicillin added and the plates were incubated at 37ºC for 16 hours. Only TOP10 cells which were successfully transformed would survive since the pIRES-neo2 vector contained an ampicillin resistance cassette. Eight surviving colonies were picked for expansion, inoculated into 4mL of LB medium containing carbenicillin and the tubes were shaken vertically at 225 rpm at 37ºC for 16 hours in an orbital shaker. Bacterial cells were pelleted by centrifugation at 4,000 x g and the plasmid DNA was isolated using a Promega

Wizard Plus SV Miniprep kit. All purified plasmids were digested with *Not*I and *Hpa*I as described above to check for the appropriately sized insert.

The cloned pIRES-neo2 vector, now containing the TAP tag sequence was named pIRES-TAP, and the purified p53 sequence were digested with *Hpa*I *and Afl*II for 1 hour at 37ºC in a 20 μL reaction containing 50 mM potassium acetate, 20 mM Tris-acetate, 10 mM magnesium acetate, 1 mM dithiothreitol (pH 7.9), 0.1 μg/μL BSA, 10 U *Afl*II and 10 U *Hpa*I. Following the digest, the products were electrophoresed, purified and their concentrations were determined as stated above. The pIRES-TAP plasmid and the purified p53 sequence insert were ligated as stated above with 43.7 ng of the insert and 25 ng of the plasmid. The ligation was transformed into TOP10 cells, surviving colonies were picked and mini-prepped as described above. The eight purified plasmids were checked for the correct size insert with a digestion including *HpaI I* and *Afl*II as described above. This vector was named pIRES-TAP-p53 (Fig 3-2B).

Amplifying the 3kb p53 UTR fragment

A 3kb fragment of the p53 non-coding sequence directly after the stop codon was amplified from 50 ng of genomic DNA isolated from HCT116 cells by Fiona Turner with the Downstream p53 sense primer and the Downstream p53 Antisense primer (Table 3-1) in a 25 μL reaction containing 12.5 μL Hot StartTaq Master Mix, 0.5 U PfuTurbo DNA Polymerase and 0.3 μM of each primer. The PCR program started with a 15 minute incubation at 95ºC followed by 35 cycles of 94ºC for 45 seconds, 60ºC for 45 seconds and 72ºC for 3 minutes, and finished with an extension for 15 minutes at 72ºC. The product was electrophoresed, purified and the concentration was determined as previously described and the sequence was checked.

Cloning the pAAV-MCS p53 TAP vector

Homology Arm Amplification

The left homology arm was designed to contain 900 bp of p53 sequence upstream from the stop codon and the sequence encoding the TAP tag which would provide sufficient homologous sequence with the endogenous p53 allele to allow for homologous recombination to occur with the vector. These sequences were amplified from the pIRES-TAP-p53 vector which contained 3kb of p53 coding sequence upstream from the endogenous stop codon and the TAP tag sequence. The primers used for this amplification contained a *Not*I restriction site in the Left homology arm sense primer and a 23 bp sequence referred to as a linker sequence which is required for subsequent PCR reactions in the Left homol. arm antisense primer (Fig 3-4, Table 3-1). The right homology arm was designed to contain 900 bp of p53 sequence directly downstream of the p53 stop codon to allow homologous recombination to occur with the endogenous p53 genomic locus. This sequence was amplified from the purified PCR product containing 3kb of p53 sequence directly after the stop codon. The primers used for this amplification contained a 23 bp sequence referred to as a linker sequence in the Right homol sense primer and a *Not*I restriction site in the Right homol arm antisense primer (Fig 3-5, Table 3.1). Both PCR reactions contained 12.5 μL Hot Start Taq Master Mix, 0.5 U *Pfu*Turbo DNA Polymerase and 0.3 μM of each primer. The PCR program started with a 15 minute incubation at 95ºC followed by 35 cycles of 94ºC for 45 seconds, a range of temperatures from 59ºC to 64ºC for 45 seconds was used to optimize the annealing temperature of the primers and 72ºC for 1 minute, and finished with an extension for 15 minutes at 72ºC. A total of 25 PCR reactions were done for each template to obtain sufficient PCR product for subsequent ligation steps. The

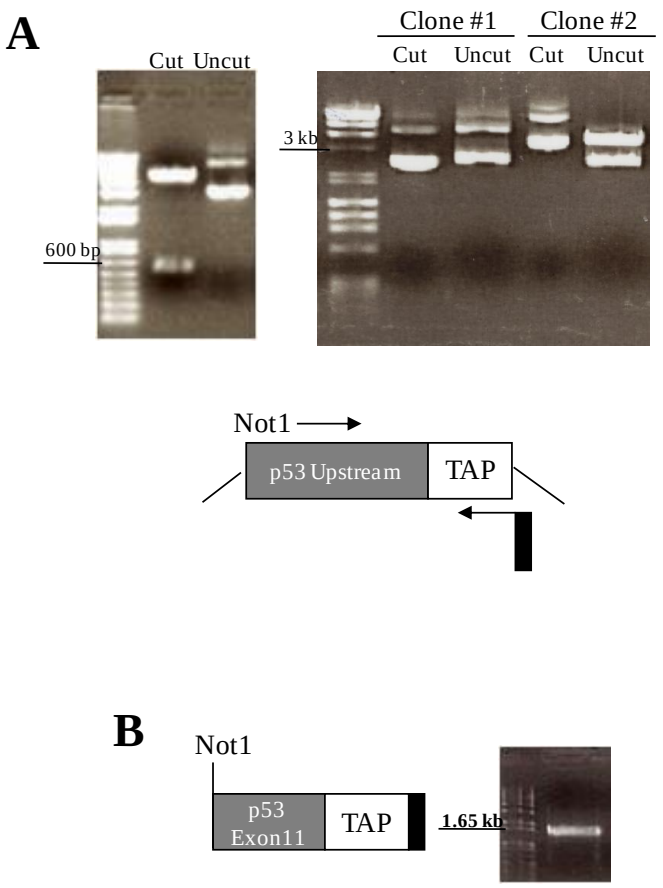

Figure 3-4. Left Homology Arm Amplification. A, Left Panel, This figure shows an agarose gel analysis of a digest of the 600 bp TAP tag sequence with *Not*I and *Hpa*I from the pIRES-TAP-p53 vector. Right Panel, This figure shows an agarose gel analysis of a digest with *Hpa*I and *Afl*II of the 3 kb p53 upstream homologous sequence from the pIRES-TAP-p53 vector. Clone 2 contained the insert of the correct size. Bottom panel, This figure is a depiction of the PCR amplification step of the Left homology arm using the sequences cloned into pIRES-TAP-p53 as template. Primer design included a sense primer with a 5′-Not1 restriction site and antisense with the 3′-23 bp linker. B, This figure is a depiction of the amplification product and agarose gel analysis of the amplified 1.5 kb product.

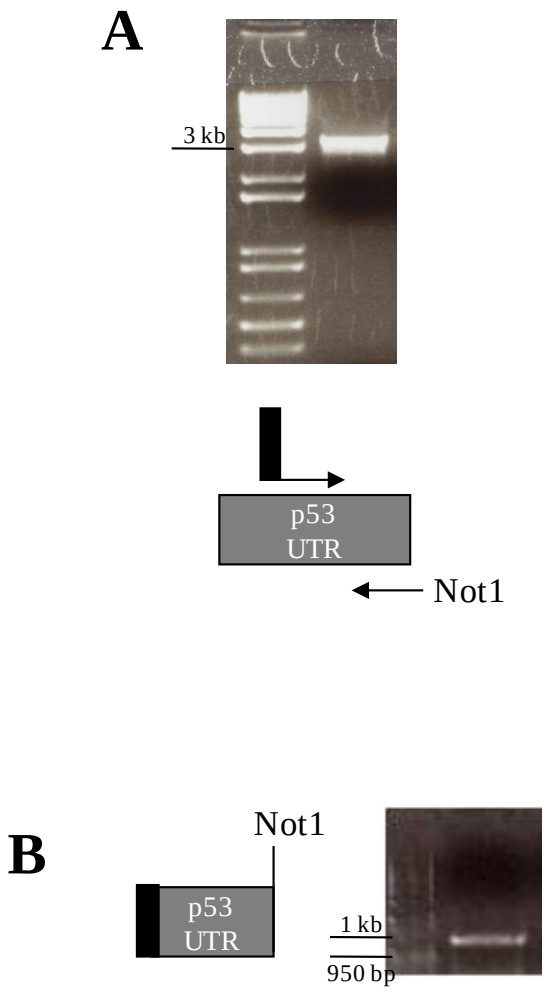

Figure 3-5. Right Homology Arm Amplification. A, Top panel, This figure is an agarose gel analysis of the 3 kb PCR product of the p53 3′-UTR sequence amplified from HCT116 genomic DNA. Primer design included an antisense primer with a 3′-Not1 restriction site and the sense primer with the 5′-23 bp linker. Bottom panel, This figure is a depiction of the PCR amplification of the right homology arm using the 3 kb PCR product as the PCR template. B, This figure is a depiction of the amplification product and agarose gel analysis of the amplified 900 bp product.

products were pooled, electrophoresed, purified and the concentrations were determined as previously described.

Digest Neomycin Cassette from pNeDaKO-Neo

The pNeDaKO-Neo vector (2 μg) (Kohli et al., 2004) was digested with *Pvu*I in a total volume of 20 μL containing 300 mM NaCl, 50 mM Tris-HCl, 10 mM $MgCl_2$, 1 mM dithiothreitol (pH 7.9), 5 U *Pvu*I, and 0.1 μg/μL BSA for 1 hour at 37ºC. The digest reaction was run on a 1% agarose gel with ethidium bromide and the 4 kb product was excised, purified and the concentration was determined as previously described. This fragment carried sequence complementary to the 23 bp linker sequence present in the primers used to amplify the homology arms.

Fusion PCR of Homology Arms and Neomycin Cassette

Figure 3-6B depicts how the linker sequences in the homology arms and neomycin cassette allowed for a 3-way PCR fusion. An equimolar PCR fusion with 30 ng of the left homology arm product and 33 ng of the neomycin cassette were incubated with the Left homol-neo sense primer designed to anneal to the 5′-end of the left homology arm sequence and the Left Homol-Neo antisense primer to anneal to the 3′-end of the neomycin cassette (Table 3-1). The 23 bp linker sequences within the homology arm and neomycin cassette acted as primers and annealed during the reaction (Fig 3-6C). The 25 μL PCR reaction contained 12.5 μL Hot StartTaq Master Mix, 0.5 U PfuTurbo DNA polymerase and 0.3 μM of each primer. The PCR program started with a 15 minute incubation at 95ºC followed by 35 cycles of 94ºC for 45 seconds, a range of temperatures from 61ºC to 64ºC for 45 seconds and 72ºC for 3.5 minutes, and

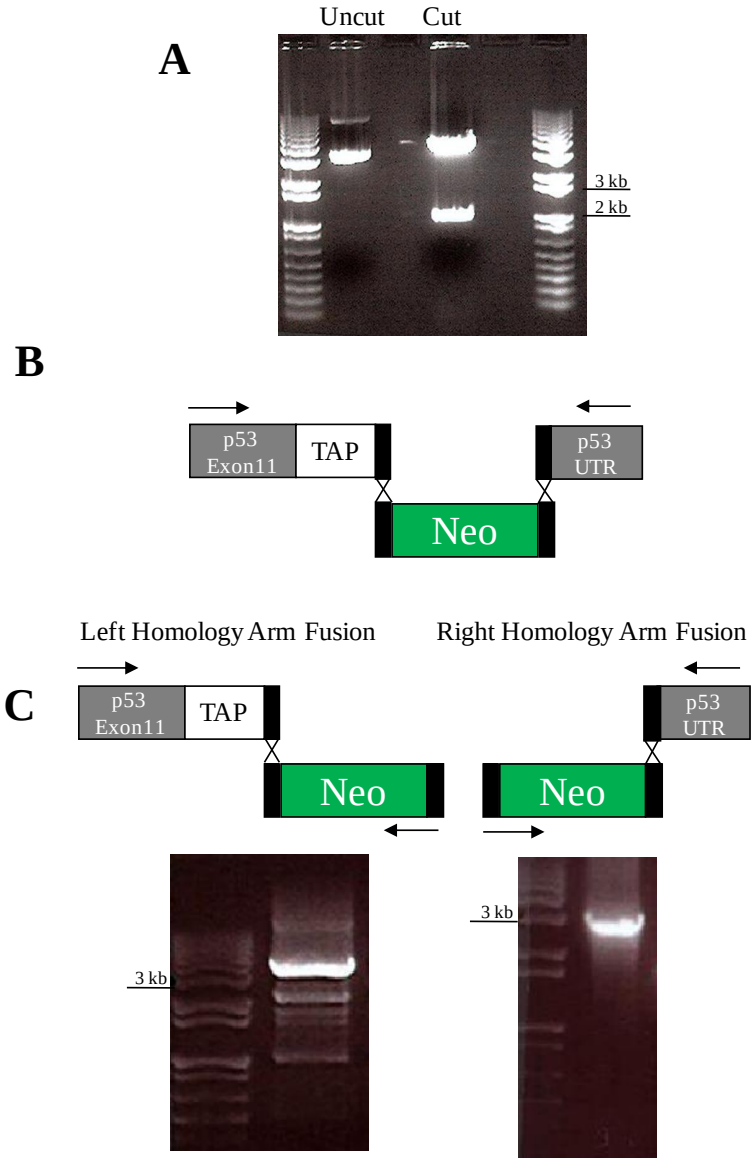

Figure 3-6. Fusion PCR of the Homology Arms with the Neomycin Resistance Cassette. A, This figure is an agarose gel analysis of a digest with *Pvu*I of the 2.2 kb neomycin cassette from the pNeDaKO-Neo vector. B, This figure is a depiction of the 3 way PCR fusion of the homology arms with the neomycin cassette which was not successfully accomplished C, This figure is a depiction of the separate PCR fusion reactions, the black rectangles depicts the 23 bp linker sequences. The agarose gel analysis of each fusion reaction is below the respective depiction.

finished with an extension for 15 minutes at 72ºC. The PCR reaction was analyzed on an 1% agarose gel, the 3.7 kb product was excised, purified and the concentration was determined as previously described. The fusion between the neomycin cassette and the right homology arm was performed in a similar fashion. The Neo-right homol sense primers were designed to anneal to the 5′-end of the neomycin cassette and the Neo-right homol antisense primer was designed to anneal to the 3′-end of the right homology arm (Table 3-1). The PCR reaction was set up as described above and the PCR program was also the same with the exception of the range of temperature used to optimize the primer annealing temperature, which was changed to 62ºC to 68ºC for this PCR fusion. The 3kb product was found to be efficiently amplified at an annealing temperature of 63ºC, it was analyzed and purified as previously stated. Both fusion products were sequenced and the sequences were compared with the known sequences of p53, the sequence encoding the TAP tag, and the known sequence of the neomycin resistance cassette.

Both resulting PCR fusions contained neomycin resistant cassettes and only one neomycin cassette is required in the final vector needed for homologous recombination. Hence, the neomycin cassette from the right homology arm was removed with a digest containing *Kpn*I. The left homology arm was also cut with *Kpn*I to generate compatible sticky ends required for the subsequent ligation with the right homology arm (Fig 3-7). The *Kpn*I digestions were performed for one hour at 37ºC in a reaction volume of 50 μL containing 10 mM Tris HCl, 10 mM $MgCl_2$, 1 mM dithiothreitol (pH 7.0), 10 U *Kpn*I and 0.1 μg/μL BSA. The reaction were analyzed on a 1% agarose gel and the 3.6 kb left homology arm and the 943 bp right homology arm were gel purified and their concentrations were determined. The two purified homology arms were ligated together for 16 hours at 16ºC in a solution contain T4 ligase and ligase buffer

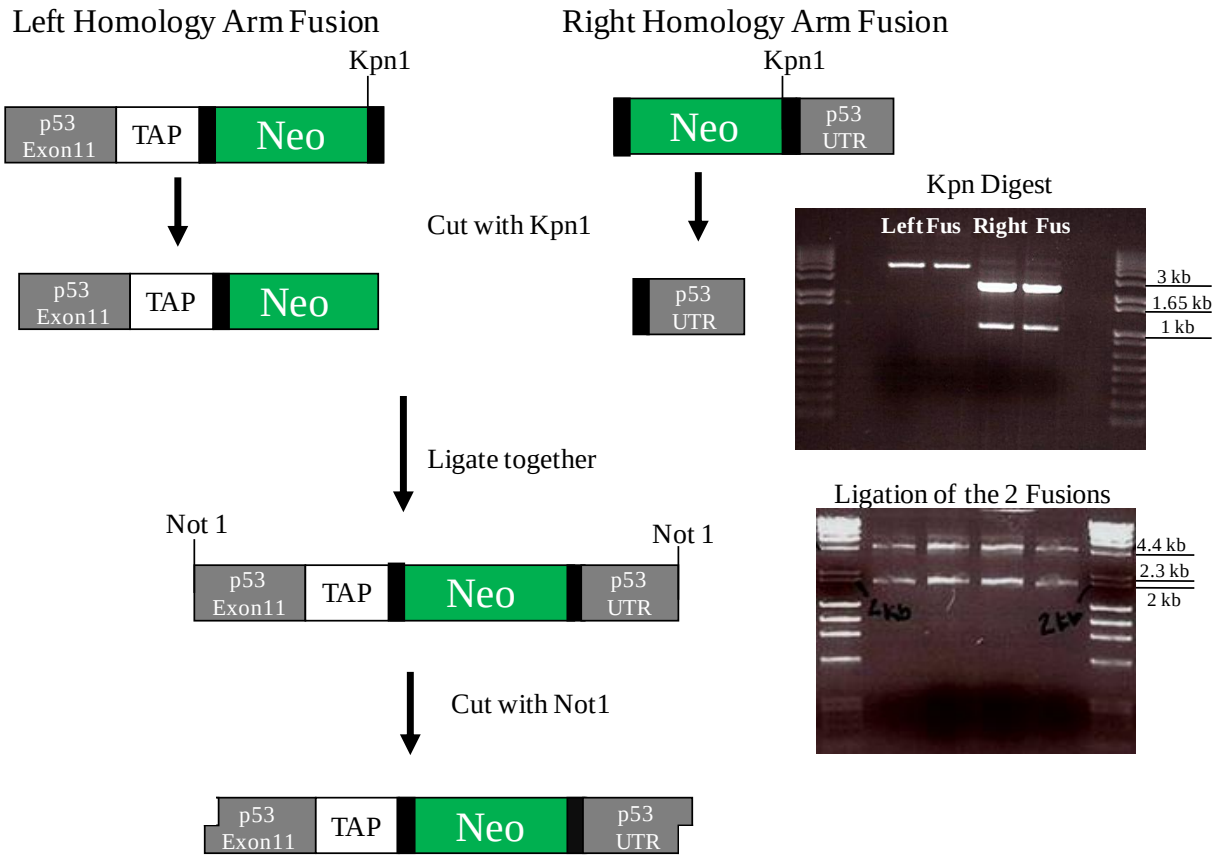

Figure 3-7. Generation of the Cloned Insert Necessary for Gene Targeting. The top half of the figure demonstrates how the left homology arm was digested with *Kpn*I to remove the 23 bp linker and right homology arm was digested with *Kpn*I to remove the neomycin cassette. Analysis by agarose gel is the right of the depiction. The bottom half demonstrates the ligation of the left and right homology arms creating the 4.5 kb insert necessary for gene targeting. Prior to cloning the fragment into the pAAV MCS vector the insert was digested with *Not*I generating compatible ends. Agarose gel analysis of the ligation is to the right of the figure, the total volume of the ligation was loaded into the four lanes.

as previously described. The ligation product was run on a 1% agarose gel and the 4.5 kb band was excised and purified as described above.

Cloning the insert into the pAAV-MCS vector

The pAAV-MCS vector was digested with *Not*I for two hours at 37ºC in a 200 μL reaction containing 300 mM NaCl, 50 mM Tris-HCl, 10 mM $MgCl_2$, 1 mM dithiothreitol (pH 7.9), 40 U *NotI*, 0.1 μg/μL BSA and 2μg of the vector. *Not*I was heat inactivated for 20 minutes at 65ºC and the vector was dephosphorylated with 20 U calf intestinal alkaline phosphatase for one hour at 37ºC. The vector was phenol:chloroform extracted by adding one volume of phenol:chloroform (ratio 1:1) to the reaction, the tube was vortexed and centrifuged at 16,100 x g for 15 minutes at 4ºC in a tabletop centrifuge. The top (aqueous) layer was recovered and 1/10 volume of 3 M NaOAc and 2 volumes of 100% ethanol were added, the tubes were vortexed and incubated at -80ºC for one hour to precipitate the DNA. The sample was thawed and spun down at 16,100 x g for 15 minutes at 4ºC to pellet the DNA. The supernatant was poured off and washed with one volume of 70% ethanol. The DNA was pelleted by centrifugation at 16,100 x g for 15 minutes at 4ºC. The supernatant was poured off and the pellet was dried for 5 minutes. The pellet was resuspended in 20 μL H_2O and the dissolved cut plasmid was purified on a 1% agarose gel and the 3 kb cut vector was isolated (Fig 3-8). The 4.5 kb insert containing the left homology arm-TAP tag sequence-right homology arm was cut with *Not*I and gel-purified.

The insert and vector were ligated at a 3:1 molar ratio as described above. The ligation reaction was transformed into TOP10 chemically competent *E. coli* cells and plated on LB plates. Fifty colonies were picked, each was inoculated in LB containing 50 μg/mL carbenicillin

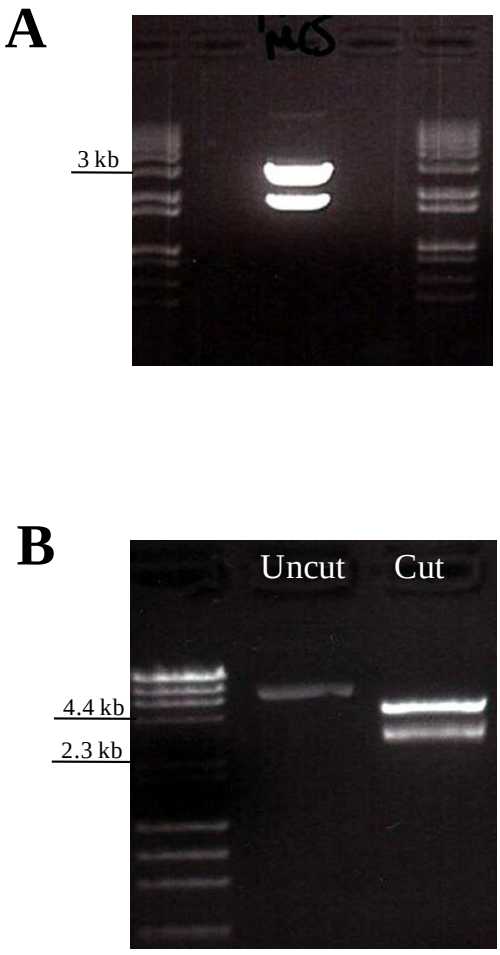

Figure 3-8. Cloning the Insert into the pAAV-MCS vector. A, This figure is an agarose gel analysis of a digest with *Not*I of the pAAV-MCS vector. The 3kb vector backbone was gel purified and used in the subsequent ligation. B, This figure is an agarose gel analysis of a digest with *Not*I to verify the 4.5 kb insert after the ligation, transformation in TOP10 competent *E. coli* cells and vector purification from the surviving colonies.

and 40 μg/ml zeocin and the cultures were incubated for 16 hours at 37ºC with shaking. Mini-prepped plasmids were prepared from each culture. The purified plasmids were digested with *Not*I to check for the correct size insert (Fig 3-8). The pAAV MCS p53TAP vectors were sequenced.

Packaging and isolating the rAAV

HEK293 cells (ATCC) were grown in DMEM supplemented with 10% dFBS and 100 U/mL of penicillin and 100 mg/mL of streptomycin at 37ºC with 5% CO_2. Cells were grown to 80% confluency in a T-75 flask prior the transfection. A mixture of 2.5 μg of pAAV MCS p53TAP and 2.5 μg of each helper plasmid, pAAV-RC and pHelper was diluted in Opti-MEM reduced serum medium to a total volume of 750 μL. Lipofectamine 2000 reagent (54 μg) was mixed with Opti-MEM medium to a total volume of 750 μL. The two tubes were combined and incubated at 25ºC for 15 minutes. The HEK293 cells were washed with 10 mL Hank's Balanced Salt solution and 7.5 mL of Opti-MEM medium was added to the flask. The transfection mixture was added drop-wise to the flask and incubated for four hours. The Opti-MEM medium was removed and replaced with DMEM medium and the flask was incubated at 37ºC. Forty-eight hours after the transfection, the packaged adeno-associated virus was collected from the HEK293 cells (Fig 3-9). The DMEM medium was aspirated and the cells were scraped off into 1.5 mL of PBS. The cells were freeze thawed three times in a 70% ethanol and dry ice bath for 10 minutes with intermediate thaws in a 37ºC water bath. The cells were pelleted at 12,000 x g at 25ºC for 10 minutes and the supernatant was stored in three 500 μL aliquots at -80ºC.

Transducing HCT116 cells with the packaged rAAV

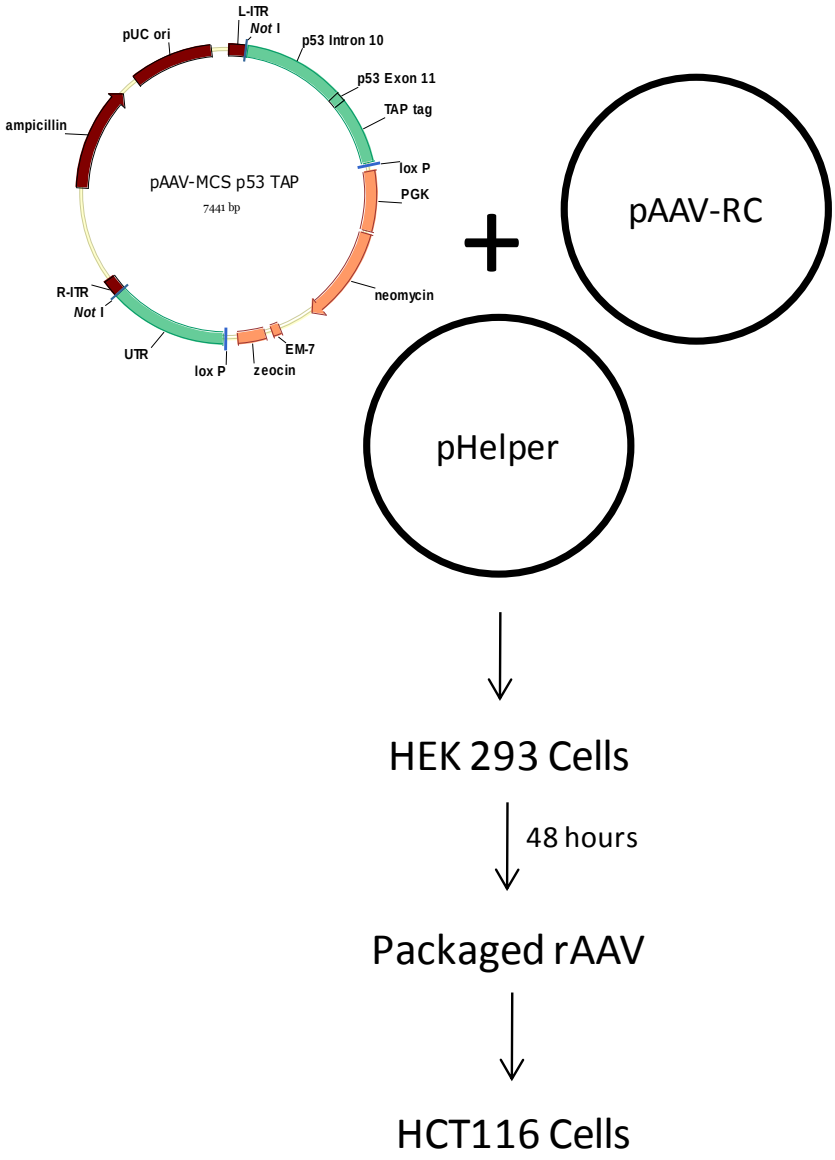

Figure 3-9. The process of packaging the rAAV with the pAAV-MCS p53 TAP vector. The cloned pAA-MCS p53 TAP vector, pHELPER and pAAV-RC helper vectors were cotransfected into HEK 293 cells. The rAAV was extracted from the cells after 48 hours and an aliquot of the isolated virus was used to transduce HCT116 cells**.**

HCT116 cells (ATCC) were grown in RPMI 1640 supplemented with 10% dFBS and 100 U/mL of penicillin and 100 mg/mL of streptomycin at 37ºC with 5% CO_2. A 75% confluent culture in a T-75 flask was washed once with Hanks Balanced Salt Solution, an aliquot of the isolated rAAV was thawed on ice and added to the culture mixed with 4 mL of RPMI 1640. After two and a half hours, the virus mixture was removed and 8 mL of fresh RPMI 1640 was added to the flask. The cells were plated out under 0.4 mg/mL geneticin (G418) selection in ten-96 well plates at 200 μL per well, 48 hours after transduction. The plates were wrapped with parafilm to minimize evaporation and placed in the incubator for 10 days. Wells clearly containing only one cell clone were marked. The medium was aspirated and 100 μL of trypsin was added to each marked well and incubated at 37ºC for two minutes. Duplicate plates were made with the trypsinized clones by adding 50 μL of each cell suspension to 150 μL RPMI 1640 with 10% dFBS, 100 U/mL of penicillin and 100mg/mL of streptomycin and 0.4 mg/mL G418 (complete medium) in new 96-well plates. A total of 144 single cell clones were re-plated in duplicate. After four days the cells were expanded into duplicate 24-well plates by trypsinization. One set of 24 well plates were used for screen the clones for correct recombination while the other duplicate plate was placed in -80ºC after addition of 300 μL of freezing medium (10% DMSO in dFBS).

Screening cell clones for correct insertion of the TAP tag into the endogenous *p53* locus

The Exon 10 screening sense primer was designed to anneal to exon 10 in the endogenous p53 genomic locus and the TAP screen antisense primer was designed to anneal to TAP tag sequence within the insert (Fig 3-10, Table 3-1). The primer placement allowed for screening for the correct orientation of the TAP tag insertion by homologous recombination

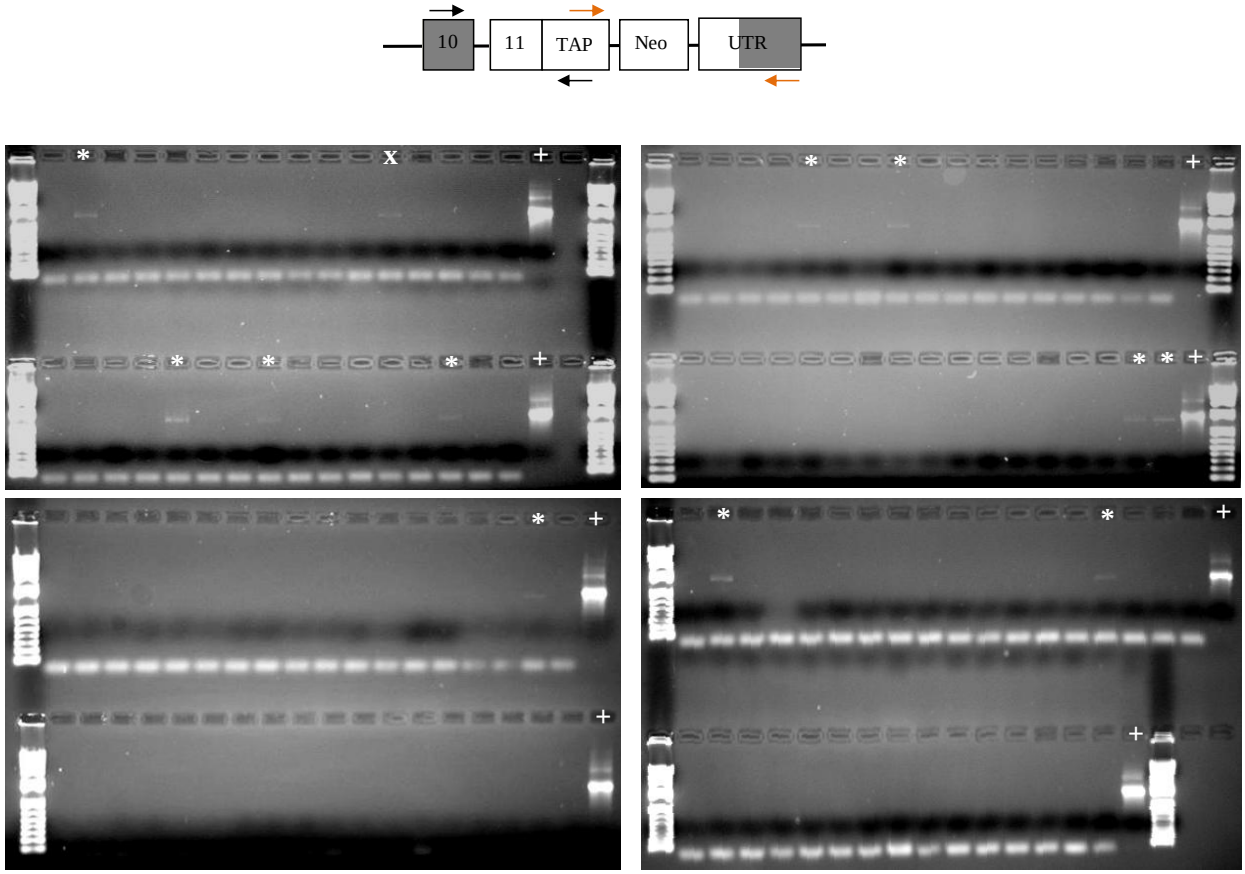

Figure 3-10. PCR screening for the correct insertion of the TAP tag into the p53 genomic locus by homologous recombination. The top of the figure depicts the screening process including the strategic placement of the black screening primers with one primer located in the genomic sequence outside of the cloned insert and the other placed inside the insert. The orange primers denote the 3′ screening process. The bottom figure is the agarose gel analysis of 140 clones screened with the 5′-screening primers (black). The plus sign denotes the lanes containing the positive control, the asterisks denote clones containing the correct location of insertion as verified by the 1.4 kb PCR product of the insert and the X denotes a false positive that was determined in subsequent PCR reactions.

since one screening primer was located outside of the insert and the other was placed within the insert. The pIRES-p53-TAP vector was used as the positive control for the screening process. The PCR program was optimized with the positive control vector in a 25 μL reaction volume containing 12.5 μL Hot StartTaq Master Mix and 0.6 μM of each primer. The PCR program started with a 15 minute incubation at 95ºC followed by 30 cycles of 94ºC for 45 seconds, 57ºC for 45 seconds and 72ºC for 1.5 minutes, and finished with an extension for 10 minutes. The reaction was analyzed on a 1% agarose gel containing ethidium bromide. Genomic DNA was isolated from the 24-well plates using the Promega Wizard SV genomic DNA purification system and the concentration was determined by sample absorbance at 260 nm. All genomic DNA samples were diluted down to a concentration of 50 ng/mL with H_2O; 1 μL of each gDNA sample was added to the previously described PCR reaction. A positive control and a blank reaction containing water was including in all screening reactions. The PCR products were run out on a 1% agarose gel and analyzed for a 1.4 kb product indicating correct homologous recombination. The PCR product from the screening procedure from 4 clones containing the TAP tag at the correct orientation were excised from the agarose gel and purified as previously described. The purified PCR screening product was cloned into the pCR4-TOPO vector for sequencing using the TOPO TA Cloning Kit for Sequencing (Invitrogen). A 6 μL reaction containing 0.2 M NaCl and 10 mM $MgCl_2$ (Salt Solution), 4 μL of purified DNA and 1 μL pCR4-TOPO was incubated at 25ºC for 30 minutes. TOP10 chemically competent *E. coli* cells were transformed with 2 μL of each reaction. Bacteria were plated, expanded and mini-prepped. The purified plasmids were cut with *EcoR*I to check for the correct insert size. The reactions were run on a 2% agarose gel containing ethidium bromide and one plasmid containing the purified product from each of the four cell clones that containing the correct insert was

sequenced. Clone number AA5 contained no mutations, the duplicate plate containing this well was removed from the -80ºC and was thawed in a water bath. A volume of 2 mL of complete medium was added to the well containing this clone and placed into a 15 mL conical tube and spun down. The pellet was resuspended in 5 mL of complete medium and plated into a T-25 flask. This cell line was named AA5 TAP. The 3′-end of this clone was screened by PCR to make sure that only the insert and no other parts of the vector homologously recombined with the p53 locus. The 3′-screening sense primer was designed to anneal within the TAP tag and the 3′ -screening antisense primer was designed to anneal within the 3′ UTR of p53 outside of the insert (Fig 3-10, Table 3-1). The PCR reaction contained primers at a concentration of 0.3 μM and started with a 15 minute incubation at 95ºC followed by 35 cycles of 94ºC for 45 seconds, 53.9ºC for 45 seconds and 72ºC for 2 minutes, and finished with an extension for 10 minutes. The PCR product was electrophoresed and the 1.3 Kb product was excised, purified and sequenced.

Western Blotting

Cellular Lysate preparation

HCT116 and AA5 TAP cells were plated at 8 x 10^5 cells/10 cm dish and allowed to adhere 24 hour prior to drug treatment. Etoposide (VP16, Sigma) was dissolved in DMSO making a 10 mM stock and then diluted in PBS to 100 μM prior to use. The 100 μM solution of VP16 was filter sterilized with a 0.22 μM filter, 1 mL of it was added to 9 mL complete medium added to the treatment plates. The no treatment plates received 9 mL complete medium with the same dilution of DMSO used in the VP16 plates. Preparations of cellular lysates and Western blotting were performed as described in Chapter 2. Briefly, 25 μg of total cellular protein was

resolved by electrophoresis on a 7.5% -polyacrylamide gel (BioRad) and transferred to a PVDF membrane. Non-specific protein binding was blocked with Blotto solution containing 5% milk, 0.1% Tween 20, 0.01 M Tri, pH 7.4, 0.15 M NaCl for 1 hour at 25ºC with gently rocking. Primary antibody was diluted in 5% milk in TBS-T and incubated with the membrane overnight at 4ºC. Primary antibodies used were p53 monoclonal Ab-6 (Calbiochem) at 1:100, p21 monoclonal Ab-1 (Calbiochem) at 1:100, TAP polyclonal (Open Biosystems CAB1001) at 1:500 and monoclonal beta Actin (Abcam) at 1:5000. Membranes were incubated with secondary antibodies conjugated to horseradish peroxidase (Pierce) diluted in 5% milk in TBS-T for 1 hour at 25°C. Complexes were detected by enhanced chemiluminescence using the Supersignal West Pico Chemiluminescent Substrate Kit (Pierce).

Removing the neomycin cassette with cre recombinase

Dr. Jolene Windle generously provided a plasmid, pMC1 CRE, in which the *cre* recombinase can be expressed in mammalian cells under the control of a thymidine kinase promoter. This plasmid was transformed into TOP10 chemically competent *E. coli* cells and purified using with the Promega Pure Yield Plasmid Midiprep System and checked with a digestion for one hour at 37ºC in a 20 μL reaction containing 10 U *Eco*RV, 10 U *Sal*I, NEB3, and 0.1 μg/μL BSA. The reaction was run on a 1% agarose gel to check correct product size. AA5 TAP cells were plated in a 60 mm dish with RPMI 1640 with 10% dFBS and allowed to reach 90% confluency. A total of 8 μg of pMCI CRE was diluted into 500 μL Opti-MEM medium and 20 μg of Lipofectamine 2000 was added to 480 μL Opti-MEM medium; both mixtures were incubated at 25ºC for 5 minutes, then combined, gently mixed and incubated for 20 minutes at 25ºC before adding the mixture to the cells. Twenty-four hours after transfection

the transfected cells were trypsinzed and plated at 0.25 cell/well in five 96-well plates in RPMI 1640 with 10% dFBS and 100 U/mL of penicillin and 100 mg/mL of streptomycin. The plates were wrapped in parafilm and placed in the incubator for 12 days. Wells containing only one cell clone were marked and trypsinzed and split into duplicate sets of 24-well plates as previously described. Cells were allowed to adhere for 24 hours, the medium was then replaced on both sets of plates. One set received complete medium containing 0.4 mg/mL G418 while the duplicate set received complete medium without G418. Five days after selection clones that were not G418 sensitive were trypsinized and expanded in T-75 flasks with complete medium not containing G418. This cell line was named CRE2 TAP.

Chromatin Immunoprecipitation

The ChIP assay was performed as described in Chapter 2. Briefly, 1 x 10^7 HCT116 cells or CRE2 TAP cells per treatment were crosslinked at room temperature with 1% formaldehyde. Aliquots of 2 x 10^6 washed cells were lysed and sonicated with the Diagenode bioruptor for a total of 18 minutes in consecutive duty cycles of 30 seconds on, 30 seconds off (for a total of 3 cycles, each being 6 minutes). These conditions were found to yield DNA fragments less than 1000 bp in size. Lysate volumes corresponding to 2 x 10^6 cells were precleared and blocked with 8 μg of BSA and 5 μg of sonicated lambda DNA, then were incubated with 2 μg of p53 Ab-6 (Calbiochem) antibody, 2 μg TAP antibody directed against the calmodulin peptide (Open Biosystems) or 2 μg IgG (Millipore) antibody overnight. Antibody-protein-DNA complexes were captured by the addition of 30 μL of 50% protein G-Sepharose bead slurry. Beads were extensively washed as previously described. Protein-DNA complexes were eluted with elution buffer containing 2% SDS, 10 mM DTT, 0.1 M $NaHCO_3$ and incubated at 65ºC overnight to

reverse the crosslinks. DNA was treated with RNase, Proteinase K, phenol-chloroform extracted, ethanol-precipitated as previously described, and dissolved in 100 μL of TE.

Quantitative PCR

Q-PCR was performed with 1 μL of input DNA or ChIP DNA per a 25 μL reaction containing 12.5 μL Quantitect SYBR Green PCR Master Mix (Qiagen), 0.3 μM of each primer. The sequences of the primers for the upstream p53 consensus binding site on the p21 promoter were 5′-CTTTCCACCTTTCACCATTCC-3′ (sense) and 5′-AAGGACAAAATAGCCACCAGC-3′ (antisense). The amplification conditions were 95ºC for 15 minutes, 40 cycles of 95ºC for 45 seconds, 53ºC for 45 seconds, 72ºC for 45 seconds with a plate read between cycles followed by a 5 minute extension at 72ºC and a determination of the melting curve from 45ºC to 100ºC. Quantities were calculated using a standard curve ranging from 100 ng to 0.8 ng of input DNA.

Tandem Affinity Purification of p53

Cellular Lysate Preparation

Approximately 8 x 10^8 CRE2 TAP cells were used for each purification. CRE2 TAP cells were plated at 4 x 10^6 cells/15 cm dish in forty dishes per drug treatment containing RPMI 1640 with 10% dFBS and allowed to adhere for 24 hours. Cells were treated for 24 hours with either VP16, HU or PALA as previously described. Cells were trypsinzed, washed twice with PBS containing 1x protease inhibitor complete cocktail (Roche) and resuspended in 8 mL Tween-20 lysis buffer containing 50 mM HEPES pH 7.5, 150 mM NaCl, 1 mM EDTA, 2.5 mM EGTA 0.1% Tween-20. All purification buffers contained 1 μg/mL aprotinin, 1 μg/mL

leupeptin, 1 mM PMSF, 1 mM Na_3VO_4, 1 mM NaF. Lysates were sonicated on ice using the Misonix Sonicator 3000 with the 1/16" microtip for 40 cycles of 1 second on, 5 seconds off at 4 ºC while on ice and then incubated on ice for 30 minutes.

IgG Purification and TEV Cleavage

Cell debris was spun down at 16,100 x g for 15 minutes at 4ºC. An aliquot (200 μL) IgG Sepharose 6 Fast Flow beads (GE Healthcare) that were washed with Tween-20 Lysis buffer and a 50 % bead slurry was added to the clarified supernatant. The IgG bead suspension was incubated at 4ºC for 4 hours while rotating end-over-end. The beads were pelleted at 2,500 x g for 1 minute at 4ºC and washed three times with Tween-20 lysis buffer and three times with TEV buffer containing 50 mM Tris pH 8.0, 0.5 mM EDTA. The p53 complex was cleaved from the IgG beads in a 300 μL reaction containing 50 mM Tris, pH 8.0, 0.5 mM EDTA, 1.0 mM DTT and 100 U AcTEV Protease (Invitrogen) TEV protease cleavage proceeded for 16 hours at 4ºC rotating end-over-end.

Calmodulin Purification

The IgG beads were pelleted at 2,500 x g for 2 minutes at 4ºC and the supernatant was removed and added to 200 μL of the 50% slurry of Calmodulin Sepharose 4B (GE Healthcare). The IgG beads were washed three times with 300 μL calmodulin binding buffer containing 10 mM Tris pH 8.0, 150 mM NaCl, 1 mM magnesium acetate, 1 mM imidazole, 0.1% NP-40, 2 mM EGTA, 10 mM 2-mercaptoethanol and each wash was added to the saved supernatant. Aliquots of a concentrated stock of 1M $CaCl_2$ was added to the lysate-calmodulin slurry to achieve a final concentration of 4 mM and the mixture was incubated for 4 hours at 4ºC while

rotating end-over-end. The beads were pelleted by centrifugation at 2,500 x g for 2 minutes at 4ºC and washed three times with calmodulin binding buffer. The p53 protein complex was eluted in eight 200 μL fractions with calmodulin eluting buffer (10 mM Tris pH 8.0, 150 mM NaCl, 1 mM magnesium acetate, 1 mM imidazole, 0.1% NP-40, 2mM EGTA, 10 mM 2-mercaptoethanol). Aliquots of IgG Beads and Calmodulin beads from this procedure were resuspended in 100 μL SDS sample buffer containing 62.5 mM Tris pH 6.8, 5% glycerol, 2% SDS, 5% 2-mercaptoethanol, boiled for five minutes, pelleted and the supernatant was saved along with samples from each step of the purification for further analysis. All samples were stored at -80ºC for further analysis.

Analysis of Tandem Affinity Purification

The concentrations of the soluble and insoluble fractions after sonication were quantitated with the Bradford assay as previously described. Samples collected throughout the purification process and eluted fractions were resolved on a 4-15% gradient SDS polyacrylamide gel. Soluble and insoluble starting materials (25 μg) were used while the remaining samples were loaded onto this gel based on estimations of their protein concentrations and equal volumes of eluted fractions were added to each well. One set of gels underwent silver staining using the Bio-Rad Silver Stain plus according to manufacturer's instructions (161-0449) while the other set was immunoblotted for the presence of p53.

Results

The experiments in Chapter 3 describe the design, development, and characterization of a HCT116-derived cell line in which one endogenous p53 locus has been manipulated to include

the TAP tag sequence in frame at the 3′ end of the p53 coding sequence. This cell line was created to allow a proteomic analysis of the molecular role of p53 during nucleotide pool imbalances. Specifically, we wished to investigate how p53 is involved in the decision to promote apoptosis or a cytostatic S-phase arrest.

Design and Molecular Cloning of the pAAV vector that will allow insertion of the TAP-tag sequence in the p53 gene

The vector that was designed and constructed in order to insert the TAP tag into the endogenous p53 locus is shown in Figure 3-3 and the strategy for construction of this targeting vector is show in Figure 3-2. Two fragments of DNA identical to regions of the p53 genomic sequence were amplified from HCT116 genomic DNA and inserted into a pAAV vector, one on each side of a sequence encoding the TAP-tag peptides. To obtain high efficiencies of gene targeting, a minimum of 900 bp of homologous sequence upstream and downstream from the gene targeting site was previously shown to be required (Kohli et al., 2004). The TAP tag sequence and approximately 3 kb of sequence upstream from the stop codon in the p53 genomic sequence was isolated by PCR and ligated into the pIRES vector (See Methods, Fig 3-2), including all of the coding sequence of exon 11 (79 nucleotides) and 2921 nucleotides of intron 10. The sequence encoding the TAP tag was excised from the pIRES-TAP vector with *Not*I and *Hpa*I to verify the correct size (Fig 3-4A, left panel). After the TAP tag sequence was ligated into pIRES, the 3 kb of p53 sequence upstream from the stop codon in the p53 genomic sequence was ligated into the vector upstream of the TAP tag sequence to create the pIRES-TAP-p53 vector (Fig 3-2). This 3 kb fragment was excised from pIRES-TAP-p53 vector with *Hpa*I and *Afl*II to verify the correct size (Fig 3-4A, right panel). The pIRES-TAP-p53 vector was used as

the template for amplifying the left homology arm needed for the targeting vector. This homology arm contained 900 bps of the upstream p53 coding sequence, which includes 79 nucleotides from exon 11 ending immediately upstream of the stop codon, 821 nucleotides of intron 10 and the TAP tag sequence. The primers for this PCR reaction were designed to contain a *Not*I restriction site on the 5′-end of the sense primer and to include a 23 bp linker sequence on the 3′-end of the antisense primer that would be required for future cloning reactions. The resulting 1.5 kb fragment amplified with these primers contained 900 bps of homologous p53 sequence followed by the TAP tag sequence, with a *Not*I site at the 5′-end and the linker sequence at the 3′-end (3-4B). The right homology arm contained 900 bp of homologous sequence from the p53 3′-untranslated region (UTR) sequence directly following the stop codon. Previously, a 3 kb fragment was amplified from HCT116 genomic DNA with primers starting after the stop codon and extending for 3 kb (Fig 3-5A). This PCR fragment was used as the template for the amplification of the 900 bp needed for the right homology arm. New primers were designed to include the 23 bp linker sequence and a *Not*I restriction site for this amplification. The resulting PCR product was a 900 bp product with the linker sequence at the 5′-end and a *Not*I restriction site at the 3′-end (Fig 3-5B). The neomycin selection cassette was digested out of the pNeDaKO-Neo plasmid obtained from the Vogelstein group (Kohli et al., 2004) with *Pvu*I (Fig 3-6A). The resulting 2.2 kb fragment contained a mammalian neomycin selection marker and a zeocin bacterial selection marker flanked with loxP sites and the 23 bp linker sequence on both ends. The 23 bp linker sequences on each end of the neomycin cassette and the complementary linker sequences on the left and right homology arms were designed to allow for a three-way PCR fusion using primers designed to anneal at the 5′-end of the left homology arm and at the 3′-end of the right homology arm (Fig 3-6B). Many variations of this

PCR fusion were attempted with several combinations of primer sets, yet the product was never amplified, so two two-way fusions with the neomycin cassette were performed (Fig 3-6C). The left homology arm was fused with the neomycin cassette with primers designed against the 5′-terminus of the left homology arm and against the 3′-end of the neomycin cassette. The 3.7 kb fusion product was amplified and purified (Fig 3-6B left). A similar reaction was performed with the right homology arm and neomycin cassette. The 3.2 kb fusion product was amplified and purified (3-6B, right panel). Each homology arm contained a neomycin cassette and only one cassette was needed in the final product, so the neomycin cassette was digested off the right homology arm fusion with *Kpn*I (Fig 3-7, top panel). The left homology arm fusion also was digested with KpnI to remove the 23 bp linker (Fig 3-7). As a result from the digest, the purified products both contained complementary sticky ends and they were easily ligated together to form the 4.5 kb insert necessary for the gene targeting (Fig 3-7, bottom panel). The insert was digested with NotI as was the pAAV MCS vector (Fig 3-7, 3-8A). The 3 kb vector backbone was mixed with an equimolar amount of the 4.5 kb insert and joined with DNA ligase. To verify that the correct ligation took place, the insert was cut from the pAAV MCS vector with *Not*I and sized on an agarose gel (Fig 3-8B). Four out of 50 screened clones contained the correct size insert. The resultant vector was named pAAV MCS p53 TAP

Generation and Characterization of the p53 TAP-tagged Cells

The cloned pAAV MCS p53TAP vector in combination with two helper vectors were transfected into HEK 293 cells for viral packaging. The virus was collected from the HEK 293 cells after 48 hours and used to transduce HCT116 cells (see methods and Fig 3-9). A total of 140 neomycin resistant cell clones were propagated and screened by PCR for correct integration

of the TAP tag in the p53 locus. Two different primer sets were used for the PCR screening for homologous recombinants; one set tested the 5′- insertion site and the other tested the 3′-insertion site. Each set contained one primer corresponding to the TAP sequence and one outside of the insert to verify insertion specifically into the p53 gene locus in the correct orientation (Fig 3-10). Out of the 140 screened cell clones, 11 contained the TAP tag inserted into the correct location within the p53 gene locus as is seen by the 1.4 kb product amplified for a 7.9% efficiency of homologous recombination (Fig 3-10). Several clones containing the TAP tag were expanded and then sequenced to ensure proper insertion and presence of all essential sequence elements. Clone A-A5 was used for all subsequent experimentation (Fig 3-11).

The sequence that was inserted into the p53 genomic locus added about 25 kDa to the mass of the expressed p53. Data from western blot experiments should show two bands when probed for p53, a band at 53 kDa for the un-altered p53 allele and one band at 78 kDa for the TAP-tagged allele. Initial experiments with the TAP tag cell line showed that the p53 that was transcribed and translated from the TAP tagged allele, was able to be stabilized, following VP16-induced DNA damage. However, the protein levels made from the TAP tagged p53 allele were not comparable to the p53 protein transcribed and translated from the wild-type, un-altered allele (Fig 3-12).

We hypothesized that insertion of the 2.2 kb neomycin resistance cassette moved the polyadenylation tail further away from the p53 coding sequence thus altering the stability of the mRNA. Since the neomycin resistance cassette had been designed to be flanked with loxP sites in the case this happened, it was removed by a transient transfection of the pMC1 CRE vector containing the *cre* recombinase gene. Duplicate plates of single cell transfected clones were propagated. One set of plates was exposed to G418 while the other set contained no selection

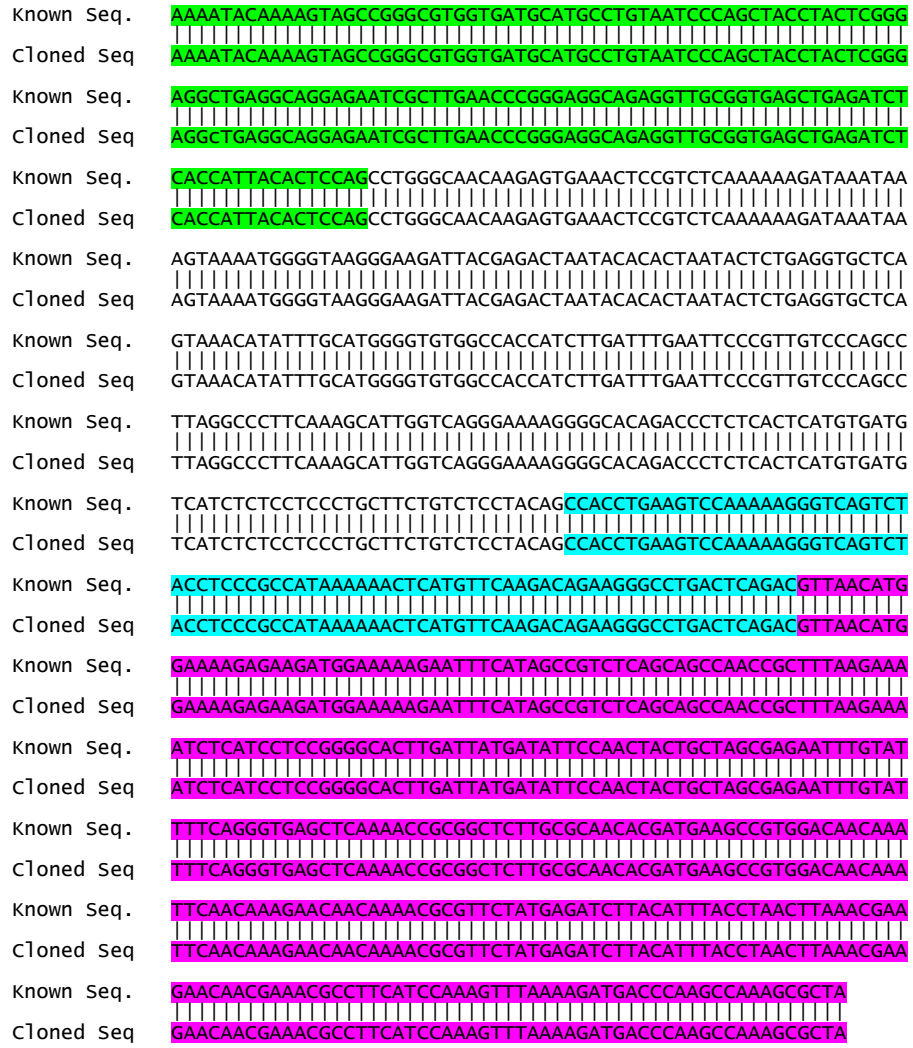

Figure 3-11. Sequence analysis of the PCR product from the screening process. The top sequence is the reference sequence and the bottom is the sequence of the screened product. A line between the two sequences indicates a match. The green highlighted sequence denotes exon 10 of p53, the non-colored sequence represents intron 10, blue denotes exon 11 of p53 and pink denotes the TAP tag sequence.

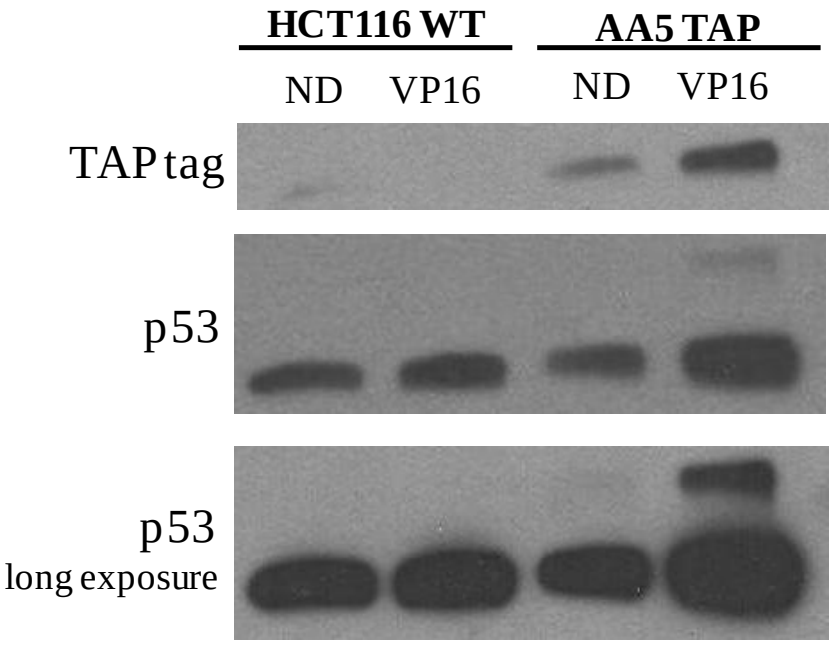

Figure 3-12. TAP tagged p53 accumulates in response to DNA damage levels lower than that of untagged p53. This figure is a western blot analysis of p53 levels in HCT116 and AA5 TAP cells exposed to 10 μM VP16 for24 hours. Total cell lysate protein (25 μg) was subjected to SDS-PAGE and immunoblotted with antibodies against p53 or the calmodulin peptide in the TAP tag were used.

(Fig 3-13). The cells which did not survive when exposed to G418 no longer contained the neomycin resistance cassette and, hence, had excised the neomycin cassette and also not fixed the pMCI CRE plasmid in the genome since this vector also carried the neomycin resistance cassette. The corresponding wells in the duplicate set without selection, were grown for further analysis. Following growth of neomycin sensitive single cell populations, p53 protein levels were assessed by western blotting. The removal of the neomycin resistance cassette from the TAP tag insert completely restored the TAP tag protein levels to wild-type p53 protein levels both in unstressed cells and also in cells treated with the topoisomerase II inhibitor, VP16 (Fig 3-14). The equivalent levels of accumulated p53 from the TAP tagged allele and the wild-type allele indicates that the TAP tag did not interfere with p53 stabilization and accumulation after DNA damage. The levels of p21 activated upon DNA damage were similar to the untagged cells suggesting that insertion of the TAP tag did not interfere with the transactivating ability of p53.

The functionality of the TAP tagged p53 was further investigated to determine whether the tag interferes with the cellular functions of the p53 encoded by the tagged allele. To assess the capability of the TAP tagged p53 to bind to gene promoters, the presence of p53 at the p21 promoter was investigated using ChIP. Two antibodies were used for the immunoprecipitation; the DO-1 antibody to pull down all cellular p53, and an antibody against the calmodulin binding peptide in the TAP tag to pull down only TAP tagged p53. Total p53 and TAP tagged p53 are poised at the upstream p53 binding site on the p21 promoter under no drug conditions and after VP16-induced DNA damage, the levels of both total and TAP-tagged p53 increase more than threefold indicating that the TAP tag does not interfere with the ability of p53 to bind to DNA (Figure 3-15).

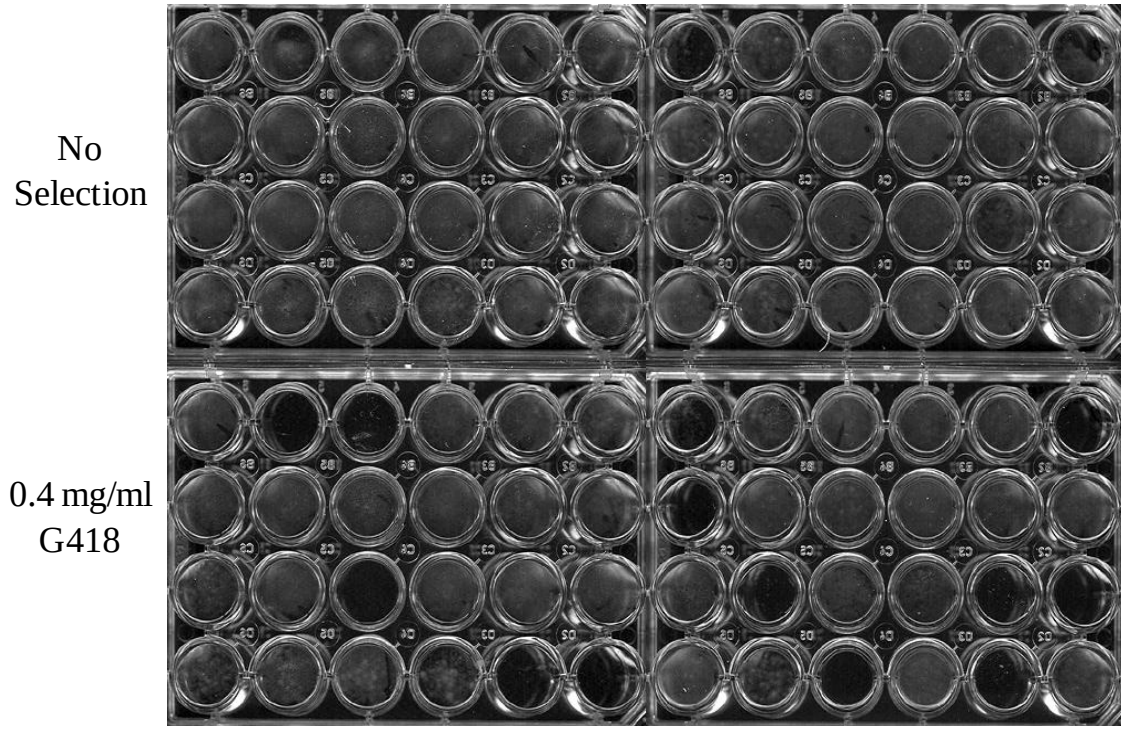

Figure 3-13. Selection of neomycin sensitive clones post transfection of a *cre* recombinase containing vector. Cre2 TAP cells were plated in duplicate post transfection. The cells which could not survive under G418 selection were propagated from the duplicate well in the no selection plate.

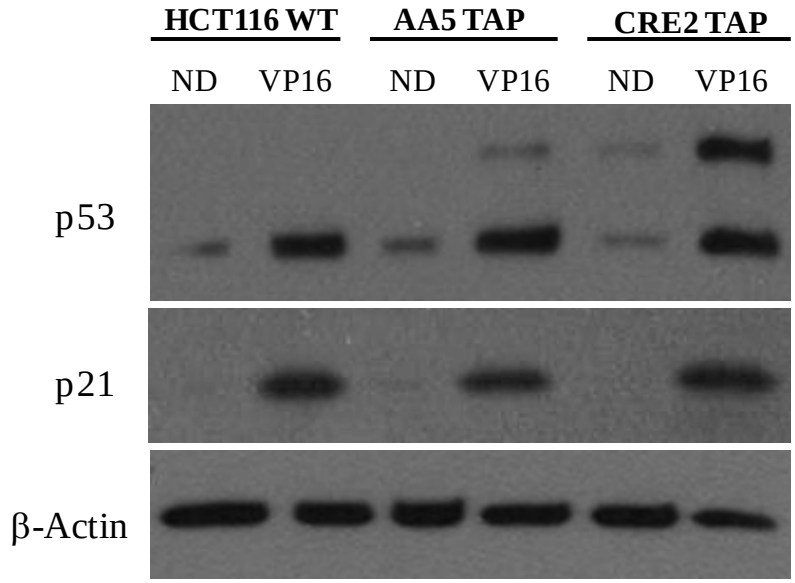

Figure 3-14. Removal of the neomycin cassette restores TAP tagged p53 levels to that of the untagged p53. This figure is a western blot analysis of p53 and p21 levels in HCT116, AA5 TAP and CRE2 TAP cells exposed to 10 μM VP16 for 24 hours. Total cell lysate protein (25 μg) was subjected to SDS-PAGE and immunoblotted with antibodies against p53 or p21 were used. Protein loading was assessed with β-Actin.

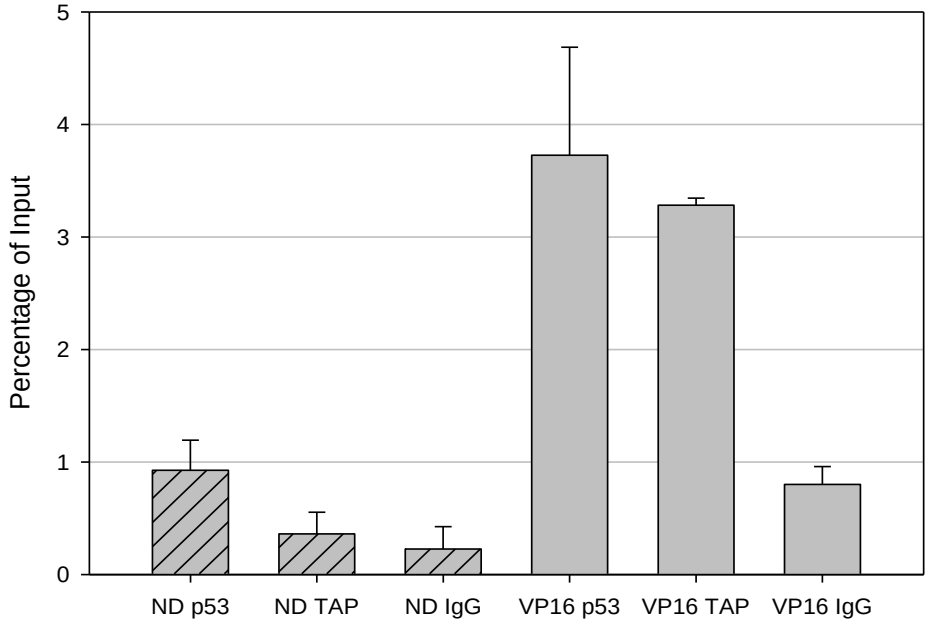

Figure 3-15. TAP tag does not interfere with the ability of p53 to bind to the p21 promoter. This figure is a ChIP analysis of p53 enrichment at the Rad51 promoter in CRE2 TAP cells after 24 hours of drug treatment. p53-DNA complexes were immunoprecipitated from formaldehyde crosslinked cells with either the DO-1 p53 or antibody against the calmodulin peptide in the TAP tag and p21 promoter levels were quantitated with Q-PCR. Standard error is depicted by the bars from two biological repeats each with triplicate Q-PCR samples. Non-specific binding was estimated using immunoprecipitation with non-specific IgG. Vehicle was PBS, VP16 was used at 10 μM.

Tandem Affinity Purification of p53

The ability of the TAP tag to pull down and isolate p53 binding partners through the tandem affinity purification protocol was evaluated using an adapted version of the published purification protocol (Bertwistle et al., 2004). TAP-tagged p53 was tandem affinity purified from VP16-treated cells, along with it any associated proteins. An aliquot from each step in the purification was saved to assess the efficiency of the protocol; the level of p53 in each fraction was determined by western blot using the DO-1 p53 antibody (Fig 3-16). There was loss of p53 at both of the binding steps. TAP tagged p53 was found in samples from the lysates that did not bind to the IgG beads. The majority of the TAP tagged p53 was lost after TEV cleavage as observed by a significant amount of p53 remaining bound to IgG beads after TEV cleavage and after the final elution from the calmodulin beads, suggesting the use of more TEV protease and more calmodulin beads would result in a larger yield of p53 (Fig 3-16).

Western blot analysis of the eight eluted fractions from the purification, probed with the DO-1 p53 antibody, resulted in two bands indicating that the TAP-tagged p53 is pulling down the wild-type p53 as a protein binding partner, an interesting result since it implies that the majority of p53 pre-exists as multimers of equal parts transcribed from each allele (Fig 3-17). The purification functionally isolated a portion of the TAP-tagged p53. Silver staining analysis of the eluted fractions revealed numerous proteins being pulled down with p53 during VP16-induced DNA damage (Fig 3-17). This purification procedure was next performed on cells which were exposed to HU to ask questions about the binding partners of p53 during nucleotide pool imbalances in comparison to the binding partners during DNA damage. A control of non-tagged HCT116 cells was also included to determine the background proteins being pulled down

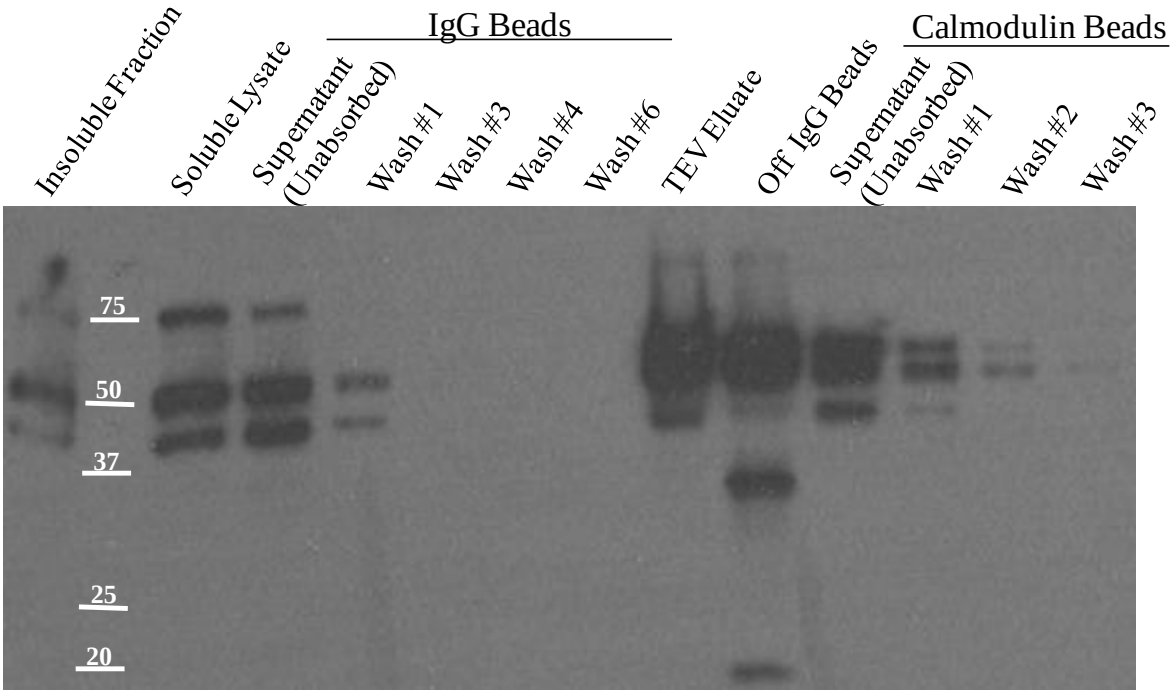

Figure 3-16. Recovery of p53 during tandem affinity purification. This figure shows a western blot analysis of the steps of the TAP purification of p53 from CRE2 TAP cells treated with VP16 for 24 hours and immunoblotted with DO-1 p53 antibody. Twenty-five μg of total protein was loaded for the insoluble fraction and soluble lysate, while the concentrations of the other fractions were estimated. Off IgG Beads is the supernatant that resulted after the IgG beads were boiled; the material remaining on IgG beads after TEV cleavage. VP16 was used at 10 μM.

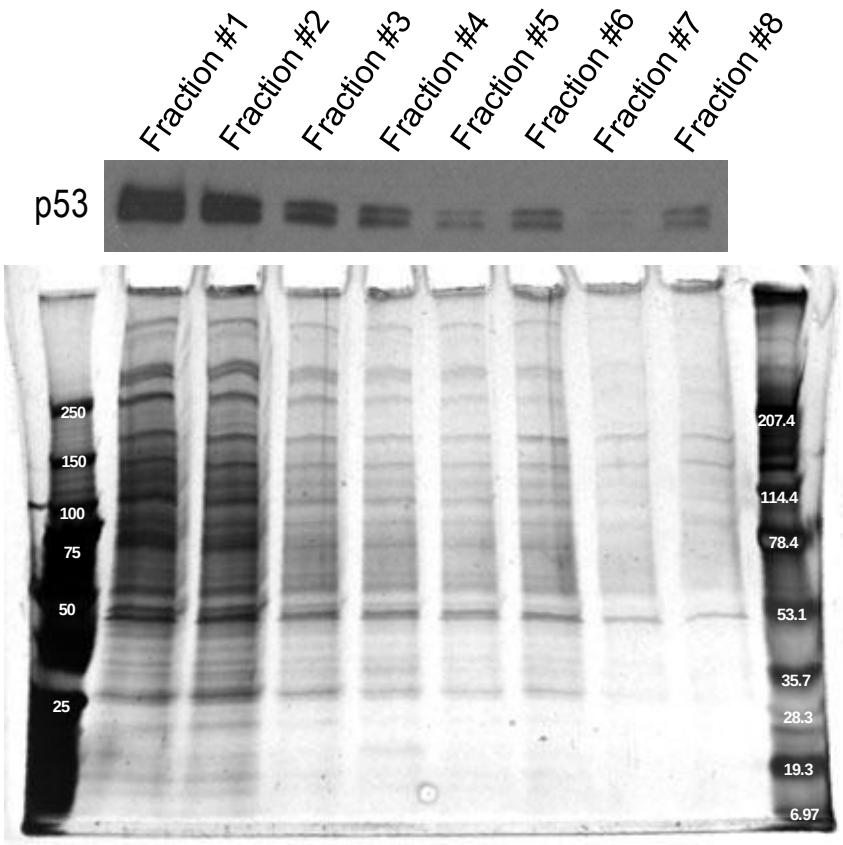

Figure 3-17. TAP tag purifies p53 with several protein binding partners. This figure is a western blot and silver stain analysis of 8 EGTA-eluted fractions from the TAP purification of p53 from CRE2 TAP cells treated with VP16 for 24 hours. 18.75% of each eluted fraction was subjected to SDS page: one polyacrylamide gel was immunoblotted with DO-1 p53 antibody while the other was silver stained. VP16 was used at 10 μM.

by the purification protocol. The silver stain of the eluted fractions showed differential binding patterns when comparing untreated cells to HU and VP16 treated cells (Fig 3-18). Although we are unable to confirm that there are indeed different proteins by mass spectrometry binding to p53 during nucleotide pools imbalances than during DNA damage, these data are encouraging. A similar purification was performed from HU- and PALA-treated cells. This was performed to investigate the different p53 binding partners during the observed S-phase arrest induced by HU treatment and the apoptosis induced by PALA treatment. In the previous purification, an equal number of cells were used in the purification, in contrast to using an equivalent amount of protein, which was done in the HU and PALA purification. PALA treatment resulted in a five-fold increase in p53 purification over that of the HU treated cells while the silver stain of the eluted fraction showed surprisingly similar protein banding patterns (Fig 3-19).

Discussion

The creation of this cell line marked the first time our lab has successfully manipulated a mammalian genomic locus by homologous recombination in a cell line. Previous attempts were made by Dr. Fiona Turner using different technologies but the screening process was laborious and after screening thousands of clones, the attempts were abandoned. This chapter demonstrates that this powerful AAV technology is possible and, indeed, highly efficient; it is a vast improvement over previous methodologies. From the cloning process to the completion of the cell line, the most challenging aspect was the cloning process, specifically attempting the three-way-fusion. This three-way fusion was never successfully accomplished in the cloning of the pAAV MCS vector. Other methodologies were used without adding significant labor to the

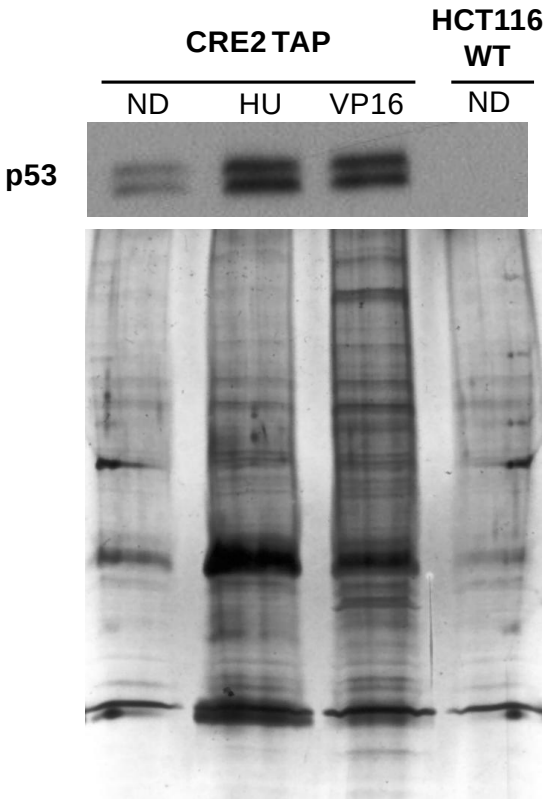

Figure 3-18. TAP tag purifies p53 with different protein binding partners after nucleotide deficiencies than after DNA damage. This figure is a western blot and silver stain analysis of the second eluted fraction from the TAP purification of p53 from CRE2 TAP cells treated with VP16 or HU for 24 hours. Purification of p53 from nontagged, HCT116 cells were used as a negative control for non specific proteins. 18.75% of each eluted fraction was subjected to SDS PAGE one polyacrylamide gel was immunoblotted with DO-1 p53 antibody while the other one was silver stained. VP16 was used at 10 μM and HU was used at 1.5 mM

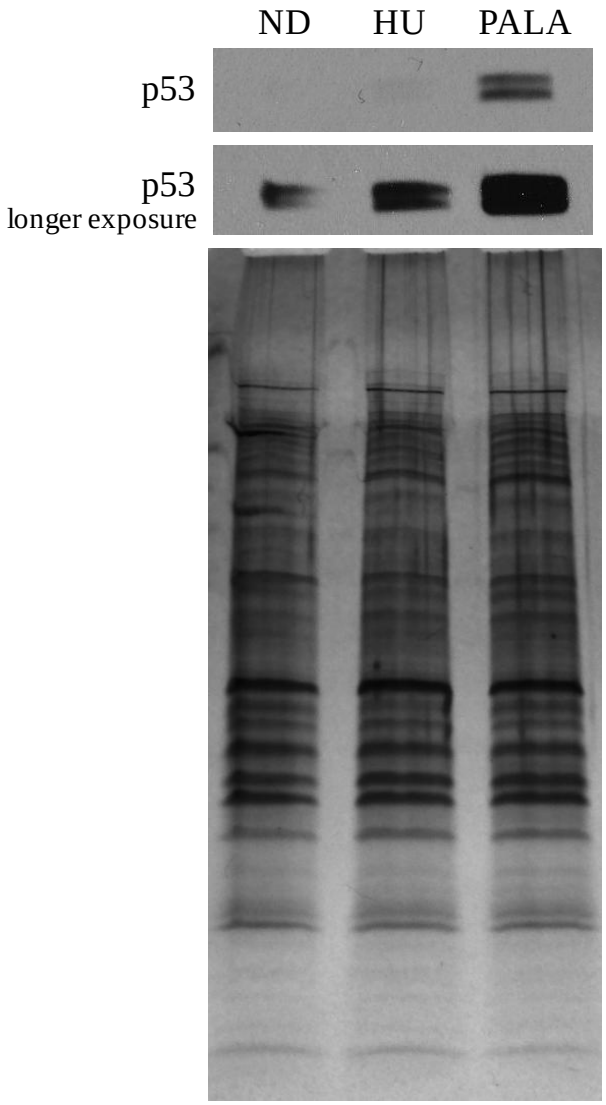

Figure 3-19. TAP tag purifies p53 with protein binding partners after nucleotide deficiencies induced by HU and PALA treatment. This figure is a western blot and silver stain analysis of the second eluted fraction from the TAP purification of p53 from CRE2 TAP cells treated with HU or PALA for 24 hours. 18.75% of each eluted fraction was subjected to SDS PAGE: one polyacrylamide gel was immunoblotted with DO-1 p53 antibody while the other was silver stained. HU was used at 1.5 mM and PALA was used at 100 μM.

process. The screening step which previously has caused the most problems was the least problematic step. With a targeting efficiency of 7.9%, it would be theoretically possible to screen fifteen clones and find one that was correct. This alone makes this methodology powerful enough to allow questions to be asked which previously were not within reach.

Does the neomycin cassette interfere with the stability of the TAP tagged p53?

The initial analysis of the stability of the TAP tagged p53 AA5 cells by western blot analysis showed for the first time that the tagged p53 is able to be stabilized and accumulated after VP16-induced DNA damage, suggesting that the large 25 kDa TAP tag is not interfering with the stabilization of p53 after genotoxic stress. The levels of accumulated p53 were not equivalent between the tagged allele and the wild-type allele (Fig 3-12). If the protein produced from a tagged allele does not reflect the behavior of the protein product from the wild-type allele, it would be difficult to draw conclusions about the protein binding partners of p53. Hence, the protein level disparity had to be addressed. Since insertion of the neomycin cassette moved the endogenous polyadenylation tail 2.2 kb further away from the end of the coding sequence, we suspected that the neomycin cassette was altering with the stability of the mRNA. Although the function of the polyadenylation tail is somewhat complex, there are several hypotheses of how it affects the stability of mRNA and the initiation of protein synthesis (reviewed in (Millevoi and Vagner, 2010)). Moving the polyadenylation tail over 2 kb downstream from its original location most likely interfered with protein binding and subsequent signaling events involved in the splicing, translocation and translation initiation of the p53-TAP mRNA. The pAAV MCS vector was designed to have loxP sites flanking the neomycin resistance cassette allowing the removal of the cassette from the endogenous p53 in the eventuality that this type of problem

arose. After the pMCI CRE plasmid containing the *cre* recombinase gene was transfected into the AA5 cells, cells were selected for the acquisition of sensitivity to G418 (Fig 3-13). In cell lines which the cre excision removed the drug resistance cassette, the protein levels of the TAP tagged p53 was restored to the endogenous levels of the wild-type protein, implying that the hypothesis that the neomycin cassette was altering translation or mRNA stability was correct (Fig 3-14).

Does the TAP tag interfere in the molecular properties of p53?

The ability of the TAP tagged p53 to accumulate after DNA damage was encouraging, but to prove that the TAP tag did not interfere in the molecular properties of p53, further experimentation was done. The ChIP analysis of the binding of both alleles of p53 at the p21 promoter demonstrated that the TAP tag did not interfere with the ability of p53 to bind to promoters. Since different antibodies were used for the TAP- and p53-immunoprecipitates, we cannot quantitatively determine the amount of TAP tagged p53 versus wild-type p53 that is at the p21 promoter. To assess the ability of the tagged p53 to bind to and modulate proteins, both BLM and HU-stabilized tagged p53 could be purified and the helicase activity of BLM could be measured. To do so, both purified proteins would be incubated with a radiolabeled X-junctions mimicking a Holliday junction where BLM is known to promote branch migration (Karow et al., 2000). If the HU stabilized p53 is able to bind to and inhibit BLM, then the X-junction would not be disrupted. If p53 does not inhibit BLM, then the X-junction would be disrupted, and two products would result; a one armed product (single stranded DNA) and a two armed product (half of the holiday junction) (Yang et al., 2002).

Purification of TAP tagged p53 along with its binding partners

The purification of tagged p53 along with interacting proteins was successful and the silver stain analysis showed that many proteins of various masses (Fig 3-18) are interacting with p53 and that these interactions change depending on the genotoxic stressor. When the western blot analysis of the eluted fraction was probed with the p53 antibody two bands resulted: the TAP tagged p53, which after the TEV protease cleavage has a mass of 59 kDa, and the band from wild-type p53. Since TAP tagged p53 is pulling down equimolar wild-type p53 in the purification, this indicates that the tag does not interfere with p53 oligomerization.

A second TAP tag could have been inserted into the wild-type p53 locus through gene targeting in the same manner as the other locus. This would have resulted in all cellular p53 being TAP tagged. Since p53 acts as a tetramer and we demonstrated that the tagged p53 interacts with the wild-type p53, there is no real desire to tag the other locus. Having an unaltered locus is a useful internal control when determining the functionality of the tagged p53.

Possible Uses for the TAP tagged p53

Post-translational Modifications

p53 is a highly post translationally modified protein. These modifications include phosphorylation, methylation, acetylation, sumoylation, neddylation and ubiquitylation and are thought to act as a barcode governing the activity of p53 (reviewed by (Murray-Zmijewski et al., 2008) (Fig 2-2). Extensive research has been done to identify the upstream kinases responsible for modifying p53 and how certain modifications impact the cellular activities of p53. The TAP tag cell line could be used to purify p53 and through mass spectroscopy, all of the PTMs could be identified under any given set of circumstances. Since the focus of this thesis is on the

different cellular responses to HU and PALA treatment, the p53 purified from CRE2 TAP cells treated with HU and PALA can be used to identify the PTMs of p53. As discussed in the previous chapter, some of the modifications of p53 during HU and PALA treatment have been investigated with western blots; the results are striking. The PTMs were asymmetrically opposed; if a specific serine was phosphorylated in HU treatment it was not phosphorylated in PALA treatment (Fig 2-8). Using the nonbiased approach of mass spectroscopy, an all inclusive PTM map of the p53 accumulated by HU- and PALA-treatment could be constructed. The upstream kinases could be elucidated and possibly give direction to the next experiment needed to understand the upstream cellular events promoting the oppositely modified p53 and subsequent different cellular outcomes.

Protein Binding Partners

Mitochondrial Fractionation

Not only can p53 be isolated from whole cells to determine what is binding to p53 but it could be purified from sub-cellular fractions to ask more specific questions. p53 has been found in the mitochondria and is known to induce mitochondrial outer membrane permeabilization triggering the release of pro-apoptotic molecules (Chipuk et al., 2004). Intact mitochondria could be fractionated from drug-treated cells and the protein binding partners of p53 could be identified. Previously, we found that PALA-treatment promoted p53-dependent apoptosis while HU-treatment did not. Thus, it would be interesting to compare the mitochondrial binding partners of p53 during these two treatments. Hypothetically, one would expect to find p53 associating with the pro-apoptotic Bcl2 family proteins during PALA treatment, such as Bax,

Bak, Bad and Bid while during HU treatment p53 may be associated with anti-apoptotic molecules Bcl-2 and Bcl-XL. The TAP tag cell line could be used to ask such questions.

Cytosolic Fractionation

The function of cytosolic p53 has recently been investigated and it has been linked to both inhibition of autophagy and to energy conservation. During metabolic stress, it is thought that AMPK phosphorylates and activates p53 (Feng et al., 2005). The accumulated p53 activates the transcription of sestrin 1 and sestrin 2. Both sestrins preferentially activate AMPK towards phosphorylating TSC2 which inhibits mTOR (Budanov and Karin, 2008). mTOR suppresses autophagy, so through its inhibition, p53 has been linked to activating autophagy during metabolic stress while basal levels of cytosolic p53 have been implicated in the inhibition of autophagy (Tasdemir et al., 2008). Through inhibition of mTOR the cell is able to conserve energy and prolong viability. This is fairly new and rapidly growing field, and with the TAP tag cell line, the involvement of p53 could be further examined. Questions about the direct interactions between p53 and AMPK could be addressed, as well as identifying all proteins which interact with p53 in the cytosol. Since cytosolic p53 has been associated with AMPK signaling, one would imagine at least some of the proteins binding to p53 will have a role in this signaling pathway.

Nuclear Fractionation

The majority of p53 research has been focused on the nuclear functions of the tumor suppressor, specifically its functions as a transcription factor activating the transcription of cell cycle and apoptosis regulatory proteins. The mechanism involved in determining which set of

genes p53 activates is not fully understood. There are two theories: one is the p53-centric theory, in which the cellular fate of the cell depends on the activities of p53 which are regulated by the PTMs and protein interactions of p53. The other theory is the p53-autonomous model that states that the cellular fate is determined independently of p53 activity and that, although p53 may be found at the promoter, the activation of transcription is dependent on other transcription factors (Gomes and Espinosa, 2010). TAP purification of nuclear p53 from cells undergoing apoptosis (PALA-treated) versus cell cycle arrested cells (HU-treated) could be used to compare the PTMs and protein interaction of p53 between both cellular fates. The similarities and differences may lead to further understanding of how the cellular fate is decided and if indeed p53 is a key regulator in the decision.

Transcriptional Regulation

The enrichment of p53 at promoters does not necessarily indicate that transcription is activated. There are instances where p53 is found at the p21 promoter yet it is not activating transcription. Previously in our lab, Julie Bronder identified one of these instances where, during DDATHF treatment, p53 was found at the p21 promoter but due to the lack of PTMs of p53 and the closed chromatin structure of the promoter, transcription was not activated (Bronder and Moran, 2003). During this dissertation work, two more instances were found, both HU and pemetrexed treatment resulted in a defect in significant p21 transcription even though p53 was found at the p21 promoter (Heyer, Racanelli and Moran, unpublished results and (Gottifredi et al., 2001), and Figs 2-6, 2-7). This was not found during PALA treatment. The hydroxyurea observation was previously identified and thought to be due to a decrease in the phosphorylation of RNA polymerase II which is required for transcriptional elongation (Mattia et al., 2007). The

causative event for this defect was never identified. Prior to any cellular stress, basal levels of p53 are at the p21 promoter and establish a gradient of paused RNA polymerase II at the promoter. Upon stress, the RNA polymerase is converted to the elongation form via CTD phosphorylation, resulting in gene transcription. This process requires the recruitment of several elongation factors including P-TEFb, FACT, DSIP, TPIIF and TFIIH. This suggests that gene transcription of p53-dependent promoters depends on the protein complexes recruited after cellular stress (Espinosa et al., 2003; Gomes et al., 2006). Nuclear purified TAP tagged p53 from both HU- and PALA-treated cells would help to investigate the different protein complexes associating with p53 at promoters where in one instance p21 transcription is activated and in the other, it is not. Promoter complexes could first be isolated through immunoprecipitation of a component of the preinitiation complex and then subjected to the TAP purification to isolate p53 binding proteins. With mass spectroscopy, the identities of the protein that are present or missing in both treatments could be achieved. The PTMs of promoter bound p53 could also be identified and may possibly lead to an understanding of the signaling events required for transcriptional activation.

S-phase Checkpoint

Another nuclear role of p53 is the S-phase checkpoint, which was described in depth in the previous chapter. Since the role of p53 is still to be elucidated in this pathway, the TAP tag would be useful in expanding the knowledge in this field. It appears that p53 exerts its tumor suppressor activity as a protein modulator in this pathway more than as a transcription factor. By isolating p53 and all interacting proteins from nuclear extracts, or specifically from chromatin, the protein complexes could be identified. To further enrich for stalled replication forks, an

initial immunoprecipitation could be performed with an antibody against a specific replication fork protein such as BLM, RPA or Rad51. Then this pool of proteins could be subjected to the TAP purification resulting in isolation of the proteins which interact with p53 solely at stalled replication forks. Identification of these proteins may lead to discovering new proteins previously not identified in the S-phase checkpoint, leading to further understanding of the signaling events occurring after a replication fork stalls.

Modifications of the TAP tag

Since the development of the CRE2 TAP cell line, several other tandem affinity tags have been developed. The weakness of the TAP tag was found to be the calmodulin binding peptide. TAP tagged p53 was not completely captured by the calmodulin beads as it was found in all the washes and a larger amount of protein remained on the calmodulin beads after the elution (Calmodulin supernatant (unabsorbed) and Cal Wash #1 & #2, Fig 3-16). Since a large amount of the purified protein complex was lost at this step, upwards of 800 million cells had to be used to yield enough protein for analysis. Different versions of the TAP tag have been engineered. The calmodulin peptide has been replaced with a FLAG tag or a streptavidin binding peptide. Protein A has been replaced with Protein G which is thought to have a slightly higher binding affinity for a broader range of IgGs (Sauer-Eriksson et al., 1995). The modified TAP tag where the calmodulin binding peptide was replaced with the FLAG tag and the completely changed tag where both protein G binding units replaced the protein A units and the streptavidin binding peptide replaced the calmodulin peptide had a significant increase in purified protein yield (Burckstummer et al., 2006; Tsai and Carstens, 2006). Recovery increased to 80% and 50 million cells were used to obtain protein yields similar to what were achieved in my studies with

1 billion cells with the original TAP tag. Interestingly, the original TAP tag paper tested combinations of calmodulin binding peptide, FLAG tag, histidine tag, streptavidin binding peptide, and chitin-binding domain and found the protein A and protein calmodulin binding peptide combination to yield the most efficiently recovered protein complexes in yeast cells (Rigaut et al., 1999). Although there have been significant modifications in the TAP tag, the CRE2 TAP cells still have endless possibilities, the starting cell number simply needs to be adjusted to account for a lower efficiency of purification.

Chapter 4: Perspectives

Through the course of this dissertation, I have identified that human colon carcinoma cells respond differently to two nucleotide synthesis inhibitors, HU and PALA. The difference lies at the level of activation of the S-phase checkpoint: whereas HU treatment activates the checkpoint resulting in Chk1 phosphorylation, PALA treatment fails to, resulting in p53-dependent apoptosis. Despite the wealth of information obtained regarding the molecular events occurring after treatment with both antimetabolites, several fundamental questions remain unanswered about why these differences exist. These questions will be addressed within this chapter from a specific standpoint as well as from a global standpoint in regards to the clinical utility of antimetabolites.

Why do colon carcinoma cells respond differently to an inhibitor of dNTP synthesis versus an inhibitor of pyrimidine synthesis?

The nucleotide concentrations after drug treatment were not measured in the course of this dissertation work. These concentrations may lead to a better understanding of why the HCT116 cells responds in such different manners to HU and PALA treatment. There is some evidence that nucleotide levels may affect the DNA binding capacity of p53 in that increased levels of ADP and dADP stabilize p53-DNA complexes whereas ATP, dATP, GTP and dGTP facilitate the release of p53 (Okorokov and Milner, 1999). Further investigation would be

necessary to determine if the pyrimidine dNTPs would have an impact on the DNA binding capacity of p53 as well as to determine the nucleotide levels in HCT116 cells after HU or PALA treatment. The original suggestion that p53 is capable of sensing nucleotide levels concluded that antimetabolites primarily affecting dNTP levels arrest early in S-phase, independent of p53 status, while CTP, UTP and GMP synthesis inhibitors induce a p53-dependent G_1 arrest (Linke et al., 1996). Therefore, the idea that p53 is able to detect nucleotide levels is not universal, and is only relevant for some nucleotides. A more probable explanation is that p53 senses changes in the signal transduction pathways rather than the direct changes in nucleotide levels. The changes in the signal transduction pathways after treatment with nucleotide synthesis inhibitors ultimately could determine the cellular fate. Interestingly, we observed a difference in phosphorylation of p53 between HU, PALA and the DNA damaging agent VP16. p53 was phosphorylated at all investigated serines when cells were treated with VP16, a topoisomerase II inhibitor, which does not inhibit nucleotide synthesis. Only a fraction of these residues were phosphorylated after either HU or PALA-induced nucleotide synthesis inhibition, suggesting that the signal transduction pathways after nucleotide deficiencies were different than that after DNA damage.

Why during PALA treatment is there a greater level of stabilized p53 than during HU treatment? The dissimilar PTMs of p53 after treatment with HU or PALA may help to gain insight to as to why there is a difference in the total amount of accumulated p53. During HU treatment, p53 is modified at serines 15 and 20, the hallmark sites known to inhibit MDM-induced degradation of p53, while these residues are not modified during PALA treatment. Serine 392 is phosphorylated in PALA-treated cells (Fig 2-8). This phosphorylation is known to enhance tetramerization which masks the nuclear export signal, possibly trapping PALA-stabilized p53 within the nucleus and therefore protecting it from degradation. If the level of p53

is the causative event promoting apoptosis or S-phase arrest, then understanding why there is a differing level is crucial for our understanding and the clinical implications of this dissertation work.

To further address the differences observed between HU treatment and PALA treatment in HCT116 cells, the question of how cells are traversing through S-phase with a limited pool of nucleotides should be addressed. Are the cells accumulating DNA damage while synthesizing DNA with limiting nucleotides? Does this DNA damage differ between drugs? If so, is this the signal that causes the activation of the two different pathways? The studies performed throughout this dissertation work suggest that cells are progressing through S-phase at a much reduced rate compared with the untreated cells. HU treatment does not completely exhaust the nucleotide pools, but it is hard to imagine the small percentages remaining during treatment are enough to provide the nucleotides required to progress through an entire S-phase (Koc et al., 2004). If extensive DNA damage was occurring, the measured γH2AX levels would be higher, similar to what was observed during VP16 treatment. Also, during PALA treatment, if cells were accumulating DNA damage, why did they bypass the G_1 arrest and enter S-phase? Further experimentation to address these questions will build on the observations made during this dissertation, as well as understanding how drugs inhibiting enzymes within the nucleotide synthesis pathway can have such dissimilar cellular consequences.

The events responsible for the differing responses to HU and PALA treatment remain to be completely elucidated. It may be due to the levels of nucleotides within the cell, the differing levels of accumulated p53, or it may be peculiar for HCT116 cells. Either way we discovered that colon carcinoma cells do not respond equally to nucleotide synthesis inhibitors and the clinical implications of these findings will now be discussed.

Clinical Implications

The hypothesis that the level of accumulated p53 may cause the differential cellular response to HU and PALA treatment could aid in targeted chemotherapy. PALA treatment resulted in a p53-dependent apoptosis, a higher level of accumulated p53 and higher levels of p53 bound to all investigated promoters compared to promoter residence after VP16 or HU treatment. Conversely, HU treatment resulted in a cytostatic S-phase arrest, a lower level of accumulated p53, and significant p53 enrichment only at high affinity promoters. Overall, it appears that the high level of accumulated p53 during PALA treatment is able to bind specific promoters and transactivate these genes, resulting in programmed cell death. Cancer in which p53 is over expressed due to deletion of Mdm2, might be pushed towards apoptosis while the normal stem cells would arrest in S-phase until treatment subsides. If it is true that the level of accumulated p53 determines the cellular fate during nucleotide stress, then cancer cells over expressing a wild-type form of p53 could be treated with a nucleotide synthesis inhibitor. Prior to any treatment, p53 would be poised at proapoptotic promoters, and after nucleotide synthesis is inhibited, p53 levels would increase activating the transcription of these genes causing apoptosis. In the normal cells, p53 levels would be low prior to any treatment; after treatment, p53 levels would increase, but not to the extent observed in the cancer cells, resulting in S-phase arrest, similar to what we observed after HU treatment. This would result in cytotoxicity of the cancer cells and a reversible cytostatic arrest in the normal cells.

In light of the current ability to sequence the cancer genome, identifying the upstream pathways regulating p53 after inhibition of nucleotide synthesis would be very informative. The genetics of cancer is exhaustively being studied in hopes of finding common mutational trends

within cancer types. If the upstream modulators of p53 after HU and PALA treatment are identified, then cancers known to contain mutations of these modulators perhaps will have a higher response rate to nucleotide synthesis inhibitors. The PTMs of p53 after treatment with either HU or PALA suggest different upstream signaling pathways are activated during the two treatments, resulting in the diametrically opposed pattern of phosphorylation. If our hypothesis is true that p53 does not directly sense nucleotide levels but does sense changes in signaling from stalled replication intermediates, then the identification of the specific p53 activating pathway being activated would be beneficial. Specifically, in the case of PALA treatment, where the PTMs of p53 stimulate sequence-specific DNA binding and transcription of apoptotic genes, the upstream kinases responsible for phosphorylated serines 37, 46 and 392 would advance our understanding of the resulting apoptotic response. CK2 is thought to be a cancer driver since it was found at elevated levels in a number of cancers and cells containing elevated CK2 have a selective advantage for oncogenesis (reviewed in (Ruzzene and Pinna, 2010)). CK2 is known to phosphorylate p53 at serine 392 and this phosphorylation was found to enhance p53 tetramer stability, increase DNA binding and transcriptional activity of p53 (Meek et al., 1990). In cancer cells that have an elevated level of CK2, it is logical to think that CK2 is readily available to phosphorylate p53 at serine 392 after nucleotide deficiencies, promoting DNA binding and transcription, and in the case of PALA treatment, apoptosis. This concept can be extended to inactive mutant forms of ATR or Chk1; treatment with HU would hypothetically drive cells to apoptosis since the S-phase cell cycle checkpoint would not be intact, while normal surrounding cells would reversibly arrest in S-phase. Through sequencing of the cancer genome, the knowledge of probable mutations within cancer types will be available, thus allowing for chemotherapies to be designed according to the genetics of an individual cancer case,

significantly improving the treatment of cancer. Therefore, the signaling pathways involved in the cellular responses to HU and PALA need to be identified, as well as the proteins phosphorylating p53, to better understand how inhibitors of nucleotide synthesis can be used in the treatment of cancer. With the use of the TAP tagged p53 cell line generated during this dissertation work, this may now be possible.

The p53 TAP tagged cell line can also be used to identify S-phase specific p53 binding partners. A large part of the function of the S-phase checkpoint is to modulate homologous recombination proteins to ensure DNA repair does not occur in times of replicative stress. With the use of the TAP tag, new proteins can be identified which may have a high incidence of mutations within human cancers. Cancers containing mutation in S-phase proteins would be more sensitive to S-phase specific drugs since the checkpoint would not be intact. Constitutively active mutants of pro-recombinogenic proteins would result in the S-phase checkpoint losing control of DNA repair activity. If these cancer cells are treated with HU, or another S-phase specific drug, apoptosis would be induced due to increased homologous recombination at a time of genomic instability. The homologous recombination protein Rad51 has been implicated in cancer. Decreased Rad51 expression was found in 30% of the investigated 179 breast cancer cases and in sporadic invasive ductal breast cancer. In pancreatic adenocarcinoma, Rad51 was found to be over expressed (reviewed in (Thacker, 2005)). Together with the finding that cells containing a Rad51 mutant preventing phosphorylation by Chk1 are more sensitive to HU treatment, suggests that targeted therapeutics in cancers containing Rad51 mutations is possible (Sorensen et al., 2005). It is also likely that there are other proteins involved in the S-phase checkpoint which still remain to be identified and with the use of the p53 TAP tagged cell line, these multi-protein complexes can be isolated and identified.

Literature Cited

Literature Cited

1. Krumbhaar, E. B., and Krumbhaar, H. D. (1919). The blood and bone marrow in yelloe cross gas (mustard gas) poisoning: Changes produced in the bone marrow of fatal cases. *J. Med. Res., 40,* 497-508.

2. Gilman, A., and Philips, F. S. (1946). The biological actions and therapeutic applications of the B-chloroethyl amines and sulfides. *Science, 103,* 409-436.

3. Gilman, A. (1963). The initial clinical trial of nitrogen mustard. *Am. J. Surg., 105,* 574-578.

4. Farber, S., Cutler, E. C., Hawkins, J. W., Harrison, J. H., Peirce, E. C.,2nd, and Lenz, G. G. (1947). The action of pteroylglutamic conjugates on man. *Science, 106,* 619-621.

5. Farber, S., and Diamond, L. K. (1948). Temporary remissions in acute leukemia in children produced by folic acid antagonist, 4-aminopteroyl-glutamic acid. *N. Engl. J. Med., 238,* 787-793.

6. Hitchings, G. H., and Elion, G. B. (1954). The chemistry and biochemistry of purine analogs. *Ann. N. Y. Acad. Sci., 60,* 195-199.

7. Skipper, H. E., Thomson, J. R., Elion, G. B., and Hitchings, G. H. (1954). Observations on the anticancer activity of 6-mercaptopurine. *Cancer Res., 14,* 294-298.

8. Heidelberger, C., Chaudhuri, N. K., Danneberg, P., Mooren, D., Griesbach, L., Duschinsky, R., Schnitzer, R. J., Pleven, E., and Scheiner, J. (1957). Fluorinated pyrimidines, a new class of tumour-inhibitory compounds. *Nature, 179,* 663-666.

9. Heidelberger, C., Griesbach, L., Montag, B. J., Mooren, D., Cruz, O., Schnitzer, R. J., and Grunberg, E. (1958). Studies on fluorinated pyrimidines. II. effects on transplanted tumors. *Cancer Res., 18,* 305-317.

10. Collins, K. D., and Stark, G. R. (1971). Aspartate transcarbamylase. interaction with the transition state analogue N-(phosphonacetyl)-L-aspartate. *J. Biol. Chem., 246,* 6599-6605.

11. Kantrowitz, E. R., and Lipscomb, W. N. (1988). Escherichia coli aspartate transcarbamylase: The relation between structure and function. *Science, 241,* 669-674.

12. Pardee, A. B., and Yates, R. A. (1956). Control of pyrimidine biosynthesis in escherichia coli by a feed-back mechanism. *J. Biol. Chem., 221,* 757-770.

13. Gerhart, J. C., and Pardee, A. B. (1962). The enzymology of control by feedback inhibition. *J. Biol. Chem., 237,* 891-896.

14. Reichard, P., and Hanshoff, G. (1956). Aspartate carbamly transferase from *escherichia coli*.*10,* 548.

15. Collins, K. D., and Stark, G. R. (1969). Aspartate transcarbamylase. studies of the catalytic subunit by ultraviolet difference spectroscopy. *J. Biol. Chem., 244,* 1869-1877.

16. Cohen, R. E., and Schachman, H. K. (1986). Kinetics of the interaction of N-(phosphonacetyl)-L-aspartate with the catalytic subunit of aspartate transcarbamoylase. A slow conformational change subsequent to binding. *J. Biol. Chem., 261,* 2623-2631.

17. Swyryd, E. A., Seaver, S. S., and Stark, G. R. (1974). N-(phosphonacetyl)-L-aspartate, a potent transition state analog inhibitor of aspartate transcarbamylase, blocks proliferation of mammalian cells in culture. *J. Biol. Chem., 249,* 6945-6950.

18. Johnson, R. K., Inouye, T., Goldin, A., and Stark, G. R. (1976). Antitumor activity of N-(phosphonacetyl)-L-aspartic acid, a transition-state inhibitor of aspartate transcarbamylase. *Cancer Res., 36,* 2720-2725.

19. Moyer, J. D., and Handschumacher, R. E. (1979). Selective inhibition of pyrimidine synthesis and depletion of nucleotide pools by N-(phosphonacetyl)-L-aspartate. *Cancer Res., 39,* 3089-3094.

20. Tsuboi, K. K., Edmunds, N. H., and Kwong, L. K. (1977). Selective inhibition of pyrimidine biosynthesis and effect on proliferative growth of colonic cancer cells. *Cancer Res., 37,* 3080-3087.

21. Johnson, R. K., Swyryd, E. A., and Stark, G. R. (1978). Effects of N-(phosphonacetyl)-L-aspartate on murine tumors and normal tissues in vivo and in vitro and the relationship of sensitivity to rate of proliferation and level of aspartate transcarbamylase. *Cancer Res., 38,* 371-378.

22. Moyer, J. D., Smith, P. A., Levy, E. J., and Handschumacher, R. E. (1982). Kinetics of N-(phosphonacetyl)-L-aspartate and pyrazofurin depletion of pyrimidine ribonucleotide and deoxyribonucleotide pools and their relationship to nucleic acid synthesis in intact and permeabilized cells. *Cancer Res., 42,* 4525-4531.

23. Erlichman, C., Strong, J. M., Wiernik, P. H., McAvoy, L. M., Cohen, M. H., Levine, A. S., Hubbard, S. M., and Chabner, B. A. (1979). Phase I trial of N-(phosphonacetyl)-L-aspartate. *Cancer Res., 39,* 3992-3995.

24. Van Echo, D. A., Diggs, C. H., Scoltock, M., and Wiernik, P. H. (1980). Phase II evaluation of N-(phosphonacetyl)-L-aspartic acid (PALA) in metastatic adenocarcinoma of the colon or rectum. *Cancer Treat. Rep., 64,* 339-342.

25. Carroll, D. S., Gralla, R. J., and Kemeny, N. E. (1980). Phase II evaluation of N-(phosphonacetyl-L-aspartic acid (PALA) in patients with advanced colorectal carcinoma. *Cancer Treat. Rep., 64,* 349-351.

26. Casper, E. S., Gralla, R. J., Kelsen, D. P., Houghton, A., Golbey, R. B., and Young, C. W. (1980). Phase II evaluation of N-(phosphonacetyl)-L-aspartic acid (PALA) in patients with non-small cell carcinoma of the lung. *Cancer Treat. Rep., 64,* 705-707.

27. Moran, R. G., Spears, C. P., and Heidelberger, C. (1979). Biochemical determinants of tumor sensitivity to 5-fluorouracil: Ultrasensitive methods for the determination of 5-fluoro-2'-deoxyuridylate, 2'-deoxyuridylate, and thymidylate synthetase. *Proc. Natl. Acad. Sci. U. S. A., 76,* 1456-1460.

28. Liang, C. M., Donehower, R. C., and Chabner, B. A. (1982). Biochemical interactions between N-(phosphonacetyl)-L-aspartate and 5-fluorouracil. *Mol. Pharmacol., 21,* 224-230.

29. Meshad, M. W., Ervin, T. J., Kufe, D., Johnson, R. K., Blum, R. H., and Frei, E.,3rd. (1981). Phase I trial of combination therapy with PALA and 5-FU. *Cancer Treat. Rep., 65,* 331-334.

30. Weiss, G. R., Ervin, T. J., Meshad, M. W., and Kufe, D. W. (1982). Phase II trial of combination therapy with continuous-infusion PALA and bolus-injection 5-FU. *Cancer Treat. Rep., 66,* 299-303.

31. Woodcock, T. M., Martin, D. S., Damin, L. A., Kemeny, N. E., and Young, C. W. (1980). Combination clinical trials with thymidine and fluorouracil: A phase I and clinical pharmacologic evaluation. *Cancer, 45,* 1135-1143.

32. O'Connell, M. J., Moertel, C. G., Rubin, J., Hahn, R. G., Kvols, L. K., and Schutt, A. J. (1984). Clinical trial of sequential N-phosphonacetyl-L-aspartate, thymidine, and 5-fluorouracil in advanced colorectal carcinoma. *J. Clin. Oncol., 2,* 1133-1138.

33. Kemeny, N., Schneider, A., Martin, D. S., Colofiore, J., Sawyer, R. C., Derby, S., and Salvia, B. (1989). Phase I trial of N-(phosphonacetyl)-L-aspartate, methotrexate, and 5-fluorouracil with leucovorin rescue in patients with advanced cancer. *Cancer Res., 49,* 4636-4639.

34. Grem, J. L., King, S. A., O'Dwyer, P. J., and Leyland-Jones, B. (1988). Biochemistry and clinical activity of N-(phosphonacetyl)-L-aspartate: A review. *Cancer Res., 48,* 4441-4454.

35. Markman, M., Chan, T. C., Cleary, S., and Howell, S. B. (1987). Phase I trial of combination therapy of cancer with N-phosphonacetyl-L-aspartic acid and dipyridamole. *Cancer Chemother. Pharmacol., 19,* 80-83.

36. Dresler, W. F. C., and Stein, R. (1869). Ueber den hydroxylharnstoff.*150,* 242-252.

37. Krakoff, I. H., Brown, N. C., and Reichard, P. (1968). Inhibition of ribonucleoside diphosphate reductase by hydroxyurea. *Cancer Res., 28,* 1559-1565.

38. Reichard, P., and Ehrenberg, A. (1983). Ribonucleotide reductase--a radical enzyme. *Science, 221,* 514-519.

39. Brown, N. C., Eliasson, R., Reichard, P., and Thelander, L. (1969). Spectrum and iron content of protein B2 from ribonucleoside diphosphate reductase. *Eur. J. Biochem., 9,* 512-518.

40. Atkin, C. L., Thelander, L., Reichard, P., and Lang, G. (1973). Iron and free radical in ribonucleotide reductase. exchange of iron and mossbauer spectroscopy of the protein B2 subunit of the escherichia coli enzyme. *J. Biol. Chem., 248,* 7464-7472.

41. Reichard, P. (1993). From RNA to DNA, why so many ribonucleotide reductases? *Science, 260,* 1773-1777.

42. Brown, N. C., and Reichard, P. (1969). Role of effector binding in allosteric control of ribonucleoside diphosphate reductase. *J. Mol. Biol., 46,* 39-55.

43. Reichard, P. (1987). Regulation of deoxyribotide synthesis. *Biochemistry, 26,* 3245-3248.

44. Shao, J., Zhou, B., Zhu, L., Bilio, A. J., Su, L., Yuan, Y. C., Ren, S., Lien, E. J., Shih, J., and Yen, Y. (2005). Determination of the potency and subunit-selectivity of ribonucleotide reductase inhibitors with a recombinant-holoenzyme-based in vitro assay. *Biochem. Pharmacol., 69,* 627-634.

45. Lassmann, G., Thelander, L., and Graslund, A. (1992). EPR stopped-flow studies of the reaction of the tyrosyl radical of protein R2 from ribonucleotide reductase with hydroxyurea. *Biochem. Biophys. Res. Commun., 188,* 879-887.

46. Lewis, W. H., and Wright, J. A. (1978). Ribonucleotide reductase from wild type and hydroxyurea-resistant chinese hamster ovary cells. *J. Cell. Physiol., 97,* 87-97.

47. Shao, J., Zhou, B., Chu, B., and Yen, Y. (2006). Ribonucleotide reductase inhibitors and future drug design. *Curr. Cancer. Drug Targets, 6,* 409-431.

48. Neuhard, J. (1967). Studies on the acid-soluble nucleotide pool in escherichia coli. IV. effects of hydroxyurea. *Biochim. Biophys. Acta, 145,* 1-6.

49. Bianchi, V., Pontis, E., and Reichard, P. (1986). Changes of deoxyribonucleoside triphosphate pools induced by hydroxyurea and their relation to DNA synthesis. *J. Biol. Chem., 261,* 16037-16042.

50. Rosenthal, F., Wislicki, L., and Kollek, L. (1928). Ueber die beziehungen von schwersten blutgiften zu abbauprodukten des eiweisses. beitrag zum entstehungsmechanismus der perniziosen. *Anamie. Klin. Wschr., 7,* 972.

51. Ostruszka, L. J., and Shewach, D. S. (2003). The role of DNA synthesis inhibition in the cytotoxicity of 2',2'-difluoro-2'-deoxycytidine. *Cancer Chemother. Pharmacol., 52,* 325-332.

52. Stearns, B., Losee, K. A., and Bernstein, J. (1963). Hydroxyurea. a new type of potential antitumor agent. *J. Med. Chem., 6,* 201.

53. Thurman, W. G., Bloedow, C., Howe, C. D., Levin, W. C., Davis, P., Lane, M., Sullivan, M. P., and Griffith, K. M. (1963). A phase I study of hydroxyurea. *Cancer Chemother. Rep., 29,* 103-107.

54. Fishbein, W. N., Carbone, P. P., Freireich, E. J., Misra, D., and Frei, E.,3rd. (1964). Clinical trials of hydroxyurea in patients with cancer and leukemia. *Clin. Pharmacol. Ther., 5,* 574-580.

55. Kennedy, B. J., and Yarbro, J. W. (1966). Metabolic and therapeutic effects of hydroxyurea in chronic myeloid leukemia. *JAMA, 195,* 1038-1043.

56. Kennedy, B. J. (1972). Hydroxyurea therapy in chronic myelogenous leukemia. *Cancer, 29,* 1052-1056.

57. von Bubnoff, N., and Duyster, J. (2010). Chronic myelogenous leukemia: Treatment and monitoring. *Dtsch. Arztebl Int., 107,* 114-121.

58. Sinclair, W. K. (1968). The combined effect of hydroxyurea and x-rays on chinese hamster cells in vitro. *Cancer Res., 28,* 198-206.

59. Richards, G. J.,Jr, and Chambers, R. G. (1969). Hydroxyurea: A radiosensitizer in the treatment of neoplasms of the head and neck. *Am. J. Roentgenol. Radium Ther. Nucl. Med., 105,* 555-565.

60. Robichaud, N. J., and Fram, R. J. (1987). Potentiation of ara-C induced cytotoxicity by hydroxyurea in LoVo colon carcinoma cells. *Biochem. Pharmacol., 36,* 1673-1677.

61. Schilsky, R. L., Williams, S. F., Ultmann, J. E., and Watson, S. (1987). Sequential hydroxyurea-cytarabine chemotherapy for refractory non-hodgkin's lymphoma. *J. Clin. Oncol., 5,* 419-425.

62. Moran, R. G., Danenberg, P. V., and Heidelberger, C. (1982). Therapeutic response of leukemic mice treated with fluorinated pyrimidines and inhibitors of deoxyuridylate synthesis. *Biochem. Pharmacol., 31,* 2929-2935.

63. Lokich, J. J., Pitman, S. W., and Skarin, A. T. (1975). Combined 5-fluorouracil and hydroxyurea therapy for gastrointestinal cancer. *Oncology, 32,* 34-37.

64. Platt, O. S., Orkin, S. H., Dover, G., Beardsley, G. P., Miller, B., and Nathan, D. G. (1984). Hydroxyurea enhances fetal hemoglobin production in sickle cell anemia. *J. Clin. Invest., 74,* 652-656.

65. Rodgers, G. P. (1992). Spectrum of fetal hemoglobin responses in sickle cell patients treated with hydroxyurea: The national institutes of health experience. *Semin. Oncol., 19,* 67-73.

66. Yin, Y., Tainsky, M. A., Bischoff, F. Z., Strong, L. C., and Wahl, G. M. (1992). Wild-type p53 restores cell cycle control and inhibits gene amplification in cells with mutant p53 alleles. *Cell, 70,* 937-948.

67. Linke, S. P., Clarkin, K. C., Di Leonardo, A., Tsou, A., and Wahl, G. M. (1996). A reversible, p53-dependent G0/G1 cell cycle arrest induced by ribonucleotide depletion in the absence of detectable DNA damage. *Genes Dev., 10,* 934-947.

68. Linke, S. P., Sengupta, S., Khabie, N. *et al.* (2003). p53 interacts with hRAD51 and hRAD54, and directly modulates homologous recombination. *Cancer Res., 63,* 2596-2605.

69. Agarwal, M. L., Agarwal, A., Taylor, W. R., Chernova, O., Sharma, Y., and Stark, G. R. (1998). A p53-dependent S-phase checkpoint helps to protect cells from DNA damage in response to starvation for pyrimidine nucleotides. *Proc. Natl. Acad. Sci. U. S. A., 95,* 14775-14780.

70. Taylor, W. R., Agarwal, M. L., Agarwal, A., Stacey, D. W., and Stark, G. R. (1999). p53 inhibits entry into mitosis when DNA synthesis is blocked. *Oncogene, 18,* 283-295.

71. Agarwal, M. K., Hastak, K., Jackson, M. W., Breit, S. N., Stark, G. R., and Agarwal, M. L. (2006). Macrophage inhibitory cytokine 1 mediates a p53-dependent protective arrest in S phase in response to starvation for DNA precursors. *Proc. Natl. Acad. Sci. U. S. A., 103,* 16278-16283.

72. Hastak, K., Paul, R. K., Agarwal, M. K. *et al.* (2008). DNA synthesis from unbalanced nucleotide pools causes limited DNA damage that triggers ATR-CHK1-dependent p53 activation. *Proc. Natl. Acad. Sci. U. S. A., 105,* 6314-6319.

73. Sinclair, W. K. (1965). Hydroxyurea: Differential lethal effects on cultured mammalian cells during the cell cycle. *Science, 150,* 1729-1731.

74. Tobey, R. A., and Crissman, H. A. (1972). Use of flow microfluorometry in detailed analysis of effects of chemical agents on cell cycle progression. *Cancer Res., 32,* 2726-2732.

75. Enoch, T., Carr, A. M., and Nurse, P. (1992). Fission yeast genes involved in coupling mitosis to completion of DNA replication. *Genes Dev., 6,* 2035-2046.

76. Lane, D. P., and Crawford, L. V. (1979). T antigen is bound to a host protein in SV40-transformed cells. *Nature, 278,* 261-263.

77. Linzer, D. I., Maltzman, W., and Levine, A. J. (1979). The SV40 A gene product is required for the production of a 54,000 MW cellular tumor antigen. *Virology, 98,* 308-318.

78. Wolf, D., and Rotter, V. (1984). Inactivation of p53 gene expression by an insertion of moloney murine leukemia virus-like DNA sequences. *Mol. Cell. Biol., 4,* 1402-1410.

79. Oren, M., and Levine, A. J. (1983). Molecular cloning of a cDNA specific for the murine p53 cellular tumor antigen. *Proc. Natl. Acad. Sci. U. S. A., 80,* 56-59.

80. Benchimol, S., Lamb, P., Crawford, L. V., Sheer, D., Shows, T. B., Bruns, G. A., and Peacock, J. (1985). Transformation associated p53 protein is encoded by a gene on human chromosome 17. *Somat. Cell Mol. Genet., 11,* 505-510.

81. Lamb, P., and Crawford, L. (1986). Characterization of the human p53 gene. *Mol. Cell. Biol., 6,* 1379-1385.

82. Fields, S., and Jang, S. K. (1990). Presence of a potent transcription activating sequence in the p53 protein. *Science, 249,* 1046-1049.

83. Seto, E., Usheva, A., Zambetti, G. P., Momand, J., Horikoshi, N., Weinmann, R., Levine, A. J., and Shenk, T. (1992). Wild-type p53 binds to the TATA-binding protein and represses transcription. *Proc. Natl. Acad. Sci. U. S. A., 89,* 12028-12032.

84. Thut, C. J., Chen, J. L., Klemm, R., and Tjian, R. (1995). p53 transcriptional activation mediated by coactivators TAFII40 and TAFII60. *Science, 267,* 100-104.

85. Zhang, Y., and Xiong, Y. (2001). A p53 amino-terminal nuclear export signal inhibited by DNA damage-induced phosphorylation. *Science, 292,* 1910-1915.

86. Walker, K. K., and Levine, A. J. (1996). Identification of a novel p53 functional domain that is necessary for efficient growth suppression. *Proc. Natl. Acad. Sci. U. S. A., 93,* 15335-15340.

87. Sakamuro, D., Sabbatini, P., White, E., and Prendergast, G. C. (1997). The polyproline region of p53 is required to activate apoptosis but not growth arrest. *Oncogene, 15,* 887-898.

88. Kern, S. E., Kinzler, K. W., Bruskin, A., Jarosz, D., Friedman, P., Prives, C., and Vogelstein, B. (1991). Identification of p53 as a sequence-specific DNA-binding protein. *Science, 252,* 1708-1711.

89. el-Deiry, W. S., Kern, S. E., Pietenpol, J. A., Kinzler, K. W., and Vogelstein, B. (1992). Definition of a consensus binding site for p53. *Nat. Genet., 1,* 45-49.

90. Cho, Y., Gorina, S., Jeffrey, P. D., and Pavletich, N. P. (1994). Crystal structure of a p53 tumor suppressor-DNA complex: Understanding tumorigenic mutations. *Science, 265,* 346-355.

91. Kraiss, S., Quaiser, A., Oren, M., and Montenarh, M. (1988). Oligomerization of oncoprotein p53. *J. Virol., 62,* 4737-4744.

92. Jeffrey, P. D., Gorina, S., and Pavletich, N. P. (1995). Crystal structure of the tetramerization domain of the p53 tumor suppressor at 1.7 angstroms. *Science, 267,* 1498-1502.

93. Pietenpol, J. A., Tokino, T., Thiagalingam, S., el-Deiry, W. S., Kinzler, K. W., and Vogelstein, B. (1994). Sequence-specific transcriptional activation is essential for growth suppression by p53. *Proc. Natl. Acad. Sci. U. S. A., 91,* 1998-2002.

94. Stommel, J. M., Marchenko, N. D., Jimenez, G. S., Moll, U. M., Hope, T. J., and Wahl, G. M. (1999). A leucine-rich nuclear export signal in the p53 tetramerization domain: Regulation of subcellular localization and p53 activity by NES masking. *EMBO J., 18,* 1660-1672.

95. Hupp, T. R., and Lane, D. P. (1995). Two distinct signaling pathways activate the latent DNA binding function of p53 in a casein kinase II-independent manner. *J. Biol. Chem., 270,* 18165-18174.

96. McKinney, K., Mattia, M., Gottifredi, V., and Prives, C. (2004). p53 linear diffusion along DNA requires its C terminus. *Mol. Cell, 16,* 413-424.

97. Addison, C., Jenkins, J. R., and Sturzbecher, H. W. (1990). The p53 nuclear localisation signal is structurally linked to a p34cdc2 kinase motif. *Oncogene, 5,* 423-426.

98. Shaulsky, G., Goldfinger, N., Ben-Ze'ev, A., and Rotter, V. (1990). Nuclear accumulation of p53 protein is mediated by several nuclear localization signals and plays a role in tumorigenesis. *Mol. Cell. Biol., 10,* 6565-6577.

99. Honda, R., Tanaka, H., and Yasuda, H. (1997). Oncoprotein MDM2 is a ubiquitin ligase E3 for tumor suppressor p53. *FEBS Lett., 420,* 25-27.

100. Kastan, M. B., Onyekwere, O., Sidransky, D., Vogelstein, B., and Craig, R. W. (1991). Participation of p53 protein in the cellular response to DNA damage. *Cancer Res., 51,* 6304-6311.

101. Shieh, S. Y., Ikeda, M., Taya, Y., and Prives, C. (1997). DNA damage-induced phosphorylation of p53 alleviates inhibition by MDM2. *Cell, 91,* 325-334.

102. Toledo, F., and Wahl, G. M. (2006). Regulating the p53 pathway: In vitro hypotheses, in vivo veritas. *Nat. Rev. Cancer., 6,* 909-923.

103. Fuchs, B., O'Connor, D., Fallis, L., Scheidtmann, K. H., and Lu, X. (1995). P53 phosphorylation mutants retain transcription activity. *Oncogene, 10,* 789-793.

104. Lambert, P. F., Kashanchi, F., Radonovich, M. F., Shiekhattar, R., and Brady, J. N. (1998). Phosphorylation of p53 serine 15 increases interaction with CBP. *J. Biol. Chem., 273,* 33048-33053.

105. Gu, W., and Roeder, R. G. (1997). Activation of p53 sequence-specific DNA binding by acetylation of the p53 C-terminal domain. *Cell, 90,* 595-606.

106. Tibbetts, R. S., Brumbaugh, K. M., Williams, J. M., Sarkaria, J. N., Cliby, W. A., Shieh, S. Y., Taya, Y., Prives, C., and Abraham, R. T. (1999). A role for ATR in the DNA damage-induced phosphorylation of p53. *Genes Dev., 13,* 152-157.

107. Chehab, N. H., Malikzay, A., Stavridi, E. S., and Halazonetis, T. D. (1999). Phosphorylation of ser-20 mediates stabilization of human p53 in response to DNA damage. *Proc. Natl. Acad. Sci. U. S. A., 96,* 13777-13782.

108. Shieh, S. Y., Ahn, J., Tamai, K., Taya, Y., and Prives, C. (2000). The human homologs of checkpoint kinases Chk1 and Cds1 (Chk2) phosphorylate p53 at multiple DNA damage-inducible sites. *Genes Dev., 14,* 289-300.

109. Dohoney, K. M., Guillerm, C., Whiteford, C., Elbi, C., Lambert, P. F., Hager, G. L., and Brady, J. N. (2004). Phosphorylation of p53 at serine 37 is important for transcriptional activity and regulation in response to DNA damage. *Oncogene, 23,* 49-57.

110. Sakaguchi, K., Herrera, J. E., Saito, S., Miki, T., Bustin, M., Vassilev, A., Anderson, C. W., and Appella, E. (1998). DNA damage activates p53 through a phosphorylation-acetylation cascade. *Genes Dev., 12,* 2831-2841.

111. Oda, K., Arakawa, H., Tanaka, T. *et al.* (2000). p53AIP1, a potential mediator of p53-dependent apoptosis, and its regulation by ser-46-phosphorylated p53. *Cell, 102,* 849-862.

112. D'Orazi, G., Cecchinelli, B., Bruno, T. *et al.* (2002). Homeodomain-interacting protein kinase-2 phosphorylates p53 at ser 46 and mediates apoptosis. *Nat. Cell Biol., 4,* 11-19.

113. Mayo, L. D., Seo, Y. R., Jackson, M. W., Smith, M. L., Rivera Guzman, J., Korgaonkar, C. K., and Donner, D. B. (2005). Phosphorylation of human p53 at serine 46 determines promoter selection and whether apoptosis is attenuated or amplified. *J. Biol. Chem., 280,* 25953-25959.

114. Sakaguchi, K., Sakamoto, H., Lewis, M. S., Anderson, C. W., Erickson, J. W., Appella, E., and Xie, D. (1997). Phosphorylation of serine 392 stabilizes the tetramer formation of tumor suppressor protein p53. *Biochemistry, 36,* 10117-10124.

115. Hupp, T. R., Meek, D. W., Midgley, C. A., and Lane, D. P. (1992). Regulation of the specific DNA binding function of p53. *Cell, 71,* 875-886.

116. Keller, D. M., Zeng, X., Wang, Y., Zhang, Q. H., Kapoor, M., Shu, H., Goodman, R., Lozano, G., Zhao, Y., and Lu, H. (2001). A DNA damage-induced p53 serine 392 kinase complex contains CK2, hSpt16, and SSRP1. *Mol. Cell, 7,* 283-292.

117. Milne, D. M., Palmer, R. H., and Meek, D. W. (1992). Mutation of the casein kinase II phosphorylation site abolishes the anti-proliferative activity of p53. *Nucleic Acids Res., 20,* 5565-5570.

118. Jordan, J. J., Menendez, D., Inga, A., Noureddine, M., Bell, D. A., and Resnick, M. A. (2008). Noncanonical DNA motifs as transactivation targets by wild type and mutant p53. *PLoS Genet., 4,* e1000104.

119. Inga, A., Storici, F., Darden, T. A., and Resnick, M. A. (2002). Differential transactivation by the p53 transcription factor is highly dependent on p53 level and promoter target sequence. *Mol. Cell. Biol., 22,* 8612-8625.

120. Weinberg, R. L., Veprintsev, D. B., Bycroft, M., and Fersht, A. R. (2005). Comparative binding of p53 to its promoter and DNA recognition elements. *J. Mol. Biol., 348,* 589-596.

121. Samuels-Lev, Y., O'Connor, D. J., Bergamaschi, D., Trigiante, G., Hsieh, J. K., Zhong, S., Campargue, I., Naumovski, L., Crook, T., and Lu, X. (2001). ASPP proteins specifically stimulate the apoptotic function of p53. *Mol. Cell, 8,* 781-794.

122. Lill, N. L., Grossman, S. R., Ginsberg, D., DeCaprio, J., and Livingston, D. M. (1997). Binding and modulation of p53 by p300/CBP coactivators. *Nature, 387,* 823-827.

123. Espinosa, J. M., Verdun, R. E., and Emerson, B. M. (2003). p53 functions through stress- and promoter-specific recruitment of transcription initiation components before and after DNA damage. *Mol. Cell, 12,* 1015-1027.

124. Marshall, N. F., Peng, J., Xie, Z., and Price, D. H. (1996). Control of RNA polymerase II elongation potential by a novel carboxyl-terminal domain kinase. *J. Biol. Chem., 271,* 27176-27183.

125. Zhu, Y., Pe'ery, T., Peng, J., Ramanathan, Y., Marshall, N., Marshall, T., Amendt, B., Mathews, M. B., and Price, D. H. (1997). Transcription elongation factor P-TEFb is required for HIV-1 tat transactivation in vitro. *Genes Dev., 11,* 2622-2632.

126. Ramanathan, Y., Rajpara, S. M., Reza, S. M., Lees, E., Shuman, S., Mathews, M. B., and Pe'ery, T. (2001). Three RNA polymerase II carboxyl-terminal domain kinases display distinct substrate preferences. *J. Biol. Chem., 276,* 10913-10920.

127. Claudio, P. P., Cui, J., Ghafouri, M. *et al.* (2006). Cdk9 phosphorylates p53 on serine 392 independently of CKII. *J. Cell. Physiol., 208,* 602-612.

128. Murphy, M., Ahn, J., Walker, K. K., Hoffman, W. H., Evans, R. M., Levine, A. J., and George, D. L. (1999). Transcriptional repression by wild-type p53 utilizes histone deacetylases, mediated by interaction with mSin3a. *Genes Dev., 13,* 2490-2501.

129. Lee, K. C., Crowe, A. J., and Barton, M. C. (1999). p53-mediated repression of alpha-fetoprotein gene expression by specific DNA binding. *Mol. Cell. Biol., 19,* 1279-1288.

130. Arias-Lopez, C., Lazaro-Trueba, I., Kerr, P., Lord, C. J., Dexter, T., Iravani, M., Ashworth, A., and Silva, A. (2006). p53 modulates homologous recombination by transcriptional regulation of the RAD51 gene. *EMBO Rep., 7,* 219-224.

131. Yonish-Rouach, E., Resnitzky, D., Lotem, J., Sachs, L., Kimchi, A., and Oren, M. (1991). Wild-type p53 induces apoptosis of myeloid leukaemic cells that is inhibited by interleukin-6. *Nature, 352,* 345-347.

132. Miyashita, T., and Reed, J. C. (1995). Tumor suppressor p53 is a direct transcriptional activator of the human bax gene. *Cell, 80,* 293-299.

133. Selvakumaran, M., Lin, H. K., Miyashita, T., Wang, H. G., Krajewski, S., Reed, J. C., Hoffman, B., and Liebermann, D. (1994). Immediate early up-regulation of bax expression by p53 but not TGF beta 1: A paradigm for distinct apoptotic pathways. *Oncogene, 9,* 1791-1798.

134. Riley, T., Sontag, E., Chen, P., and Levine, A. (2008). Transcriptional control of human p53-regulated genes. *Nat. Rev. Mol. Cell Biol., 9,* 402-412.

135. Haupt, Y., Rowan, S., Shaulian, E., Vousden, K. H., and Oren, M. (1995). Induction of apoptosis in HeLa cells by trans-activation-deficient p53. *Genes Dev., 9,* 2170-2183.

136. Marchenko, N. D., Zaika, A., and Moll, U. M. (2000). Death signal-induced localization of p53 protein to mitochondria. A potential role in apoptotic signaling. *J. Biol. Chem., 275,* 16202-16212.

137. Leu, J. I., Dumont, P., Hafey, M., Murphy, M. E., and George, D. L. (2004). Mitochondrial p53 activates bak and causes disruption of a bak-Mcl1 complex. *Nat. Cell Biol., 6,* 443-450.

138. Chipuk, J. E., Kuwana, T., Bouchier-Hayes, L., Droin, N. M., Newmeyer, D. D., Schuler, M., and Green, D. R. (2004). Direct activation of bax by p53 mediates mitochondrial membrane permeabilization and apoptosis. *Science, 303,* 1010-1014.

139. Mihara, M., Erster, S., Zaika, A., Petrenko, O., Chittenden, T., Pancoska, P., and Moll, U. M. (2003). P53 has a direct apoptogenic role at the mitochondria. *Mol. Cell, 11,* 577-590.

140. Tomita, Y., Marchenko, N., Erster, S., Nemajerova, A., Dehner, A., Klein, C., Pan, H., Kessler, H., Pancoska, P., and Moll, U. M. (2006). WT p53, but not tumor-derived mutants,

bind to Bcl2 via the DNA binding domain and induce mitochondrial permeabilization. *J. Biol. Chem., 281,* 8600-8606.

141. Nelson, W. G., and Kastan, M. B. (1994). DNA strand breaks: The DNA template alterations that trigger p53-dependent DNA damage response pathways. *Mol. Cell. Biol., 14,* 1815-1823.

142. Huang, L. C., Clarkin, K. C., and Wahl, G. M. (1996). Sensitivity and selectivity of the DNA damage sensor responsible for activating p53-dependent G1 arrest. *Proc. Natl. Acad. Sci. U. S. A., 93,* 4827-4832.

143. Vogelstein, B. (1990). Cancer. A deadly inheritance. *Nature, 348,* 681-682.

144. Kato, S., Han, S. Y., Liu, W., Otsuka, K., Shibata, H., Kanamaru, R., and Ishioka, C. (2003). Understanding the function-structure and function-mutation relationships of p53 tumor suppressor protein by high-resolution missense mutation analysis. *Proc. Natl. Acad. Sci. U. S. A., 100,* 8424-8429.

145. Hollstein, M., Sidransky, D., Vogelstein, B., and Harris, C. C. (1991). P53 mutations in human cancers. *Science, 253,* 49-53.

146. Baker, S. J., Fearon, E. R., Nigro, J. M. *et al.* (1989). Chromosome 17 deletions and p53 gene mutations in colorectal carcinomas. *Science, 244,* 217-221.

147. Milner, J., and Medcalf, E. A. (1991). Cotranslation of activated mutant p53 with wild type drives the wild-type p53 protein into the mutant conformation. *Cell, 65,* 765-774.

148. Wolf, D., Harris, N., and Rotter, V. (1984). Reconstitution of p53 expression in a nonproducer ab-MuLV-transformed cell line by transfection of a functional p53 gene. *Cell, 38,* 119-126.

149. Huberman, J. A., and Riggs, A. D. (1966). Autoradiography of chromosomal DNA fibers from chinese hamster cells. *Proc. Natl. Acad. Sci. U. S. A., 55,* 599-606.

150. Bell, S. P., and Stillman, B. (1992). ATP-dependent recognition of eukaryotic origins of DNA replication by a multiprotein complex. *Nature, 357,* 128-134.

151. Moyer, S. E., Lewis, P. W., and Botchan, M. R. (2006). Isolation of the Cdc45/Mcm2-7/GINS (CMG) complex, a candidate for the eukaryotic DNA replication fork helicase. *Proc. Natl. Acad. Sci. U. S. A., 103,* 10236-10241.

152. Sheu, Y. J., and Stillman, B. (2006). Cdc7-Dbf4 phosphorylates MCM proteins via a docking site-mediated mechanism to promote S phase progression. *Mol. Cell, 24,* 101-113.

153. Sheu, Y. J., and Stillman, B. (2010). The Dbf4-Cdc7 kinase promotes S phase by alleviating an inhibitory activity in Mcm4. *Nature, 463,* 113-117.

154. Aparicio, O. M., Weinstein, D. M., and Bell, S. P. (1997). Components and dynamics of DNA replication complexes in S. cerevisiae: Redistribution of MCM proteins and Cdc45p during S phase. *Cell, 91,* 59-69.

155. Aparicio, O. M., Stout, A. M., and Bell, S. P. (1999). Differential assembly of Cdc45p and DNA polymerases at early and late origins of DNA replication. *Proc. Natl. Acad. Sci. U. S. A., 96,* 9130-9135.

156. Dimitrova, D. S., and Gilbert, D. M. (2000). Stability and nuclear distribution of mammalian replication protein A heterotrimeric complex. *Exp. Cell Res., 254,* 321-327.

157. Zhou, B. B., and Bartek, J. (2004). Targeting the checkpoint kinases: Chemosensitization versus chemoprotection. *Nat. Rev. Cancer., 4,* 216-225.

158. Kastan, M. B., and Bartek, J. (2004). Cell-cycle checkpoints and cancer. *Nature, 432,* 316-323.

159. Tercero, J. A., Longhese, M. P., and Diffley, J. F. (2003). A central role for DNA replication forks in checkpoint activation and response. *Mol. Cell, 11,* 1323-1336.

160. Davies, S. L., North, P. S., and Hickson, I. D. (2007). Role for BLM in replication-fork restart and suppression of origin firing after replicative stress. *Nat. Struct. Mol. Biol., 14,* 677-679.

161. Petermann, E., Orta, M. L., Issaeva, N., Schultz, N., and Helleday, T. (2010). Hydroxyurea-stalled replication forks become progressively inactivated and require two different RAD51-mediated pathways for restart and repair. *Mol. Cell, 37,* 492-502.

162. Weinert, T., Kaochar, S., Jones, H., Paek, A., and Clark, A. J. (2009). The replication fork's five degrees of freedom, their failure and genome rearrangements. *Curr. Opin. Cell Biol., 21,* 778-784.

163. Atkinson, J., and McGlynn, P. (2009). Replication fork reversal and the maintenance of genome stability. *Nucleic Acids Res., 37,* 3475-3492.

164. Budzowska, M., and Kanaar, R. (2009). Mechanisms of dealing with DNA damage-induced replication problems. *Cell Biochem. Biophys., 53,* 17-31.

165. Petermann, E., and Helleday, T. (2010). Pathways of mammalian replication fork restart. *Nat. Rev. Mol. Cell Biol., 11,* 683-687.

166. Shiloh, Y. (2001). ATM and ATR: Networking cellular responses to DNA damage. *Curr. Opin. Genet. Dev., 11,* 71-77.

167. Durocher, D., and Jackson, S. P. (2001). DNA-PK, ATM and ATR as sensors of DNA damage: Variations on a theme? *Curr. Opin. Cell Biol., 13,* 225-231.

168. Wright, J. A., Keegan, K. S., Herendeen, D. R., Bentley, N. J., Carr, A. M., Hoekstra, M. F., and Concannon, P. (1998). Protein kinase mutants of human ATR increase sensitivity to UV and ionizing radiation and abrogate cell cycle checkpoint control. *Proc. Natl. Acad. Sci. U. S. A., 95,* 7445-7450.

169. Cliby, W. A., Roberts, C. J., Cimprich, K. A., Stringer, C. M., Lamb, J. R., Schreiber, S. L., and Friend, S. H. (1998). Overexpression of a kinase-inactive ATR protein causes sensitivity to DNA-damaging agents and defects in cell cycle checkpoints. *EMBO J., 17,* 159-169.

170. Cortez, D., Guntuku, S., Qin, J., and Elledge, S. J. (2001). ATR and ATRIP: Partners in checkpoint signaling. *Science, 294,* 1713-1716.

171. Sogo, J. M., Lopes, M., and Foiani, M. (2002). Fork reversal and ssDNA accumulation at stalled replication forks owing to checkpoint defects. *Science, 297,* 599-602.

172. Wold, M. S. (1997). Replication protein A: A heterotrimeric, single-stranded DNA-binding protein required for eukaryotic DNA metabolism. *Annu. Rev. Biochem., 66,* 61-92.

173. Longhese, M. P., Neecke, H., Paciotti, V., Lucchini, G., and Plevani, P. (1996). The 70 kDa subunit of replication protein A is required for the G1/S and intra-S DNA damage checkpoints in budding yeast. *Nucleic Acids Res., 24,* 3533-3537.

174. Zou, L., and Elledge, S. J. (2003). Sensing DNA damage through ATRIP recognition of RPA-ssDNA complexes. *Science, 300,* 1542-1548.

175. Liu, Q., Guntuku, S., Cui, X. S. *et al.* (2000). Chk1 is an essential kinase that is regulated by atr and required for the G(2)/M DNA damage checkpoint. *Genes Dev., 14,* 1448-1459.

176. Weiss, R. S., Leder, P., and Vaziri, C. (2003). Critical role for mouse Hus1 in an S-phase DNA damage cell cycle checkpoint. *Mol. Cell. Biol., 23,* 791-803.

177. Zou, L., Cortez, D., and Elledge, S. J. (2002). Regulation of ATR substrate selection by Rad17-dependent loading of Rad9 complexes onto chromatin. *Genes Dev., 16,* 198-208.

178. Volkmer, E., and Karnitz, L. M. (1999). Human homologs of schizosaccharomyces pombe rad1, hus1, and rad9 form a DNA damage-responsive protein complex. *J. Biol. Chem., 274,* 567-570.

179. Greer, D. A., Besley, B. D., Kennedy, K. B., and Davey, S. (2003). hRad9 rapidly binds DNA containing double-strand breaks and is required for damage-dependent topoisomerase II beta binding protein 1 focus formation. *Cancer Res., 63,* 4829-4835.

180. Mordes, D. A., Glick, G. G., Zhao, R., and Cortez, D. (2008). TopBP1 activates ATR through ATRIP and a PIKK regulatory domain. *Genes Dev., 22,* 1478-1489.

181. Unsal-Kacmaz, K., and Sancar, A. (2004). Quaternary structure of ATR and effects of ATRIP and replication protein A on its DNA binding and kinase activities. *Mol. Cell. Biol., 24,* 1292-1300.

182. Furuya, K., Poitelea, M., Guo, L., Caspari, T., and Carr, A. M. (2004). Chk1 activation requires Rad9 S/TQ-site phosphorylation to promote association with C-terminal BRCT domains of Rad4TOPBP1. *Genes Dev., 18,* 1154-1164.

183. Brown, E. J., and Baltimore, D. (2000). ATR disruption leads to chromosomal fragmentation and early embryonic lethality. *Genes Dev., 14,* 397-402.

184. Takai, H., Tominaga, K., Motoyama, N., Minamishima, Y. A., Nagahama, H., Tsukiyama, T., Ikeda, K., Nakayama, K., Nakanishi, M., and Nakayama, K. (2000). Aberrant cell cycle checkpoint function and early embryonic death in Chk1(-/-) mice. *Genes Dev., 14,* 1439-1447.

185. Zhao, H., and Piwnica-Worms, H. (2001). ATR-mediated checkpoint pathways regulate phosphorylation and activation of human Chk1. *Mol. Cell. Biol., 21,* 4129-4139.

186. Lopez-Girona, A., Tanaka, K., Chen, X. B., Baber, B. A., McGowan, C. H., and Russell, P. (2001). Serine-345 is required for Rad3-dependent phosphorylation and function of checkpoint kinase Chk1 in fission yeast. *Proc. Natl. Acad. Sci. U. S. A., 98,* 11289-11294.

187. Walker, M., Black, E. J., Oehler, V., Gillespie, D. A., and Scott, M. T. (2009). Chk1 C-terminal regulatory phosphorylation mediates checkpoint activation by de-repression of Chk1 catalytic activity. *Oncogene, 28,* 2314-2323.

188. Kemp, M. G., Akan, Z., Yilmaz, S. *et al.* (2010). Tipin-replication protein A interaction mediates Chk1 phosphorylation by ATR in response to genotoxic stress. *J. Biol. Chem., 285,* 16562-16571.

189. Kumagai, A., and Dunphy, W. G. (2000). Claspin, a novel protein required for the activation of Chk1 during a DNA replication checkpoint response in xenopus egg extracts. *Mol. Cell, 6,* 839-849.

190. Chini, C. C., and Chen, J. (2003). Human claspin is required for replication checkpoint control. *J. Biol. Chem., 278,* 30057-30062.

191. Bahassi, E. M., Ovesen, J. L., Riesenberg, A. L., Bernstein, W. Z., Hasty, P. E., and Stambrook, P. J. (2008). The checkpoint kinases Chk1 and Chk2 regulate the functional associations between hBRCA2 and Rad51 in response to DNA damage. *Oncogene, 27,* 3977-3985.

192. Sorensen, C. S., Hansen, L. T., Dziegielewski, J., Syljuasen, R. G., Lundin, C., Bartek, J., and Helleday, T. (2005). The cell-cycle checkpoint kinase Chk1 is required for mammalian homologous recombination repair. *Nat. Cell Biol., 7,* 195-201.

193. Sanchez, Y., Wong, C., Thoma, R. S., Richman, R., Wu, Z., Piwnica-Worms, H., and Elledge, S. J. (1997). Conservation of the Chk1 checkpoint pathway in mammals: Linkage of DNA damage to cdk regulation through Cdc25. *Science, 277,* 1497-1501.

194. Tripathi, V., Kaur, S., and Sengupta, S. (2008). Phosphorylation-dependent interactions of BLM and 53BP1 are required for their anti-recombinogenic roles during homologous recombination. *Carcinogenesis, 29,* 52-61.

195. Wang, X., Kennedy, R. D., Ray, K., Stuckert, P., Ellenberger, T., and D'Andrea, A. D. (2007). Chk1-mediated phosphorylation of FANCE is required for the fanconi anemia/BRCA pathway. *Mol. Cell. Biol., 27,* 3098-3108.

196. Davies, S. L., North, P. S., Dart, A., Lakin, N. D., and Hickson, I. D. (2004). Phosphorylation of the bloom's syndrome helicase and its role in recovery from S-phase arrest. *Mol. Cell. Biol., 24,* 1279-1291.

197. Chen, J. (2000). Ataxia telangiectasia-related protein is involved in the phosphorylation of BRCA1 following deoxyribonucleic acid damage. *Cancer Res., 60,* 5037-5039.

198. Gatei, M., Zhou, B. B., Hobson, K., Scott, S., Young, D., and Khanna, K. K. (2001). Ataxia telangiectasia mutated (ATM) kinase and ATM and Rad3 related kinase mediate phosphorylation of Brca1 at distinct and overlapping sites. in vivo assessment using phospho-specific antibodies. *J. Biol. Chem., 276,* 17276-17280.

199. Furuta, T., Takemura, H., Liao, Z. Y. *et al.* (2003). Phosphorylation of histone H2AX and activation of Mre11, Rad50, and Nbs1 in response to replication-dependent DNA double-strand breaks induced by mammalian DNA topoisomerase I cleavage complexes. *J. Biol. Chem., 278,* 20303-20312.

200. Cimprich, K. A., and Cortez, D. (2008). ATR: An essential regulator of genome integrity. *Nat. Rev. Mol. Cell Biol., 9,* 616-627.

201. Pages, V., and Fuchs, R. P. (2003). Uncoupling of leading- and lagging-strand DNA replication during lesion bypass in vivo. *Science, 300,* 1300-1303.

202. Umezu, K., Nakayama, K., and Nakayama, H. (1990). Escherichia coli RecQ protein is a DNA helicase. *Proc. Natl. Acad. Sci. U. S. A., 87,* 5363-5367.

203. Harmon, F. G., and Kowalczykowski, S. C. (1998). RecQ helicase, in concert with RecA and SSB proteins, initiates and disrupts DNA recombination. *Genes Dev., 12,* 1134-1144.

204. Chaganti, R. S., Schonberg, S., and German, J. (1974). A manyfold increase in sister chromatid exchanges in bloom's syndrome lymphocytes. *Proc. Natl. Acad. Sci. U. S. A., 71,* 4508-4512.

205. Karow, J. K., Constantinou, A., Li, J. L., West, S. C., and Hickson, I. D. (2000). The bloom's syndrome gene product promotes branch migration of holliday junctions. *Proc. Natl. Acad. Sci. U. S. A., 97,* 6504-6508.

206. Sharples, G. J., Ingleston, S. M., and Lloyd, R. G. (1999). Holliday junction processing in bacteria: Insights from the evolutionary conservation of RuvABC, RecG, and RusA. *J. Bacteriol., 181,* 5543-5550.

207. Yang, Q., Zhang, R., Wang, X. W. *et al.* (2002). The processing of holliday junctions by BLM and WRN helicases is regulated by p53. *J. Biol. Chem., 277,* 31980-31987.

208. Sengupta, S., Linke, S. P., Pedeux, R. *et al.* (2003). BLM helicase-dependent transport of p53 to sites of stalled DNA replication forks modulates homologous recombination. *EMBO J., 22,* 1210-1222.

209. van Gent, D. C., Hoeijmakers, J. H., and Kanaar, R. (2001). Chromosomal stability and the DNA double-stranded break connection. *Nat. Rev. Genet., 2,* 196-206.

210. Johnson, R. D., and Jasin, M. (2000). Sister chromatid gene conversion is a prominent double-strand break repair pathway in mammalian cells. *EMBO J., 19,* 3398-3407.

211. Flygare, J., Benson, F., and Hellgren, D. (1996). Expression of the human RAD51 gene during the cell cycle in primary human peripheral blood lymphocytes. *Biochim. Biophys. Acta, 1312,* 231-236.

212. Benson, F. E., Stasiak, A., and West, S. C. (1994). Purification and characterization of the human Rad51 protein, an analogue of E. coli RecA. *EMBO J., 13,* 5764-5771.

213. Baumann, P., Benson, F. E., and West, S. C. (1996). Human Rad51 protein promotes ATP-dependent homologous pairing and strand transfer reactions in vitro. *Cell, 87,* 757-766.

214. Sturzbecher, H. W., Donzelmann, B., Henning, W., Knippschild, U., and Buchhop, S. (1996). p53 is linked directly to homologous recombination processes via RAD51/RecA protein interaction. *EMBO J., 15,* 1992-2002.

215. Yoon, D., Wang, Y., Stapleford, K., Wiesmuller, L., and Chen, J. (2004). P53 inhibits strand exchange and replication fork regression promoted by human Rad51. *J. Mol. Biol., 336,* 639-654.

216. Iwabuchi, K., Bartel, P. L., Li, B., Marraccino, R., and Fields, S. (1994). Two cellular proteins that bind to wild-type but not mutant p53 *Proc. Natl. Acad. Sci. U. S. A., 91,* 6098-6102.

217. Schultz, L. B., Chehab, N. H., Malikzay, A., and Halazonetis, T. D. (2000). p53 binding protein 1 (53BP1) is an early participant in the cellular response to DNA double-strand breaks. *J. Cell Biol., 151,* 1381-1390.

218. Sengupta, S., Robles, A. I., Linke, S. P. *et al.* (2004). Functional interaction between BLM helicase and 53BP1 in a Chk1-mediated pathway during S-phase arrest. *J. Cell Biol., 166,* 801-813.

219. Lu, X., Nannenga, B., and Donehower, L. A. (2005). PPM1D dephosphorylates Chk1 and p53 and abrogates cell cycle checkpoints. *Genes Dev., 19,* 1162-1174.

220. Fiscella, M., Zhang, H., Fan, S., Sakaguchi, K., Shen, S., Mercer, W. E., Vande Woude, G. F., O'Connor, P. M., and Appella, E. (1997). Wip1, a novel human protein phosphatase that is induced in response to ionizing radiation in a p53-dependent manner. *Proc. Natl. Acad. Sci. U. S. A., 94,* 6048-6053.

221. Rossi, M., Demidov, O. N., Anderson, C. W., Appella, E., and Mazur, S. J. (2008). Induction of PPM1D following DNA-damaging treatments through a conserved p53 response element coincides with a shift in the use of transcription initiation sites. *Nucleic Acids Res., 36,* 7168-7180.

222. Bronder, J. L., and Moran, R. G. (2003). A defect in the p53 response pathway induced by de novo purine synthesis inhibition. *J. Biol. Chem., 278,* 48861-48871.

223. Mendez, J., and Stillman, B. (2000). Chromatin association of human origin recognition complex, cdc6, and minichromosome maintenance proteins during the cell cycle: Assembly of prereplication complexes in late mitosis. *Mol. Cell. Biol., 20,* 8602-8612.

224. Mattia, M., Gottifredi, V., McKinney, K., and Prives, C. (2007). p53-dependent p21 mRNA elongation is impaired when DNA replication is stalled. *Mol. Cell. Biol., 27,* 1309-1320.

225. Gottifredi, V., Shieh, S., Taya, Y., and Prives, C. (2001). p53 accumulates but is functionally impaired when DNA synthesis is blocked. *Proc. Natl. Acad. Sci. U. S. A., 98,* 1036-1041.

226. Smith, P. J., Soues, S., Gottlieb, T., Falk, S. J., Watson, J. V., Osborne, R. J., and Bleehen, N. M. (1994). Etoposide-induced cell cycle delay and arrest-dependent modulation of DNA topoisomerase II in small-cell lung cancer cells. *Br. J. Cancer, 70,* 914-921.

227. Ivanov, A., Cragg, M. S., Erenpreisa, J., Emzinsh, D., Lukman, H., and Illidge, T. M. (2003). Endopolyploid cells produced after severe genotoxic damage have the potential to repair DNA double strand breaks. *J. Cell. Sci., 116,* 4095-4106.

228. Leung-Pineda, V., Ryan, C. E., and Piwnica-Worms, H. (2006). Phosphorylation of Chk1 by ATR is antagonized by a Chk1-regulated protein phosphatase 2A circuit. *Mol. Cell. Biol., 26,* 7529-7538.
229. Kaeser, M. D., and Iggo, R. D. (2002). Chromatin immunoprecipitation analysis fails to support the latency model for regulation of p53 DNA binding activity in vivo. *Proc. Natl. Acad. Sci. U. S. A., 99,* 95-100.

230. Rogakou, E. P., Pilch, D. R., Orr, A. H., Ivanova, V. S., and Bonner, W. M. (1998). DNA double-stranded breaks induce histone H2AX phosphorylation on serine. 139 *J. Biol. Chem., 273,* 5858-5868.

231. Zou, H., Li, Y., Liu, X., and Wang, X. (1999). An APAF-1.cytochrome c multimeric complex is a functional apoptosome that activates procaspase-9. *J. Biol. Chem., 274,* 11549-11556.

232. Kennedy, B. K., Barbie, D. A., Classon, M., Dyson, N., and Harlow, E. (2000). Nuclear organization of DNA replication in primary mammalian cells. *Genes Dev., 14,* 2855-2868.

233. Mekeel, K. L., Tang, W., Kachnic, L. A., Luo, C. M., DeFrank, J. S., and Powell, S. N. (1997). Inactivation of p53 results in high rates of homologous recombination. *Oncogene, 14,* 1847-1857.

234. Rosse, T., Olivier, R., Monney, L., Rager, M., Conus, S., Fellay, I., Jansen, B., and Borner, C. (1998). Bcl-2 prolongs cell survival after bax-induced release of cytochrome c. *Nature, 391,* 496-499.

235. Ellis, N. A., Groden, J., Ye, T. Z., Straughen, J., Lennon, D. J., Ciocci, S., Proytcheva, M., and German, J. (1995). The bloom's syndrome gene product is homologous to RecQ helicases. *Cell, 83,* 655-666.

236. Karow, J. K., Chakraverty, R. K., and Hickson, I. D. (1997). The bloom's syndrome gene product is a 3'-5' DNA helicase. *J. Biol. Chem., 272,* 30611-30614.

237. Rigaut, G., Shevchenko, A., Rutz, B., Wilm, M., Mann, M., and Seraphin, B. (1999). A generic protein purification method for protein complex characterization and proteome exploration. *Nat. Biotechnol., 17,* 1030-1032.

238. Parks, T. D., Leuther, K. K., Howard, E. D., Johnston, S. A., and Dougherty, W. G. (1994). Release of proteins and peptides from fusion proteins using a recombinant plant virus proteinase. *Anal. Biochem., 216,* 413-417.

239. Gavin, A. C., Bosche, M., Krause, R. *et al.* (2002). Functional organization of the yeast proteome by systematic analysis of protein complexes. *Nature, 415,* 141-147.

240. Vasileva, A., and Jessberger, R. (2005). Precise hit: Adeno-associated virus in gene targeting. *Nat. Rev. Microbiol., 3,* 837-847.

241. Sedivy, J. M., and Sharp, P. A. (1989). Positive genetic selection for gene disruption in mammalian cells by homologous recombination. *Proc. Natl. Acad. Sci. U. S. A., 86,* 227-231.

242. Kohli, M., Rago, C., Lengauer, C., Kinzler, K. W., and Vogelstein, B. (2004). Facile methods for generating human somatic cell gene knockouts using recombinant adeno-associated viruses. *Nucleic Acids Res., 32,* e3.

243. Hirata, R., Chamberlain, J., Dong, R., and Russell, D. W. (2002). Targeted transgene insertion into human chromosomes by adeno-associated virus vectors. *Nat. Biotechnol., 20,* 735-738.

244. Carter, B. J. (1992). Adeno-associated virus vectors. *Curr. Opin. Biotechnol., 3,* 533-539.

245. Russell, D. W., and Hirata, R. K. (1998). Human gene targeting by viral vectors. *Nat. Genet., 18,* 325-330.

246. Bertwistle, D., Sugimoto, M., and Sherr, C. J. (2004). Physical and functional interactions of the arf tumor suppressor protein with nucleophosmin/B23. *Mol. Cell. Biol., 24,* 985-996.

247. Millevoi, S., and Vagner, S. (2010). Molecular mechanisms of eukaryotic pre-mRNA 3' end processing regulation. *Nucleic Acids Res., 38,* 2757-2774.

248. Murray-Zmijewski, F., Slee, E. A., and Lu, X. (2008). A complex barcode underlies the heterogeneous response of p53 to stress. *Nat. Rev. Mol. Cell Biol., 9,* 702-712.

249. Feng, Z., Zhang, H., Levine, A. J., and Jin, S. (2005). The coordinate regulation of the p53 and mTOR pathways in cells. *Proc. Natl. Acad. Sci. U. S. A., 102,* 8204-8209.

250. Budanov, A. V., and Karin, M. (2008). p53 target genes sestrin1 and sestrin2 connect genotoxic stress and mTOR signaling. *Cell, 134,* 451-460.

251. Tasdemir, E., Maiuri, M. C., Galluzzi, L. *et al.* (2008). Regulation of autophagy by cytoplasmic p53. *Nat. Cell Biol., 10,* 676-687.

252. Gomes, N. P., and Espinosa, J. M. (2010). Differential regulation of p53 target genes: It's (core promoter) elementary. *Genes Dev., 24,* 111-114.

253. Gomes, N. P., Bjerke, G., Llorente, B., Szostek, S. A., Emerson, B. M., and Espinosa, J. M. (2006). Gene-specific requirement for P-TEFb activity and RNA polymerase II phosphorylation within the p53 transcriptional program. *Genes Dev., 20,* 601-612.

254. Sauer-Eriksson, A. E., Kleywegt, G. J., Uhlen, M., and Jones, T. A. (1995). Crystal structure of the C2 fragment of streptococcal protein G in complex with the fc domain of human IgG. *Structure, 3,* 265-278.

255. Burckstummer, T., Bennett, K. L., Preradovic, A., Schutze, G., Hantschel, O., Superti-Furga, G., and Bauch, A. (2006). An efficient tandem affinity purification procedure for interaction proteomics in mammalian cells. *Nat. Methods, 3,* 1013-1019.

256. Tsai, A., and Carstens, R. P. (2006). An optimized protocol for protein purification in cultured mammalian cells using a tandem affinity purification approach. *Nat. Protoc., 1,* 2820-2827.

257. Okorokov, A. L., and Milner, J. (1999). An ATP/ADP-dependent molecular switch regulates the stability of p53-DNA complexes. *Mol. Cell. Biol., 19,* 7501-7510.

258. Koc, A., Wheeler, L. J., Mathews, C. K., and Merrill, G. F. (2004). Hydroxyurea arrests DNA replication by a mechanism that preserves basal dNTP pools. *J. Biol. Chem., 279,* 223-230.

259. Ruzzene, M., and Pinna, L. A. (2010). Addiction to protein kinase CK2: A common denominator of diverse cancer cells? *Biochim. Biophys. Acta, 1804,* 499-504.

260. Meek, D. W., Simon, S., Kikkawa, U., and Eckhart, W. (1990). The p53 tumour suppressor protein is phosphorylated at serine 389 by casein kinase II. *EMBO J., 9,* 3253-3260.

261. Thacker, J. (2005). The RAD51 gene family, genetic instability and cancer. *Cancer Lett., 219,* 125-135.

VITA

Cortney Lynne Heyer was born on March 20, 1983 in Waukesha, Wisconsin. She graduated from Homer Central High School (Homer, New York) in 2001 and attended St. Bonaventure University in the following fall. She was inducted into the Phi Eta Sigma National Honor Society and earned her Bachelor of Science in Biochemistry, *cum laude*. She started her graduate studies at Virginia Commonwealth University in the department of Pharmacology and Toxicology in the fall of 2005, where she later joined the laboratory of Richard G. Moran in the spring of 2006. At Virginia Commonwealth University she presented a poster on her dissertation work at the AACR 101st Annual Meeting in 2010. As a chairperson of Women in Science in 2007, Cortney helped in the establishment of this organization. In 2009, she was a chairperson for the Virginia Academy of Sciences and aided in the organization and execution of the Medical Sciences section of the 87th annual meeting.